DIPLOMARBEIT | DIPLOMA THESIS

Titel | Title

Synthesis and characterization of silica-based nano-detoxifiers

verfasst von | submitted by

Lisa Grötzl BSc

angestrebter akademischer Grad | in partial fulfilment of the requirements for the degree of

Diplom-Ingenieurin (Dipl.-Ing.)

Wien | Vienna, 2024

Studienkennzahl lt. Studienblatt | Degree programme code as it appears on the student record sheet:	UE 066 658
Studienrichtung lt. Studienblatt | Degree programme as it appears on the student record sheet:	Masterstudium Chemie und Technologie der Materialien
Betreut von | Supervisor:	Univ.-Prof. Dr. Freddy Kleitz

Abstract

Intoxication is a major problem affecting all ages.[1] Whether through unintentional contact in household, overdosing on easily accessible analgesics, intentional drug abuse or suicide attempts, poisoning could lead to serious harm.[2] Several ways of toxin removal from the body have been applied in the medical field so far. Antidotes have been found to offer the most reliable solution. However, they are limited to only a few toxins and the identity of the harmful substance must be known.[3] As an alternative, mesoporous silica nanoparticles were herein introduced with mesopores large enough to confine small organic molecules.[4] Synthesis strategies were explored to obtain suitable silica-based oral nano-detoxifiers. Three different morphologies of particles were synthesized: dendritic- in a size of 120 nm and pore size of 3.8 nm, virus-like- in a diameter of 100 nm with a broad pore size range and nanorod silica nanoparticles with 170 nm length, aspect ratio of 2.3 and 3.2 nm pore size. The particles were grafted with phosphonate-, epoxide- and polyethylene glycol groups to enhance the particle-toxin interaction and support colloidal stability. Their adsorption capacity was investigated by the loading of paracetamol, the model toxin of this project. Results showed that plain and phosphonated dendritic mesoporous silica nanoparticles captured most paracetamol in ethanol. Additional adsorption studies in simulating gastric and intestinal fluids were attempted. We herein present preliminary results for the application of mesoporous silica nanoparticles in the detoxifying field.

Abstract (Deutsche Version)

Vergiftungen, ob durch unbeabsichtigten Kontakt im Haushalt, Überdosierungen von Schmerzmitteln oder durch bewusstes Handeln, beispielsweise Drogenmissbrauch oder Suizidversuch, stellen ein bedeutendes, altersunspezifisches Problem dar.[1,2] Da Intoxikationen mittels gefährlicher Substanzen der menschlichen Gesundheit einen erheblichen Schaden anrichten können, etablierten sich im medizinischen Bereich Methoden, um jene Toxine aus dem Körper zu entfernen. Antidote erwiesen sich als sehr wirksam, jedoch muss für deren Anwendung die Identität der zu entfernenden Substanz bekannt sein, da diese nur sehr spezifisch eingesetzt werden können. Zudem existieren Gegenmittel nur für wenige ausgewählte Toxine.[3] Vorliegende Arbeit schlägt daher die orale Anwendung von Silica Nanopartikeln zur Entfernung (unabsichtlich) aufgenommener Toxine vor. Kleine organische Moleküle können gut in den Mesoporen der Silica Nanopartikeln adsorbiert werden.[4] Um den Anforderungen eines detoxifizierenden Materials nachzukommen, wurde der Einfluss einiger ausgewählter Syntheseparameter auf die Morphologie der Materialien beobachtet. Drei verschiedene Morphologien mit unterschiedlicher Oberflächenbeschaffenheit wurden synthetisiert: 120 nm große Dendritische Mesoporöse Silica Nanopartikel mit einer Porengröße von 3.8 nm, 100 nm große Virus-like Silica Nanopartikel mit einer breiten Porengrößenverteilung und 170 nm lange Nanorods Silica Nanopartikeln mit einem Seitenverhältnis von 2.3 und einer Porengröße von 3.2 nm. Um die Wechselwirkungen mit den Toxinen zu erhöhen und kolloidale Stabilität zu erzielen, wurden die Partikel mit folgenden funktionellen Gruppen ausgestattet: Phosphonaten, Epoxiden und Polyethylenglykolen. Die Adsorptionskapazitäten resultierender Partikel wurden anhand von Paracetamol untersucht, das hier als Modell für Toxine dient. Aus den Ergebnissen der Adsorbtionsstudien in Ethanol ist ersichtlich, dass durch negativ geladenen Phosphonatgruppen funktionalisierte und nicht funktionalisierte Dendritische Mesoporöse Silica Nanopartikel die höchste Aufnahme an Paracetamol erreicht wurde. Erste Adsorptionsstudien in simulierenden Magen- und Darmfluiden wurden ebenfalls im Zuge dieser Masterarbeit bearbeitet. Mit vorliegenden ersten Studien zeigen wir die Möglichkeit, Silica-basierte Nanopartikel als orale Entferner von Toxinen anzuwenden.

List of Tables, Schemes and Figures

List of abbreviations

BET	Brunauer-Emmett-Teller theory
CP/MAS	Cross-Polarization/Magic-Angle-Spinning
CTAB	Cetyltrimethylammonium bromide
DLS	Dynamic Light Scattering
DMSN	Dendritic mesoporous silica nanoparticles
eq.	Equivalents
FC4	Sodium heptafluorobutyrate
GIT	Gastrointestinal tract
h_D	Hydrodynamic diameter
MOFs	Metal-organic frameworks
MSN(s)	Mesoporous silica nanoparticle(s)
MSN_epox	Epoxide-grafted mesoporous silica nanoparticles
MSN_PEG	Polyethylene glycol-grafted mesoporous silica nanoparticles
MSN_PO_3	Phosphonate-grafted mesoporous silica nanoparticles
NAPQI	N-acetyl-p-benzoquinoneimine
NLDFT	Non-Local Density Functional Theory
NrNPs	Nanorods nanoparticles
NS	Nanospheres (from Li *et al.* (2015)[5])
NSR	Nanoparticles short rods (from Li *et al.* (2015)[5])
NLR	Nanoparticles long rods (from Li *et al.* (2015)[5])
Parac	Paracetamol-adsorbed
PEG	Polyethylene glycol
Physmix	Physical mixture
PO_3	Phosphonate
PXRD	Powdered X-Ray Diffraction
rt	Room temperature
SEM	Scanning Electron Microscope
SGF	Simulated gastric fluid
SIF	Simulated intestinal fluid
ssNMR	Solid-State Nuclear Magnetic Resonance Spectroscopy
TEM	Transmission Electron Microscopy
TEOA	Triethanolamine
TEOS	Tetraethyl orthosilicate
TGA	Thermogravimetric Analyses
THMP	3-(Trihydroxysilyl)propyl methylphosphate
VINPs	Virus-like silica nanoparticles

Table of Contents

1 Introduction

Intoxication cases through oral intake of a wide palette of substances have been found throughout all age groups in the last years. Due to the significant health problems and mortality rates, exposure to harmful substances has led to worldwide awareness.[1,2,6]

The term “poisoning” was defined by Uges (2001)[6] as “(…) medical or social unacceptable condition as a consequence of being under influence of an exogenous substance in a dose too high for the person concerned”[6], including the historical statement of Paracelsus in 1574 “(…) and nothing is without poison; but the dose makes it clear that a thing is not a poison”[7] who postulated the toxicity depends on the concentration of the substance. As the terms “poisoning” and “intoxication” were either differentiated or used indistinguishable in former literature[6], in this thesis the terms will be treated as synonyms for simplicity.

Most common intoxication cases happen due to exposure to household products, drugs, alcohol, pesticides and poisonous food.[8] Especially children are affected by the risk of poisoning through cleaning products and other chemicals found in households.[9] Common mistakes leading to accidental exposure to cleaning products are incorrect storage in regular drinking bottles and in the reach of children. In the case of adults, unintentional poisoning caused by cleaning products usually happens due to incorrect use.[10] Similarly, incorrect storage is also the reason for ethanol and drug/medicine poisoning in children.[11] In the case of adults, the main cause of acute ethanol poisoning is unintentional overdose. Acute poisonings caused by antidepressants and illegal substances are in most cases a consequence of drug abuse. The main motives are often suicidal purposes.[8] Analgesics are the most frequent causes of intoxication related to medical products.[9] One common pain killer, paracetamol, often causes life-threatening incidences due to long latencies after overdose intake. Thus, poisoning could be easily overseen until symptoms of non-reversible organ damage appear.[8,12] Similarly, long latencies can also be found for poisonings caused by some mushroom species.[8] In contrast to mushrooms with shorter latencies, which usually lead to less severe gastrointestinal syndromes, long latencies mushroom poisonings can be life-threatening. Exposure to poisonous mushrooms usually happens due to confusion with eatable species or the abuse as psychoactive substances.[13] Other food-related intoxication cases include scombroid poisoning from fish, correlating with elevated histamine levels. Thus, this is also categorized as an allergy-inducing form of poisoning.[14,15] Poisoning caused by pesticides was observed more frequently in the past.[8] A common group of pesticides associated with intoxication are organophosphates. In developing countries, organophosphates still cause numerous annual deaths despite the declining use of this substance.[16] However, organophosphates are easily accessible in these locations. Thus, intended self-harm with pesticides is tremendously more common than accidental exposure.[2]

Organophosphate poisoning has also been associated with warfare in terrorist organizations. Thus, these substances are still a threat to the whole world and reliable therapy routes need to be on hand to ensure safety.[17]

Exposure to the above-listed poisonous substances often happens through oral ingestion[10]. Thus, the gastrointestinal tract (GIT) is the first location for detoxification to stop the toxin from further distribution in the human body. For the treatment of intoxication, the use of nanotechnology was proposed. Materials suitable for medical applications with high adsorption capacities, biocompatibility and stability need to be designed via a facile and reproducible synthesis procedure.[18] In this thesis, mesoporous silica nanoparticles (MSNs) were suggested as oral nano-detoxifiers. Due to numerous oral application studies in the GIT[19–22], we expect MSNs to be suitable candidates for toxin adsorption and to prevent further long-lasting damage. It is important to investigate the following parts for a full detoxification study: the synthesis and design of suitable nano-detoxifiers, adsorption and release for proper confinement of the toxin, cell studies to investigate biocompatibility and protein corona formation to evaluate the influence of GIT fluids on the nano-detoxifiers. In addition to the regular detoxification route, strategies in the selective removal of metabolites from commercially available drugs could be applied. Herein, paracetamol and related toxic metabolites acetaminophen glucuronide and acetaminophen sulfate would be suitable models.

2 State of the Art

Intoxication cases can be distinguished between accidental exposure and intentional self-poisoning.[1,2] In 2020, 3.5 deaths per 100.000 male inhabitants and 1.1 deaths per 100.000 female inhabitants were caused by unintentional exposure to poisonous substances in the European Union. At the same time, intoxication deaths in Austria were below the European Union average. Solely 0.4 deaths per 100.000 male Austrian inhabitants and 0.3 per 100.000 female Austrian inhabitants were ascribed to accidental poisoning.[23,24] As reported by Statistik Austria (2023)[25], the category "injuries and intoxications" was the cause of 50-60 deaths per 100.000 Austrian inhabitants between 2018-2022. Noticeably, unintentional self-poisoning of children is pronounced in Austria. Every year 800 children under the age of fifteen are hospitalized due to intoxication. A quarter of these injuries were caused by exposure to medicine and bioactive substances, usually in households. About 40 % of intoxicated and hospitalized children are under five years old. These immense numbers can be explained by children's undeveloped awareness of dangerous situations. Especially colored substances in regular households, such as cleaning products, arouse their interest and they cannot fully evaluate the danger behind these products yet.[26] On the contrary, majorities of intentional self-poisonings is committed by the middle-aged Austrian inhabitant. Self-intoxication was the third most common procedure for suicide in 2023. In the last years, suicide deaths caused by poisoning increased significantly. In 2023, 13 % of suicides were ascribed to intoxication whereas in 2022 it was only 7 %.[27] As reported injuries and deaths could be preventable, we need reliable intoxication treatments.

2.1 Conventional Detoxification Routes

As outlined in the Introduction, poisonous substances follow the oral ingestion route in most cases.[28] In the medical field, generally applied methods for the removal of toxins list the use of antidotes. Antidotes work as counteragents against the consequences of toxin or drug exposure.[29,30] Ascribed to their selectivity, antidotes only exist for less than 2 % of toxic substances.[3,30] Four different mechanisms in antidote detoxification can be distinguished: **First**, the antidote directly captures the toxic substance via adsorption or chemical bond formation. One popular example is activated carbon, which is based on adsorption.[30,31] As this method can also be classified as a non-specific treatment, the administration of activated carbon will be described later. For the treatment of heavy metal poisoning, chemical binding via chelation is a commonly used procedure.[32] The **second mechanism** is either blocking

specific receptors or inhibiting enzymes with the antidotes to avoid the interaction with toxins and subsequent harmful consequences. An established method is the inhibition of alcohol dehydrogenase via the antidote “ethanol” in the case of methanol exposition.[33,34] The **third mechanism** of antidotes is the elimination of toxic metabolites. Metabolites usually originate from common nontoxic substances and drugs. One example is *N*-acetyl-p-benzoquinoneimine (NAPQI) from paracetamol, which will be further outlined in Chapter 2.4.4. Here, antidote *N*-acetylcysteine is commonly applied to selectively target the metabolite.[35,36] The **fourth mechanism** would be the use of antidotes directly against the toxic consequences of poisonous substances. A common example is the application of the antagonist vitamin K after warfarin overdose.[30,37] Although antidotes offer a suitable treatment against intoxication, they only work against a limited concentration of poisonous substances. If exposed to higher amounts, antidotes cannot be applied alone but rather as an additional tool in therapy. Additionally, the toxicity and side effects of the antidotes themselves should not be overlooked. The risks associated with the antidote as a substance should always be considered before its application in therapy.[30] Thus, the development of safer and more reliable nontoxic detoxifiers is crucial.

Enteric decontamination lists gastric lavage and induced vomiting.[28] However, they are not recommended anymore.[38,39] These treatments are associated with the rapid removal of toxins within a short time after ingestion. Due to the high risks of damaging the patient's aspiration system or perforation of the stomach, these methods are not employed in the medical field.[28,40] Ingested acidic and alkaline substances, such as cleaning products, even carry additional risks if these physical treatments are applied. Irritation of the esophagus and respiratory system due to repeated contact with the corrosive substances could increase severity and lead to longer recovery times.[28,39]

Another relevant method is the application of activated charcoal. Activated charcoal is less invasive and the administration is safer for the patient.[8] The application is based on the adsorption of toxins in the GIT. It should be orally administered within 1 h after toxic ingestion.[41] The consciousness of the intoxicated patient is mandatory for this treatment and the respiratory system needs to be secured during administration.[42] However, the application of activated charcoal is only limited to selected toxins.[3,42] It cannot be used for detoxification of metal toxins or acidic, alkaline and organic solvents. Another disadvantage of activated charcoal is the non-selective adsorption. Various substances would also be removed, including drugs that would be beneficial for the patient. Thus, activated charcoal cannot be combined with other antidotes, as they would be either removed or even compete with the real toxins for adsorption sites.[31,42] We hereby emphasize the necessity for designing more reliable materials that could be adjusted to higher selectivity towards the target.

Extracorporeally performed hemodialysis is another common method for toxin removal. It is applied to small, hydrophilic molecules, such as methanol. In contrast to the use of antidotes, hemodialysis is employed if the toxin already caused damage to

the acid-base balance of the bloodstream.[8,43] However, this procedure is limited to the removal of small molecules only. It can only be applied if the intoxication already led to distribution in the bloodstream. If early treatment after ingestion is needed, above mentioned oral procedures are recommended.[8] Additionally, oral administration is more attractive for both, patients and medical professionals due to its convenient application and absence of needle-associated pain.[44,45] Thus, in the course of this project we focused on oral detoxification solutions only.

2.2 The Gastrointestinal Tract: The Location of Detoxification

The first contact of ingested toxins with the human body is located in the GIT, as outlined in the Introduction.[28,45] Esophagus, stomach, small intestines and colon are the organs composing the GIT, illustrated in Figure 1A. For ingested substances, the first stop would be the esophagus. This organ is not significantly affected by ingested toxins due to the rapid transit through the throat.[45–47] Thus, further focus will be laid on the other parts of the GIT.

The average retention time of the stomach is 1 h. Thus, this organ is the first relevant location of the GIT after toxin ingestion. Here, detoxifiers are prone to degradation due to the harsh conditions, established by low pH 1-4 and digestive enzymes, as listed in Figure 1B. On the contrary, a beneficial aspect of the stomach is the mucus layer. Located above the epithelial cells (Figure 1C), the mucus layer blocks detoxifiers and toxins from being transported to the bloodstream.[45,47] The mucus layer of the stomach and the colon is made up of two layers, whereas the outer layer blocks toxins and detoxifiers from epithelium penetration. However, the small intestines are built up by one mucus layer only.[18,48,49] As the mucus layer of the stomach is thicker compared to the small intestines, the transport of toxins and detoxifiers into the bloodstream could be easier prevented in this location.[45,47]

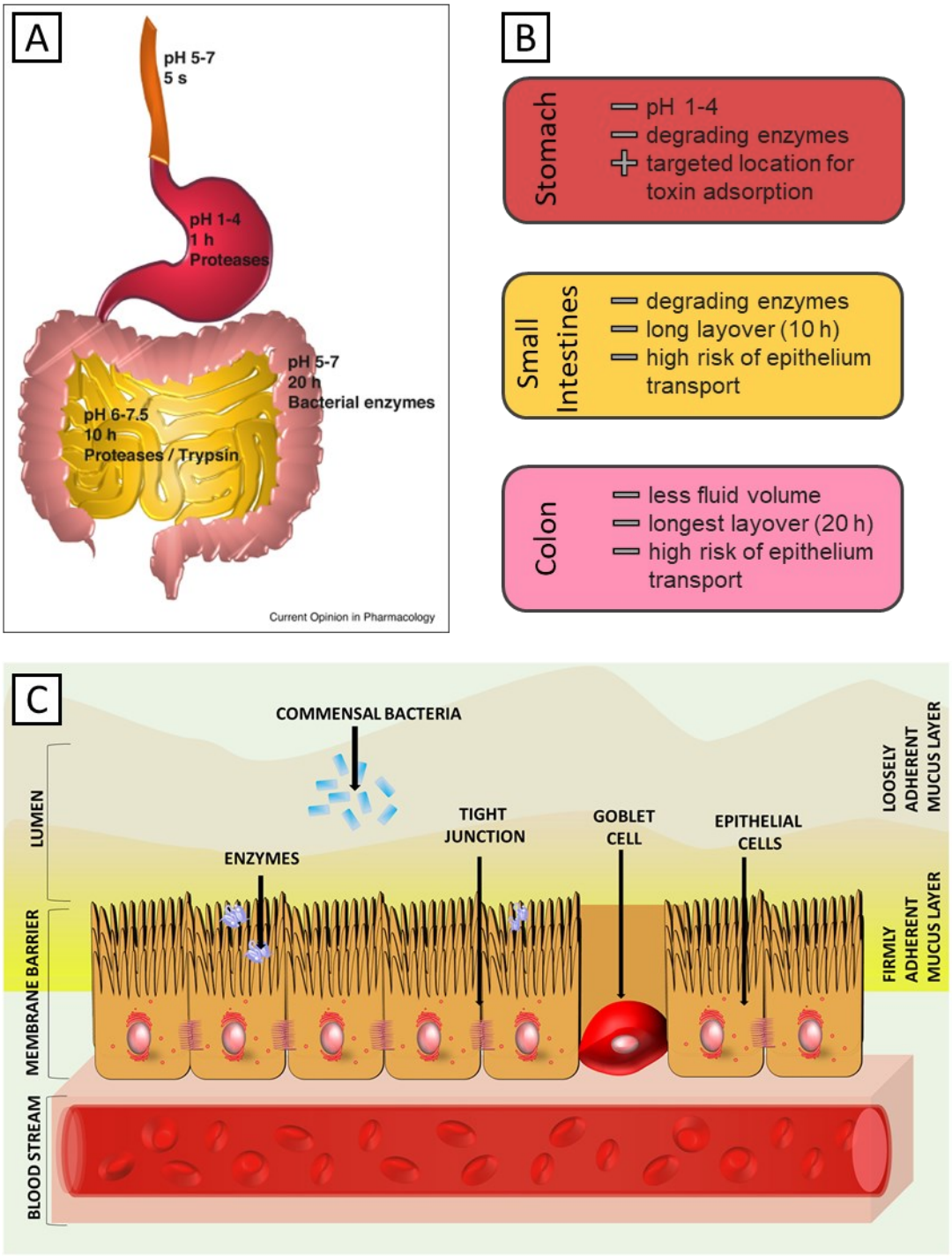

Figure 1. Schematic overview of GIT and epithelium with corresponding properties. Scheme A shows the retention time and environment of the components of the GIT. From top to bottom: Esophagus is displayed in orange, stomach in red, small intestine in yellow and colon in pink. Figure A reprinted with permission from Caffarel-Salvador *et al.* (2017)[47], Copyright (2017) Elsevier. Figure B gives an overview of the barriers for detoxifiers in the organs and marks the locations of toxin adsorption. Figure C displays a scheme of the epithelium of the GIT. Toxins and detoxifiers trespassing will be withheld by the mucus layer from the epithelial cells. Toxic substances passing through the mucus layer and the epithelial cells can be absorbed into the bloodstream and further distributed. Figure C reprinted with permission from Abeer *et al.* (2020)[19], Copyright (2020) Elsevier.

After the delay in the stomach, detoxifiers would transfer towards the small intestine. At this location, conditions are less harsh due to a neutral pH of 6-7.5.[47] However, with the presence of digestive enzymes, degradation of detoxifiers is still a risk.[50] The small intestine is commonly the targeted location for oral drug delivery approaches.[19,51,52] Thus, in detoxification studies this area should be treated with special precaution. Ingested detoxifiers face average retention times of 10 h (Figure 1A and B), being the longest layover in the GIT so far.[47] Therefore, the risk of epithelium transport of toxins and detoxifiers is significantly increased here. For drug delivery, the mucus layer of the small intestines is considered a barrier.[19] However, in detoxification the mucus layer can be seen as a beneficial barrier for unwanted transport towards the bloodstream. The epithelial cells provide an additional barrier. Selected substances can permeate the epithelial cells either directly or through the tight junctions, located in between two cells as illustrated in Figure 1C.[45,53] These pathways exhibit a risk for unintentional transport of toxins and detoxifiers and must be avoided. Thus, toxins should be safely excreted from the body without further distribution in locations other than the organs of the GIT.[54]

Before excretion, detoxifiers transfer to the last stop of the GIT, the colon (Figure 1A). Compared to the other layovers, fewer digestive enzymes occupy the colon at a neutral pH of 5-7. The detoxifiers will be forced to stay for an average retention period of 20 h. Thus, the risk of unwanted epithelium transport is still present at this location.[45]

To summarize, suitable detoxifiers resisting unwanted epithelium transport and degradation are needed.[45,53] Additionally, excellent toxin adsorption in the GIT is essential. The ideal organ for toxin adsorption would be the stomach. Thus, the risk of transport of toxins towards the bloodstream in the following organ, the small intestines, would be significantly limited. For detoxifiers, main barriers are the acidic conditions of the stomach and the presence of degrading enzymes in all organs of the GIT.[47,50] Plus, epithelium transport of the toxin-adsorbed detoxifying material must not be overseen here.[19] As this pathway could lead to further distribution of the toxin in the body,[54] a strategy for safe excretion is mandatory for detoxifiers and toxins.

2.3 Nanotechnology for Detoxification

The use of nanotechnology for biological applications has gained interest in the last few years. Outstanding high surface areas, the possibility for targeted application at the affected area and stability of nanosized materials have led to excellent performances compared to conventional therapeutics.[18,55,56] Thus, the application of nanomaterials for detoxification routes is interesting. Depending on the type of nanomaterials, different strategies have been reported for detoxification routes before:[57] nano-conjugation of heavy metals with subsequent excretion[58,59], simulating toxin-metabolism with nanomaterials[3,57], stabilization of toxin-degrading enzymes via nanomaterials[60], surface-adsorption of toxins with subsequent excretion[61] and adsorption of toxins inside the material[54].

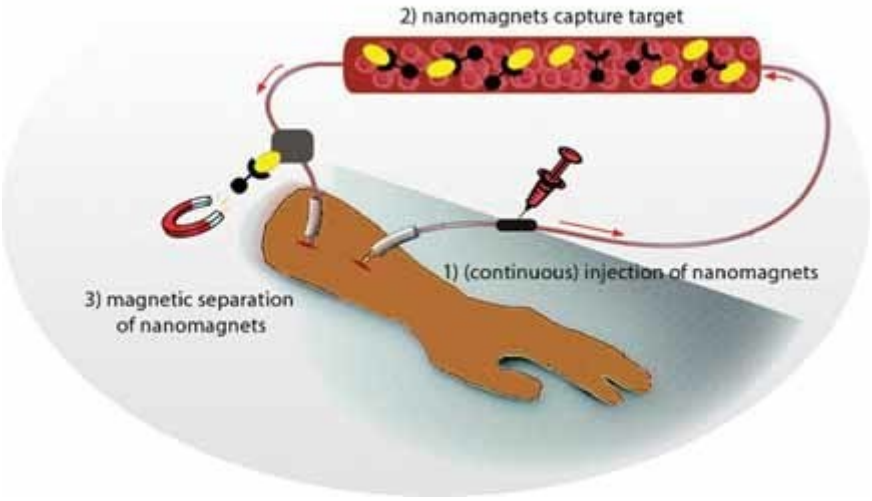

Figure 2. Intravenous pathway of heavy metal-based toxin removal via nano-conjugation as proposed by Herrmann *et al.* (2010)[62]. After injection of functionalized core-shell nano-magnets, the chelators will capture heavy metal toxins in the bloodstream. The nanomaterials will be removed together with the toxins via magnetic separation. Figure reprinted with permission from Herrmann *et al.* (2010)[62], Copyright (2010) Wiley-VCH Verlag GmbH & Co. KGaA.

Comenge *et al.* (2012)[58] presented a gold nanoparticle system based on nano-conjugation. With a pH-sensitive coordinative bond to cisplatin, specific release at the targeted location was enabled. Thus, toxic cisplatin distribution in other vulnerable organs was prevented. Hu *et al.* (2012)[59] used another nano-conjugation strategy for the detoxification of mercury via nano-aptamers. For oral lead detoxification, Lestari *et al.* (2023)[63] designed ethylenediaminetetraacetic acid functionalized metal-organic frameworks (MOFs) MIL-100(Fe). Due to high porosity and stability in GIT conditions, this material showed promising adsorption rates.

Similarly, Herrmann *et al.* (2010)[62] designed core-shell magnets functionalized with chelators for lead extraction. They proposed intravenous injection of nano-magnets for toxin adsorption with subsequent removal of the conjugated nanomaterials by magnetic separation, as illustrated in Figure 2.

Another nano-detoxification strategy was the bio-inspired reduction of toxic metabolites. During phase Ⅰ drug metabolism, toxic metabolites are formed via oxidation.[3,64] Graham *et al.* (2011)[3] proposed the design of silica nanotubes with inner surface functionalization with reducing agents. When toxic metabolites diffuse through silica nanotubes, they will be reduced to nontoxic substances at this location. A second strategy proposed by the same authors was the functionalization with glutathione. The idea was to simulate phase Ⅱ metabolism.[64] Thus, toxic structures with thiol groups could be successfully targeted via thiol bond formation.[3] These bio-inspired strategies were investigated by Xu *et al.* (2014)[65] who successfully rendered toxic organophosphorus compounds to safer dimethyl phosphate via MSNs.

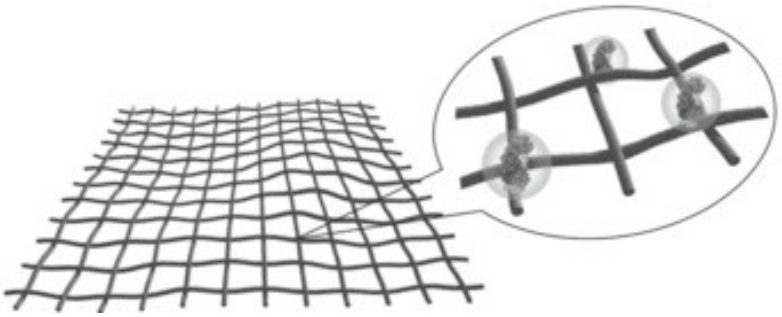

Figure 3. Schematic illustration of nano-capsules with incorporated enzyme "organophosphorus hydrolase" designed by Wei *et al.* (2013)[60]. Due to the fixation in the nano-capsules matrix, the activity and stability of the enzymes were significantly increased. Thus, the enzymatic detoxification of organophosphorus was possible. Figure adapted with permission from Wei *et al.* (2013)[60], Copyright (2013) Wiley-VCH Verlag GmbH & Co. KGaA, modification: exclusion of sub-Figures.

A formerly mentioned strategy was the stabilization of toxin-degrading enzymes via nano-capsules. Wei *et al.* (2013)[60] synthesized nano-capsules incorporated with the enzyme "organophosphorus hydrolase". These nanomaterials are illustrated in Figure 3. Although being antidotes of organophosphorus, these enzymes lack stability and cannot be applied alone or via adsorbance-based drug delivery routes. However, incorporated in nano-capsules, the activity and stability of the enzymes were significantly increased leading to enhanced performances.[57]

Adsorbance of toxins could be either performed by interaction with the outer or inner surface of nanomaterials. However, endogenous proteins may compete with toxins for the active, easily accessible adsorption sites on the outer surfaces.[57,61] For example, Howell *et al.* (2008)[61] reported difficulties in their liposomal systems for amitriptyline overdose due to protein corona formation. They suggested further development to increase the selective uptake of toxins. One way of addressing this problem is going towards inner surface adsorption. Although the formation of a protein corona could still present steric hindrance against the diffusion of the toxin inside the material[3], the toxin-protein competition for active adsorption sites could be significantly reduced.[66] Thus, more adsorption sites would be accessible for targeted toxins.

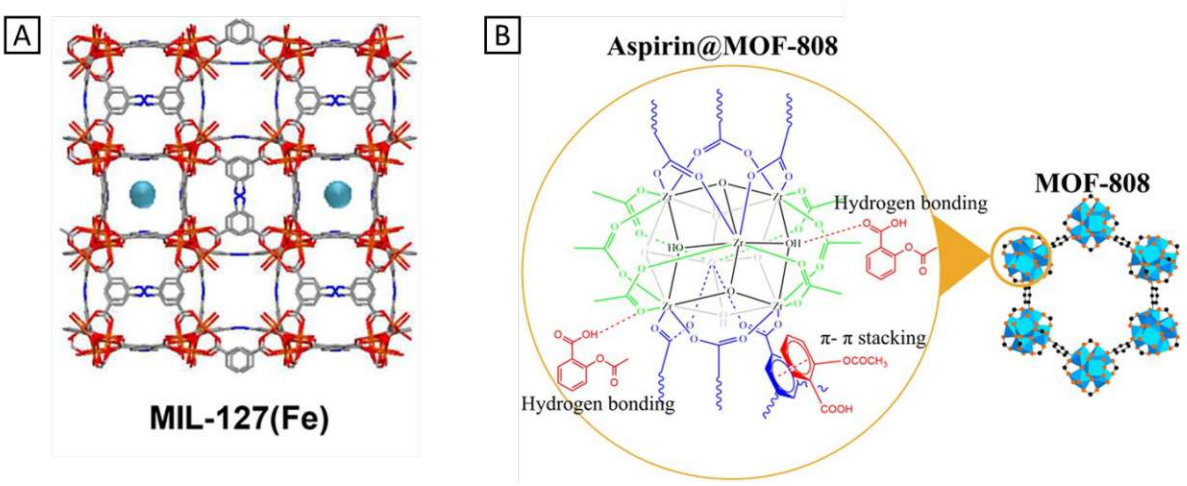

Figure 4. Schematic illustration of aspirin-adsorbing MOFs from reported studies. Figure A shows the schematic structure of MIL-127(Fe) with adsorbed aspirin (blue spheres) inside the pores from the studies of Rojas *et al.* (2018)[54]. Figure A was adapted with permission from Rojas *et al*. (2018)[54], Copyright (2018) ACS, modification: exclusion of sub-Figures. This is an unofficial adaptation of an article that appeared in an ACS publication. ACS has not endorsed the content of this adaptation or the context of its use. Figure B is the schematic illustration of aspirin- (red structure) adsorbed MOF-808 from Pangestu *et al.* (2022)[67]. Physical interactions between aspirin and the MOF's structure are labeled. Figure B was adapted with permission from Pangestu *et al.* (2022)[67], Copyright (2022) Springer Nature, modification: exclusion of sub-Figures.

So far, a bigger focus has been laid on intravenous detoxification routes via nanocarriers and proof of concept studies.[3,57,68–70] On the contrary, oral detoxification routes have only been investigated in a few cases yet. One of the alternatives includes the application of iron- and titanium-based MOFs for detoxification studies on aspirin conducted by Rojas *et al.* in 2018[54], as illustrated in Figure 4A, and by the same author in 2019[71]. Compared to other materials, iron-based MOFs MIL-127(Fe) showed good biocompatibility for biological applications, high porosity for enhanced adsorbance rates and stability in GIT conditions. The authors reported a significant decrease in the uptake of aspirin in the bloodstream after the incorporation of MOFs as adsorbents.[54]

Aside from the reported proof of concept studies by other authors, Rojas *et al.* (2019)[71] investigated the biodistribution of oral detoxifying titanium-based MOFs MIL-125-NH_2 in their follow-up work. The authors reported safe administration of the designed nano-detoxifiers, stability in GIT conditions, excellent aspirin adsorption abilities and reliable excretion. Similarly, Pangestu *et al.* (2022)[67] reported inner surface adsorption of aspirin onto MOF-808 for detoxification. Due to the proposed combination of hydrogen binding and π-π stacking (Figure 4B), the material showed sufficient aspirin adsorption.

Detoxification of paracetamol via titanate nanotubes was proposed in a recent publication by Salek *et al.* (2023)[72]. They presented an oral process, based on the toxin adsorption in intestinal conditions. Higher *in vivo* paracetamol adsorption capacities were achieved compared to activated charcoal. Thus, further studies on nano-detoxifiers could revolutionize the oral intoxication field.

Oral detoxification is located in the GIT.[28,45] As MSNs have been extensively studied for oral drug delivery applications in the past,[19,20] using these materials in nano-detoxification is promising. In contrast to drug delivery, the toxins will be adsorbed inside the GIT and not before drug administration. One former application of MSNs for detoxification was already reported in this Chapter. Not only do MSNs present excellent surface adsorption potential and bio-safety, but this material can also be combined with reducing agents or glutathione functionalities to simulate phases Ⅰ and Ⅱ of body drug metabolism.[3] Thus, MSNs provide high potential for prospects in the detoxification field and will be outlined in the following Chapter 2.4.

2.4 Mesoporous Silica Nanoparticles

MSNs in biological applications have been studied for years. Focusing on drug delivery systems, the medical performance of MSNs has been investigated in numerous studies.[73–75] The advantages of MSNs include easy availability, producibility, colloidal and thermal stability.[76] The prominent mesoporous framework is another reason for the gained interest in MSNs. These highly porous materials possess outstandingly high surface areas. The predominant structures provide excellent storage abilities for small organic molecules.[77] The tunability of morphology, size, porosity and surface functionalization enables the customization of MSNs towards the desired application.[78–80] Complex post-synthesis adaptations of therapeutics involving multiple steps face limitations in real-life applications. If further modification and development of an already complex material is necessary, it would get increasingly tedious.[45,81] Thus, easy synthesis and customization of MSNs provide a suitable basis for biological applications.

2.4.1 Safety of MSNs: Morphology, Size and Surface Chemistry

Biocompatibility of MSNs was confirmed by the Food and Drug Administration[82]. If the properties are well-tuned to the desired application, suitable performance in biological systems is enabled for MSNs. Following parameters have significant influence on the safety and applicability of MSNs for detoxification: particle morphology, size and surface chemistry.[18,83,84] Thus, these properties will be outlined in this Chapter.

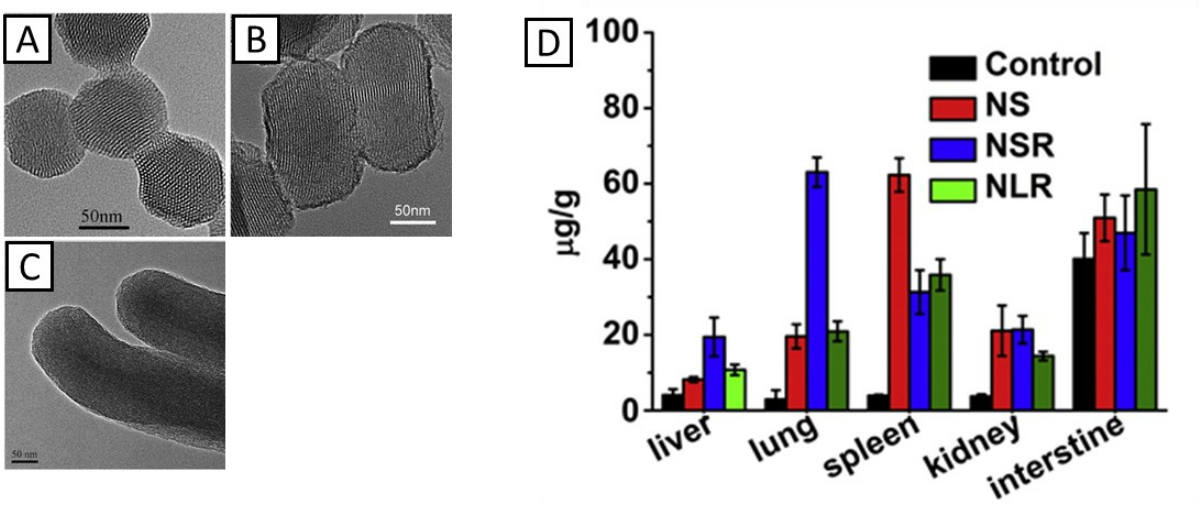

Figure 5. Figures from distribution studies of MSNs of Li *et al.* (2015)[5] depending on the morphology. TEM images (left) of mesoporous silica nanospheres (Figure A, NS), short rods (Figure B, NSR, aspect ratio 1.75) and long rods (Figure C, NLR, aspect ratio 5). Figure D gives an overview of the biodistribution studies of different morphologies in liver, lung, spleen, kidney and intestine after 2 h oral administration. Apart from the intestinal system, higher amounts of nanospheres were also found in the spleen and short nanorods in the lung. Figures adapted with permission from Li *et al.* (2015), Copyright (2015) Elsevier[5]; modification: sequence of Figures A-C and exclusion of sub-Figures.

Li *et al.* (2015)[5] investigated the toxicity of MSNs of different morphologies after oral administration. Transmission Electron Microscopy (TEM) images and results of these studies are shown in Figure 5. Spherical and nanorods-shaped MSNs were monitored in terms of acute toxicity, biodistribution and excretion. Three different morphologies of about 85 nm were investigated: spherical MSNs (Figure 5A), short rods (Figure 5B, aspect ratio 1.75) and long rods (Figure 5C, aspect ratio 5). After biodistribution analysis of the different morphologies, all three types were present in the intestines in a high quantity after 2 h administration (Figure 5D), as expected. However, considerable amounts of spherical MSNs and short nanorods accumulated in the spleen and lungs due to distribution by the bloodstream. Rods with a higher aspect ratio were predominantly found in the intestine only, as illustrated in green bars in Figure 5D. The authors showed the retention time for long rods in the intestines was enhanced compared to other morphologies. These findings were ascribed to

decreased epithelium transport and slower degradation for this morphology. Similarly, studies by Hao *et al.* (2012)[85] confirmed these observations. However, other publications reported enhanced epithelium transport of nanorods due to easier penetration of the mucus.[86,87] The reason for these opposed findings might be found in the studies' duration. Therefore, morphology has a considerable influence on the distribution in other organs apart from GIT. As the organs of the GIT are our targeted positions for oral detoxification, the use of different morphologies of MSNs could give insightful information. Hence, one focus of this project was on the design of different morphologies for the application as silica-based oral nano-detoxifiers.

In addition to the morphology, the size of MSNs influences epithelium transport in biological applications. Farjadian *et al.* (2015)[88] investigated the application of MCM-41, a previously studied silica-based material, as an adsorbent for paracetamol. Adsorption rates were found to be enhanced for this material compared to activated carbon. However, applied MSNs were smaller than 50 nm. Former studies highlighted a lower particle diameter (<100 nm) has led to enhanced epithelium transport.[75,89,90] Therefore, it is striving to design MSNs big enough not to cross the epithelium toward the bloodstream.[54] Hence, synthesizing MSNs with particle sizes ≥ 100 nm was intended in this project.

Functional groups were applied to alter the surface chemistry of MSNs.[91] The surface charge influences interparticle repulsion and performances of designed MSNs.[75] Cationic MSNs are more prone to degradation as they interact strongly with endogenous proteins, leading to the formation of large protein coronas. Thus, negatively charged MSNs are preferred in the detoxification field. If the formation of surface-blocking protein corona could be hindered, the original size and porosity of prepared MSNs could be preserved. Colloidal stability would be maintained and a significantly higher amount of toxins could be captured due to the simplified diffusion.[18,92–95] With the preservation of colloidal stability, the formation of toxic MSNs aggregates would be reduced.[96] Thus, the toxicity of MSNs could be prevented by the incorporation of functional groups. Hereby, three different functional groups were implemented via post-synthesis functionalization: phosphonate (PO_3), epoxide and polyethylene glycol (PEG) groups. PO_3 groups are known to enhance the overall negative charge on MSNs. They conserve colloidal stability due to interparticle repulsion (Figure 6B) and provide biocompatibility.[75,97] The structure of this functional group exhibits hydrogen bonding positions[98] which enhance particle-toxin interactions as illustrated in Figure 6A. Epoxide groups were introduced for the possible formation of covalent bonds if the target exhibits negatively charged structural properties, enabling stronger attachment.[99] Another possibility is the formation of hydrogen bonding[100] to hydrogen donors of toxins (Figure 6A). The third biocompatible moiety PEG was applied to repel endogenous proteins as illustrated in Figure 6C.[101–103] Thus, the formation of a dense protein corona could be prevented, leading to higher toxin adsorption due to lower steric hindrance.

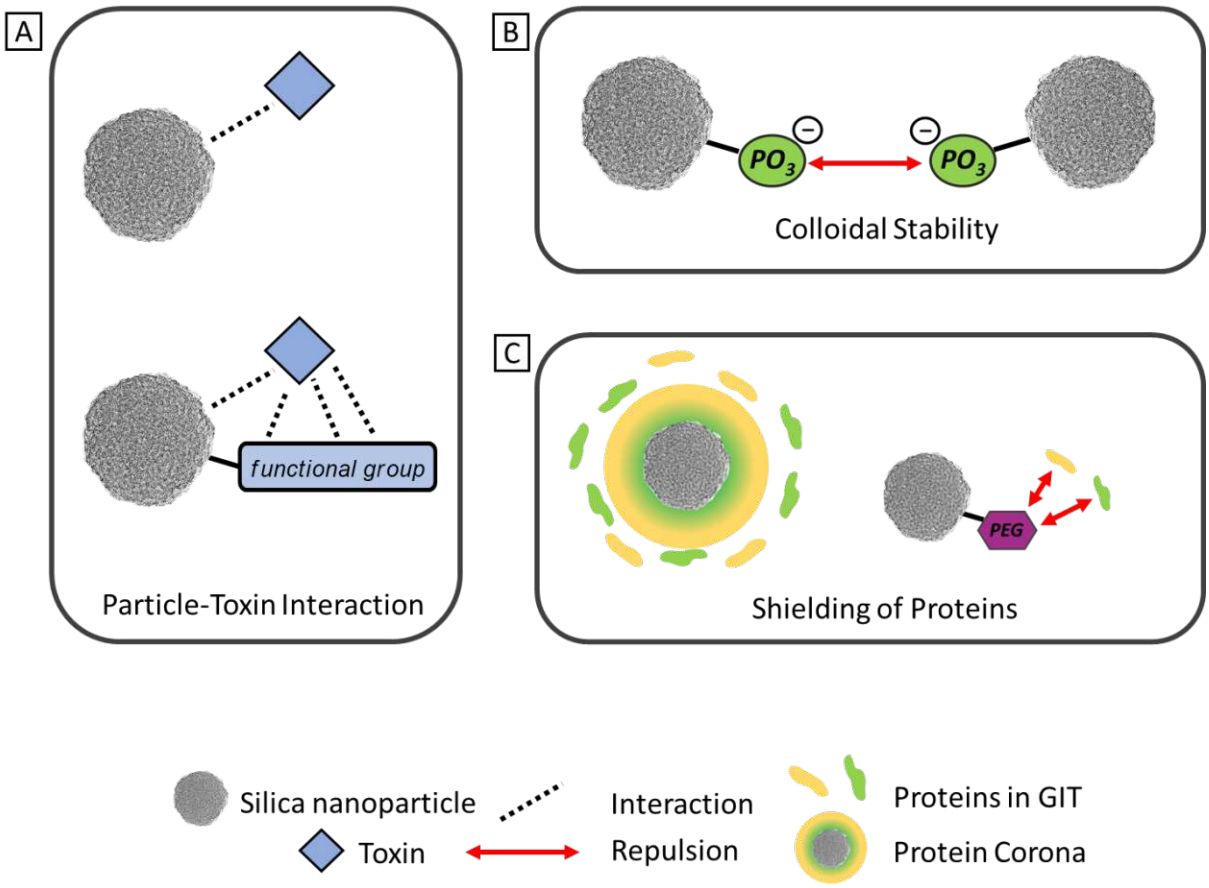

Figure 6. Schematic illustration of the benefits of functionalized MSNs. Figure A shows the enhanced toxin adsorption affinity of functionalized MSNs (bottom) compared to plain MSNs (top). Due to negatively charged PO_3 groups, interparticle repulsion prevents agglomeration and sustains colloidal stability as illustrated in Figure B. The prevention of protein corona formation by the introduction of PEG groups is shown in Figure C.

Although MSNs are considered safe, their incorporation in pre-clinical and clinical studies has been tremendously low so far. A major problem is one of the outstanding advantages of MSNs: the facile tunability. Due to the design of multitudes of MSNs shapes, all of them would need to be evaluated for cytotoxicity, biodistribution, degradation and performance. Only this way, the impact on the human body can be fully determined. Thus, this lack of data should always be considered and generalized properties should be striven for in the course of MSNs designs for medical applications.[18,104]

2.4.2 Synthesis Mechanism of Silica Nanoparticles

In 1968, Werner Stöber synthesized one of the first silica nanoparticles via a sol-gel route. As this method gave solid monodisperse particles in the nano range, the Stöber process gained in popularity and still serves as a basis for current synthesis approaches.[105] Afterwards, Unger *et al.* (1983)[106] reported one of the first drug delivery approaches with porous silica. Back then, this material was crude and not in the form of particles. With the implementation of ordered MSNs in the 1990s, higher surface areas for enhanced adsorption capacities were achieved.[18,107–109] With this, the control of further properties of MSNs started. The tunability of size and functionality to design suitable silica particles for controlled drug delivery was later shown by Lai *et al.* (2003)[110].[18]

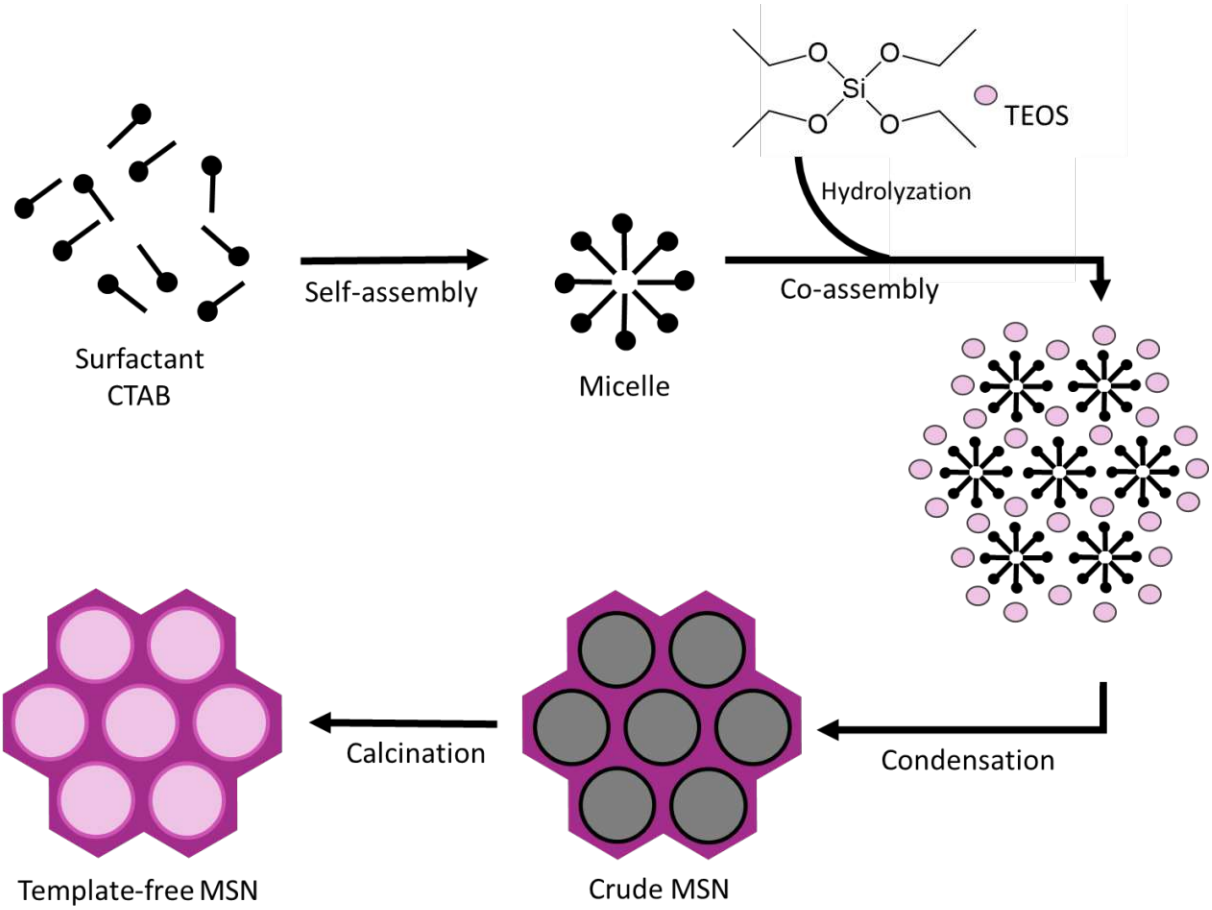

Figure 7. Scheme of MSN synthesis via micelle templating route. Micelles are formed by the self-assembly of surfactants. Together with hydrolyzed TEOS molecules, micelles co-assemble into a template defining the shape of the final product. By the condensation of TEOS, crude MSNs in the final morphology are formed. After template removal, plain MSNs (bottom left, dark violet) with mesopores (light violet) are obtained. Figure created by the author of this thesis, based on Nam *et al.* (2018)[111].

To this date, one common alteration of the Stöber process, the micelle templating route as illustrated in Figure 7, is a suitable, reliable method for the synthesis of MSNs.[112] Surfactants, e.g. Cetyltrimethylammonium bromide, in aqueous solutions self-assemble into micelles. Silica precursors, e.g. Tetraethyl orthosilicate (TEOS), hydrolyze in the presence of a catalyst (e.g. a base). Upon co-assembly of hydrolyzed TEOS with micelles, the formation of the template for the MSN structure takes place. Hydrolyzed TEOS condensates in this arrangement and forms solid, crude silica particles. After the removal of the template by calcination, plain, template-free MSNs are obtained.[107,113,114]

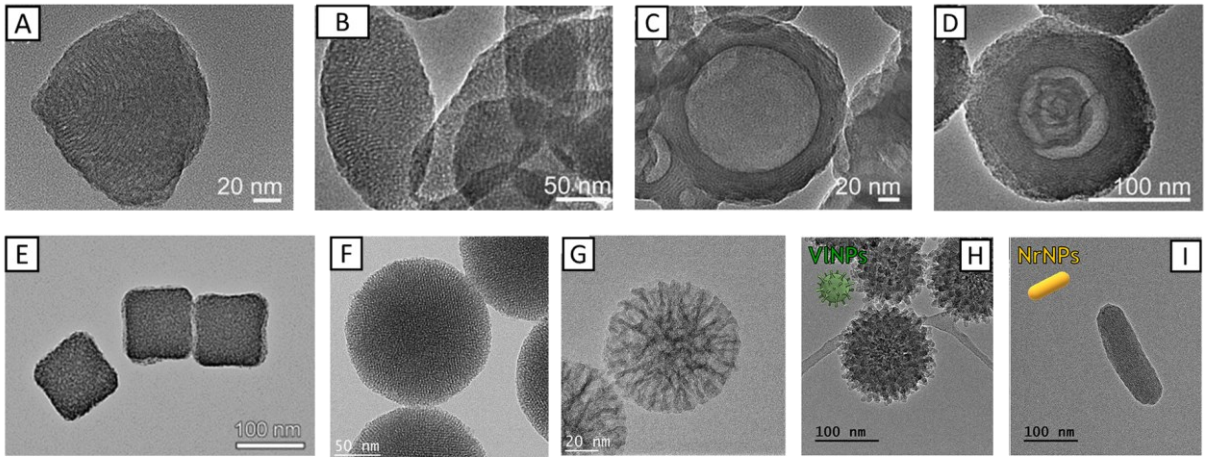

Figure 8. TEM images of selected previously reported morphologies of silica nanoparticles. Shell-like (A), rugby-like (B), hollow (C), yolk-shell (D), square (E), MCM-48 (F), dendritic (G), virus-like (H) and nanorods (I). Figures A-D adapted with permission from Han *et al.* (2013)[115], Copyright (2013) Springer Nature, modification: sequence of Figures and exclusion of sub-Figures. Figure E reprinted with permission from Li *et al.* (2007)[116], Copyright (2007) WILEY-VCH Verlag GmbH & Co. KGaA. Figures F and G adapted with permission from Juère *et al.* (2020)[21], Copyright (2020) Elsevier, modification: sequence of Figures and exclusion of sub-Figures. Figure H and I adapted with permission from Iriarte-Mesa *et al.* (2023)[52], Copyright (2023) ACS, modification: exclusion of sub-Figures. This is an unofficial adaptation of an article that appeared in an ACS publication. ACS has not endorsed the content of this adaptation or the context of its use.

Attempts of size- and morphology-controlled synthesis of MSNs have been reported previously.[86,117,118] One way of controlling the morphology outcome is the alteration of synthesis parameters such as catalyst type[119], temperature[115,120], precursor and surfactant concentration[115,117,120], reaction time[121] and stirring rate[122]. Another way is the less common hard templating synthesis procedure[116] which was not applied in the scope of this project. Various silica particle morphologies have been reported in the past: shell-like (Figure 8A), rugby-like (Figure 8B), hollow (Figure 8C) and yolk-shell[115] (Figure 8D), square[116] (Figure 8E), MCM-48 (Figure 8F) and dendritic[21] (Figure 8G), virus-like (Figure 8H) and nanorods[52] (Figure 8I), to mention a few.

However, aiming for specific structural properties is still a challenge. In this project, the synthesis of three different morphologies was investigated: Dendritic mesoporous silica nanoparticles (DMSN), virus-like silica nanoparticles (VlNPs) and nanorods nanoparticles (NrNPs). DMSN and NrNPs were synthesized by the application of the above-described micelle templating method. The generation of different aspect ratios could be achieved by the variation of synthesis parameters (e.g. triethanolamine acting as the base catalyst for spherical DMSN[120] and low precursor concentration for NrNPs[86]). The third morphology, VlNPs, was obtained by an extensive synthesis procedure, which is described in the following.

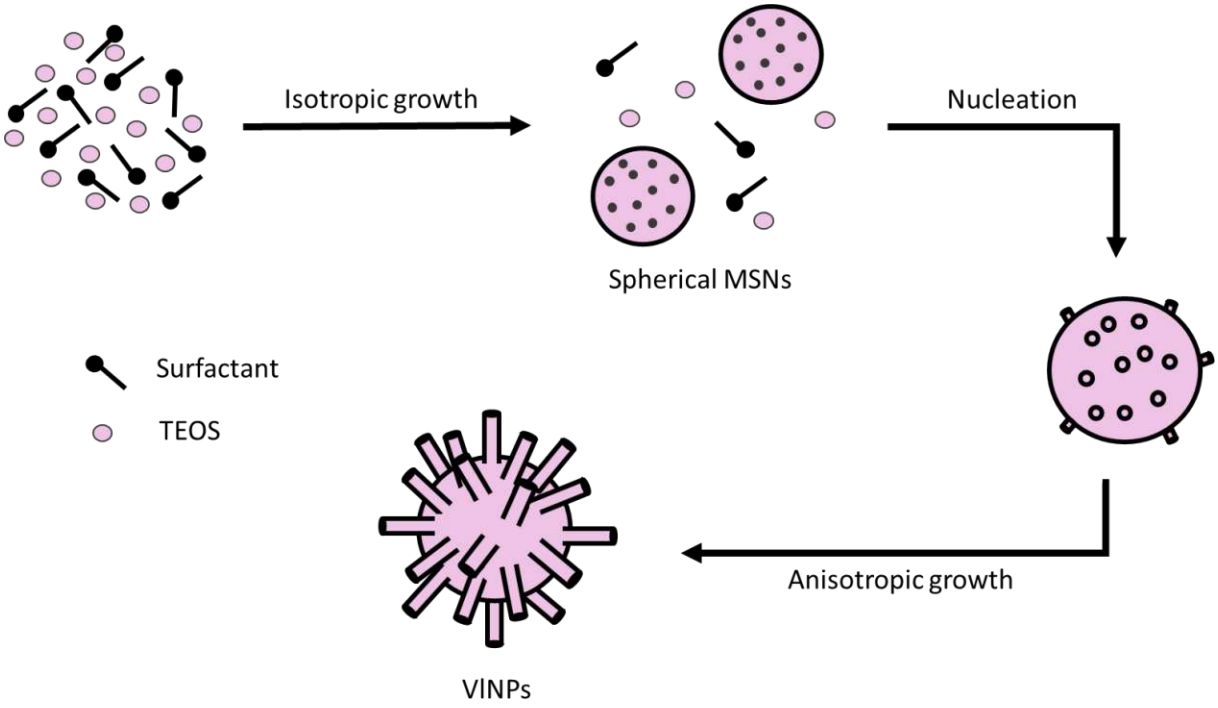

Figure 9. Formation of VlNPs by soft templating method. After simultaneous template formation by surfactants and condensation of hydrolyzed TEOS to oligomers, spherical MSNs are formed. Further condensation at lower precursor concentrations creates novel nucleation points. Subsequently, anisotropic growth of spikes on the surface results in VlNPs. Figure created by the author of this thesis, based on Wang *et al.* (2017)[121].

VlNPs are spherical MSNs with a rough, rod-like surface. Wang *et al.* (2017)[121] proposed a formation pathway of this morphology. The corresponding scheme is illustrated in Figure 9. Simultaneously with the self-assembly process of templating micelles, hydrolyzed TEOS would diffuse into the water/oil interface to form the template for the spherical MSNs. After further growth, the concentration of free surfactant and TEOS molecules decreases. Single TEOS molecules and pre-formed silica oligomers would be deposited on the surface and in the pores of the previously formed spherical particles. Upon their role as new nucleation sites, remaining precursors will be dictated to assemble into a rod-like formation. After further formation of the rough surface, virus-like morphology could finally be obtained.

Another important aspect of the synthesis of nano-detoxifiers is the ability to go towards industry scale. As this implementation is usually tedious in the field of nanotechnology[123], the possibility of up-scaling MSNs production needs to be evaluated.[18] Liu *et al.* (2021)[124] achieved an up-scaled synthesis protocol for porous silica nanoparticles. By lowering the ethanol content in the solvent, they accomplished cost reduction in production and additionally found the opportunity to change morphology through this route. They emphasized the importance of up-scaling ability for already existing MSNs shapes.

2.4.3 Examples of MSNs in Oral Applications

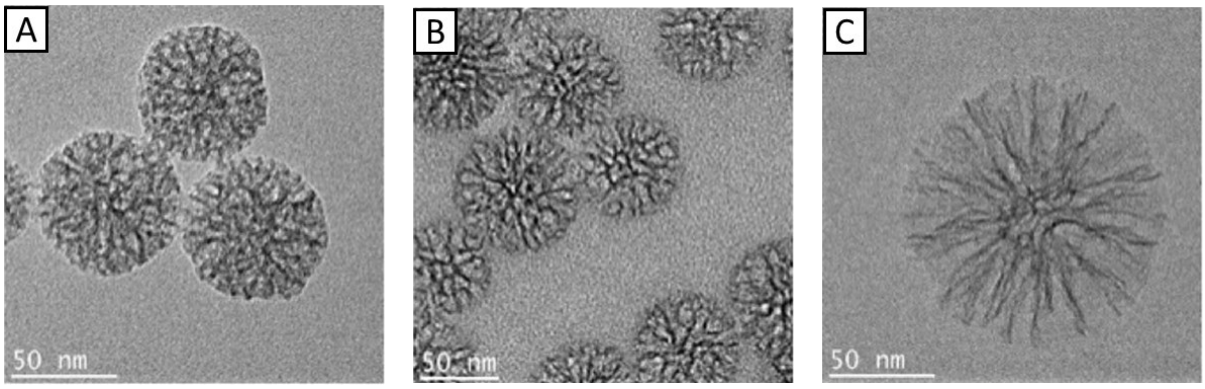

Figure 10. TEM images of DMSN from the oral insulin administration studies of Juère *et al.* (2020)[51]. Three synthesized DMSN types with altered pore sizes are shown: DMSN in Image A (pore size 7.6 nm) were synthesized with hexane, DMSN in Image B (pore size 8.4 nm) were synthesized with cyclohexane and DMSN in Image C (pore size 11.7 nm) were synthesized with toluene. Figures adapted with permission from Juère *et al.* (2020)[51], Copyright (2020) Wiley-VCH Verlag GmbH & Co. KGaA, modification: position of Figures and exclusion of sub-Figures.

MSNs have been discussed as suitable nanomaterials for oral applications in the GIT.[19,20] One example was given by Juère *et al.* (2020)[51], who proposed DMSN for the oral administration of insulin. Due to the inconvenient standard treatment of diabetes through intravenous injections of insulin and the predicted annual increase in diabetic patients[125], the aspiration to find a more patient-friendly alternative for administration arose. Thus, the authors designed insulin-adsorbed DMSN combined with β-lactoglobulin. This way, pH-responsive intestinal release of insulin was enabled, protecting the drug from premature release and degradation in the stomach. Additionally, the influence of the properties of DMSN on the application was studied. The pore size was adjusted using toluene, cyclohexane or hexane as solvents for synthesis. The authors reported three DMSN types with different pore sizes, as seen in Figure 10. The use of plain negatively charged DMSN with large pore sizes was found to be the most beneficial for oral insulin administration.[51]

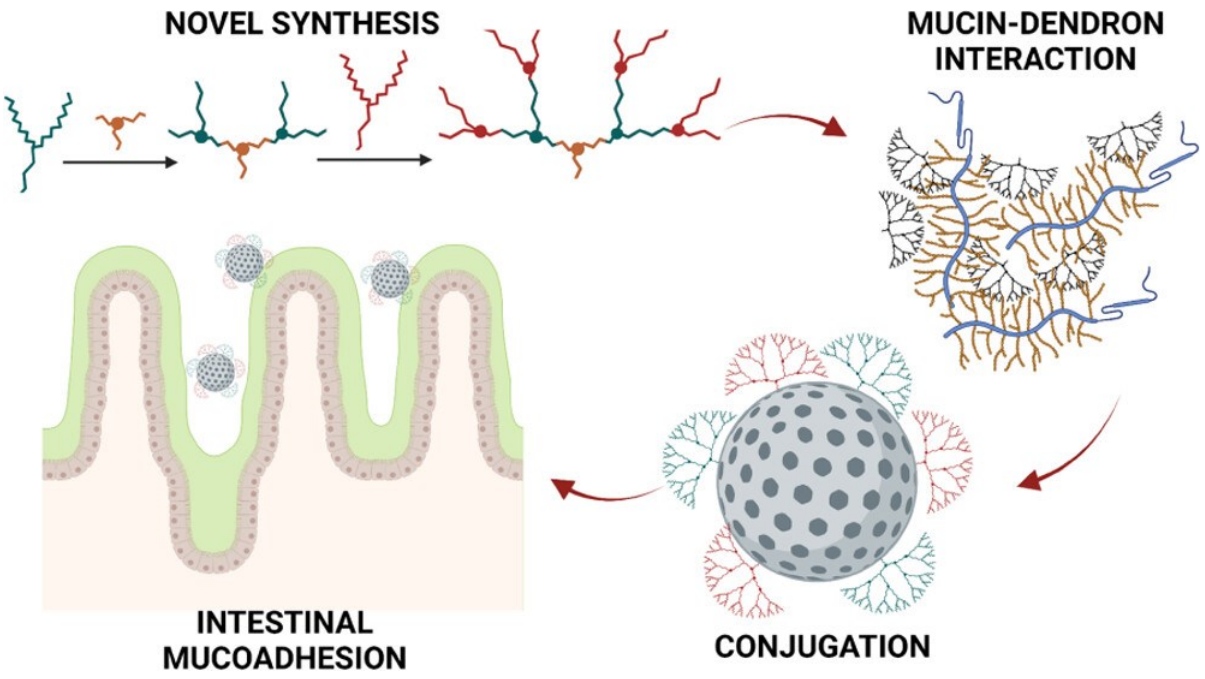

Figure 11. Schematic illustration of the proposed mucoadhesive behavior of dendron-conjugated MSNs by Tollemeto *et al.* (2023)[22]. After introducing a novel synthesis procedure of dendrons (top left), the interaction of dendrons with mucus was evaluated *in vitro* (top right). Drug delivery via conjugated dendron-MSNs (bottom right) was ensured due to the mucoadhesion of the nanoparticle system (bottom left). Thus, the drug would be easier absorbed through epithelium. Figure reprinted with permission from Tollemeto *et al.* (2023)[22], Copyright (2023) ACS.

It is still challenging to ensure proper epithelium transport of the drug. To improve the mucosal interaction of MSNs, Tollemeto *et al.* (2023)[22] recently designed dendrons-conjugated MSNs, illustrated in Figure 11. Owing to this application, a novel route for the synthesis of these polymeric-branched amine dendrons was additionally developed. The authors proposed new mucoadhesive nano-systems for oral drug delivery via MSNs and reinforced their perspective with *in vitro* studies, to ensure the enhanced interactions between mucin and dendrons.

2.4.4 Model Toxin Paracetamol and Pore Adsorption

In this project, acetaminophen, the active substance of paracetamol, was used as a model toxin for adsorption studies. Paracetamol is an easily available drug, commonly used for therapy of mild pain and fever reduction. As the administration of paracetamol happens orally in most cases[126,127], the first contact with the human body will be located in the GIT.

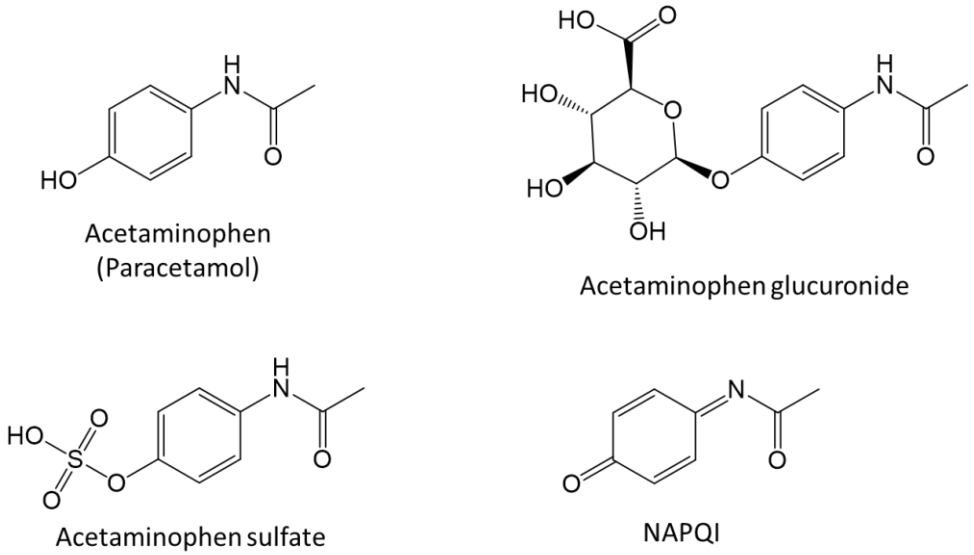

Figure 12. Chemical structures of paracetamol and associated metabolites: acetaminophen glucuronide, acetaminophen sulfate and NAPQI.

As reported by national poison control call (United States of America) statistics of 2021[1], analgesics and other medications were the number one reason for accidental and intentional fatal intoxication through all ages. Paracetamol was found to be one of the pharmaceutical drugs leading to most hospitalizations and deaths after exposure.[1] Rapid occurring hepatic failure after long latencies is still a problem.[8,12,128] Normally, non-required paracetamol is excreted in the form of glucuronided and sulfated metabolites.[129,130] If overdosed, the hepatotoxicity of paracetamol is attributed to the enzymatic metabolism of another metabolite: NAPQI.[131] The chemical structures of mentioned metabolites can be seen in Figure 12. For regular therapeutic paracetamol doses, the body removes NAPQI via glutathione.[132] In the medical field, the antidote and glutathione precursor *N*-acetylcysteine is administered. Due to enhanced glutathione production and the presence of NAPQI-binding thiol groups, liver damage from paracetamol overdose can be prevented.[133,134] Although of being commonly used, oral delivery of *N*-acetylcysteine was found to lack toleration and lead to vomiting in numerous cases due to its sulfur smell. Hence, *N*-acetylcysteine exhibits issues in application due to the need for intravenous delivery or necessary redosing after early emesis.[135,136] Thus, a better tolerable oral route for the treatment of toxin removal is necessary. MSNs could provide an interesting alternative for this problem.

The structure of paracetamol includes two possible hydrogen bond acceptors and two donors.[126] For simplicity, only the two prominent groups participating in possible hydrogen bonding are further outlined: hydroxyl groups as hydrogen donors and carbonyl groups as hydrogen acceptors, illustrated in Figure 13A.[137] When paracetamol is adsorbed by silica-based oral nano-detoxifiers, hydrogen bonds can be formed with silanol of the inner pore surfaces.[138] The pK_a of paracetamol was reported as 9.3.[126] In the GIT's pH range of 1.2 to 7.4, the paracetamol structure is mainly present in the protonated, neutral state.[139] Electronic interactions would not be favored in this state. Thus, interactions via hydrogen bonding are expected to be the predominant effect of paracetamol adsorption.

Silanol groups of MSNs contribute to hydrogen bond formation to toxins. The pK_a 6.77 was proposed for surface silanol groups on MSNs.[140,141] Thus, the conversion of protonated into deprotonated surface silanol groups could be estimated around this pH value. This value is composed of the partial-pK_a of Q^2 and Q^3 silanol (Figure 28) groups: pK_a 8.5 for predominant surface Q^2 silanol and pK_a 2-4.5 for surface Q^3 silanol.[141–143] In simulated gastric fluid (SGF) the MSNs surface is covered mainly in protonated silanol. In simulated intestinal fluid (SIF) the presence of deprotonated surface silanes is more likely. Thus, the formation of hydrogen bonds is expected to be predominant in acidic stomach-like pH conditions, as the protonated silanol participate as donor and acceptor groups[144]. Hydrogen bonds are proposed to be formed between the donors and acceptors of the MSNs[145,146] and paracetamol as illustrated in Figure 13A. Thus, higher adsorption rates of paracetamol were expected in the stomach compared to the intestines.

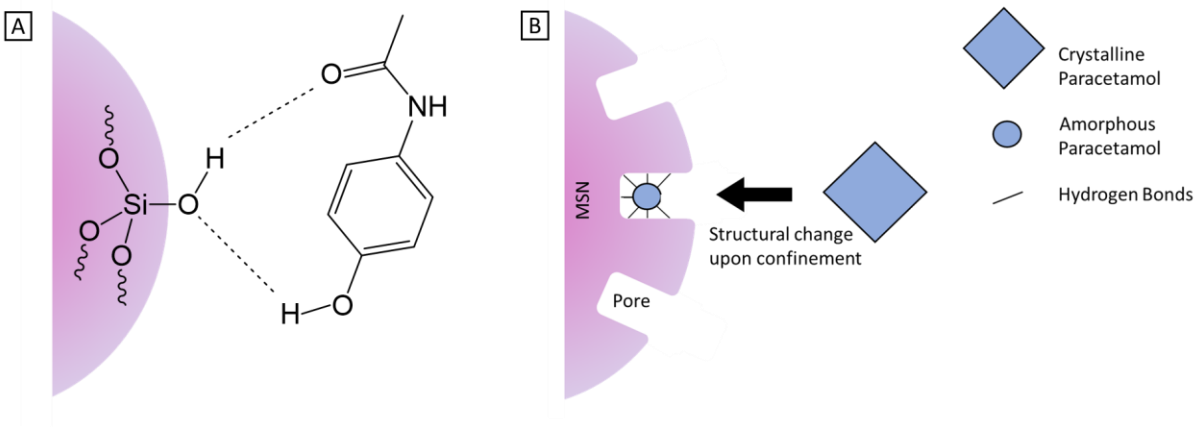

Figure 13. Schematic illustrations of the adsorption behavior of paracetamol onto MSNs. Figure A shows the proposed hydrogen bond formation between the silanol surface and paracetamol. Hydrogen bonds are represented in dashed lines either between carbonyl hydrogen acceptors of paracetamol and the hydroxyl group of silanol or the hydroxyl donors of paracetamol and the oxygen acceptor of silanol. Figure B is an illustration of a molecule's structural change from crystalline (big blue square) to amorphous (blue circle) after pore confinement. Targets inside the pores experience hydrogen bonding as illustrated by black lines. The target cannot morph into the larger crystalline form due to the limited space in the pores.

Being a useful tool in drug delivery[20,147,148], transported substances face protection against early release and biodegradation when adsorbed in the pores of MSNs. Mesopores enable the confinement of a targeted molecule. This process is ascribed to the change in the molecule structure of the target. In the crystalline state, the size of toxins is larger than the space the mesopores provide. To be confined in mesopores, toxins need to morph into the smaller, amorphous arrangement as illustrated in Figure 13B. Although energetically unfavored, the amorphous state remains as the crystalline state would claim more space than supplied by mesopores. The energy loss is compromised by the reduction of surface-free energy of MSNs. Thus, MSNs with a distinctive pore framework and the structural change of the adsorbed target are of great interest in detoxification systems.[149,150]

2.5 Aims of this Project

As far as this master's project was concerned, the aim was to design silica-based oral nano-detoxifiers and assess their applicability for the adsorbance of model toxin paracetamol. A focus was laid on the synthesis of suitable silica-based oral nano-detoxifiers. MSNs were designed towards two goals: the applicability in GIT and the adsorption of paracetamol as the model toxin. We strove to design MSNs with outstanding stability and detoxifying applicability in low pH, to simulate stomach conditions. Additionally, we tried to design particles large enough to not trespass the epithelium.[54] The morphology of particles also influences the risk of epithelium transport.[5,86,87] Thus, the synthesis of three different morphologies, DMSN, VINPs and NrNPs, was aimed for. Selected synthesis parameters were varied to observe the influence on the morphology outcome. The colloidal stability was aimed for all nano-detoxifiers, as MSNs could be toxic in aggregated form.[96] One way of influencing this parameter was by the introduction of PO_3. Interparticle repulsion from the negatively charged functional groups enhanced colloidal stability.[75,97] In fluids of stomach and small intestines, but also in the colon with lower fluid volume[45] (Figure 1B), colloidal stability provides better accessibility to the adsorption sites of the nano-detoxifiers. Thus, higher toxin adsorption rates could be achieved by reducing aggregation. To shield nano-detoxifiers from endogenous proteins, functional group PEG was introduced.[101–103] To ensure sufficient adsorption of paracetamol, particles with high surface area and mesoporosity were aimed for. Enhanced interaction was attempted by the introduction of functional groups PO_3 and epoxide for hydrogen bond formation.[98,100]

Preliminary tests on the paracetamol adsorption ability were performed to find the best silica-based oral nano-detoxifiers for model toxin paracetamol. First, adsorption of paracetamol was evaluated for designed particles in ethanol, SGF and SIF to determine the best candidates. Subsequently, release studies would be needed to investigate the confinement of paracetamol without losing the target before excretion.

Thus, designed silica-based oral nano-detoxifiers needed to be fully characterized to ensure the proposed material properties and successful adsorption of model toxin paracetamol. This was performed by numerous characterization techniques, e.g. N_2 Physisorption, Transmission Electron Microscopy and Solid-State Nuclear Magnetic Resonance Spectroscopy, outlined in Chapter 3.2.

3 Materials and Methods

3.1 Chemicals

(3-Glycidyloxypropyl)-trimethoxysilane (≥ 98 %), 3-(Trihydroxysilyl)propyl methylphosphate (THMP) (50 wt% in water), Cetyltrimethylammonium bromide (CTAB) (≥98 %), Pluronic F-127 and NaOH (≥ 98 %) were purchased from Sigma Aldrich. Silane for PEG functionalization ($(CH_3O)_3Si$-PEG-OCH_3) (2000 Dalton) was purchased from Rapp Polymere. NH_4OH solution (28-30% NH_3), Ethanol (pure, 96 %), KH_2PO_4 (99 %), TEOS (98 %) and Triethanolamine (TEOA) (≥ 98 %) were purchased from Alfa Aesar. HCl solution (37 %) was purchased from VWR Chemicals. NaCl (anhydrous) and Toluene (99.85 % over a molecular sieve) were purchased from Fisher Scientific. Sodium heptafluorobutyrate (FC4) was purchased from Fluorochem.

3.2 Characterization Techniques

For characterization of MSNs, following methods were applied: N_2 Physisorption Analyses, Thermogravimetric Analyses (TGA), Dynamic Light Scattering (DLS), Zeta Potential measurements, Solid-State Nuclear Magnetic Resonance Spectroscopy (ssNMR), Powdered X-Ray Diffraction (PXRD), UV/vis spectroscopy, TEM and Scanning Electron Microscope (SEM).

N_2 physisorption was conducted to determine surface area and porosity of MSNs. N_2 adsorption and desorption isotherms were monitored by a Quantachrome iQ3 instrument (Anton Parr) at -196 °C. For preparation, MSNs were outgassed overnight at 150 °C (plain MSNs), 80 °C (functionalized MSNs), 35 °C (paracetamol-adsorbed MSNs). BET (Brunauer-Emmett-Teller theory) was utilized for the determination of specific surface area (S_{BET}) in the range of 0.05-0.025 P/P_0 for DMSN, 0.05-0.3 P/P_0 for VINPs and 0.05-0.13 P/P_0 for NrNPs. Total pore volume was taken at P_0=0.8. Equilibrium NLDFT (Non-Local Density Functional Theory) model for cylindrical pore geometry was used to determine the pore size of MSNs. To get pore size values for VINPs, cumulative pore volume was consulted for the assessment of the N_2 monolayer.

TGA was performed to quantify functionalization rates of MSNs and adsorbed paracetamol. Measurements were done on a Netzsch STA 449-F3 Jupiter instrument in a temperature range between ambient temperature to 800 °C with a ramp rate of 10 °C min^{-1} and airflow and protective gas (N_2) flow rate of 20 mL min^{-1}. Measurements were performed on powdered solid MSNs. Calculations of mass loss were extracted from the temperature range of 150-800 °C. To quantify grafted moieties, mass loss of

plain MSNs was subtracted from mass loss of functionalized MSNs. For the paracetamol adsorption rate, mass loss of unloaded MSNs was subtracted from mass loss of loaded MSNs.

DLS and zeta potential were performed for the evaluation of colloidal stability, surface charge and hydrodynamic diameter (h_D) of MSNs. Measurements were performed on a Malvern Zetasizer Nano ZS instrument. Measurements were conducted on aqueous suspensions of MSNs (0.7 mg mL^{-1}) at 25 °C. Prior to the analysis, MSNs were dispersed by ultrasonication for at least 90 min combined with vortex shaking. For long-term stability tests, solely the h_D was measured by DLS without any dispersing operation in between. Stability over the range of pH 8-2 was conducted by automatic titration with measurements of average zeta potential. Aqueous HCl solution (0.025 M) was used as the titrant. Prior to titration, aqueous sample solutions were manually adjusted to pH 8 by NaOH (0.1 and 0.01 M).

ssNMR spectra were measured by a Bruker AVANCE NEO 500 wide bore instrument combined with a 4 mm triple resonance magic angle spinning probe for solid samples. Plain MSNs were measured with ^{29}Si (CP/MAS, Cross-Polarization/Magic-Angle-Spinning) only. Functionalized and paracetamol-adsorbed MSNs were monitored by ^{29}Si (CP/MAS) and ^{13}C (CP/MAS). ^{31}P (CP/MAS) spectra were additionally taken for phosphonated MSNs.

PXRD technique was conducted to confirm the confinement of paracetamol. A PANalytical Empyrean diffractometer was used for obtaining PXRD patterns of MSNs. Measurements were performed in reflection mode. $K\alpha_{1+2}$ radiation was induced by an X-ray Cu source at 45 kV 40 mA. PXRD patterns were recorded in continuous mode, step size 2θ of 0.013° with 175 s measurement time for each step. Physical mixtures were prepared by mixing paracetamol (amounts as prior quantified from adsorption studies) with the corresponding MSNs.

UV/vis spectroscopy was applied to monitor release rates. Absorption spectra were monitored on an Agilent 8453 UV-visible Spectroscopy System at 243 nm in SGF and SIF. To investigate release rates, the concentration of the measured solution was determined. Absorption rates of calibration lines of known concentrations were used for calculation. The concentration range of calibration lines was 0.0025-0.015 mg mL^{-1} for all dilution reagents.

To observe morphology and size of the particles, **TEM and SEM** imaging were performed. For sample preparation, 0.6 mg mL^{-1} suspensions of particles in ethanol were prepared, sonicated for 90 min, drop-casted directly onto a TEM grid and dried under air. Images were obtained from a Philips CM200 transmission electron microscope and SEM images were collected on a Zeiss Supra 55 VP instrument. Evaluation of size from images was conducted via software “ImageJ” by the average of twice measured cross section of each nanoparticle in one image.

3.3 Synthesis Procedure of MSNs

The following Chapters report the experimental procedures for the synthesis of MSNs in three morphologies: DMSN, VINPs and NrNPs. In every Chapter, first, implemented synthesis procedures for further studies are given. Second, varied parameters to observe the influence on the resulting morphology are listed, if applicable.

3.3.1 Synthesis Procedure of DMSN

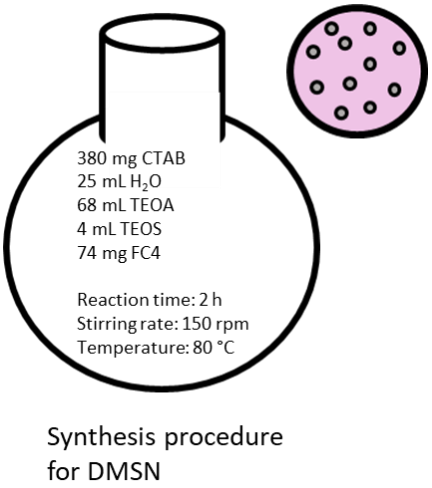

Figure 14. Summarized synthesis parameters for the regular synthesis procedure for the preparation of DMSN.

For the preparation of DMSN, a synthesis procedure adapted from Wang *et al.* (2018)[120] was performed. 68 mL TEOA was introduced in a 100 mL round-bottom flask and dissolved in 25 mL H_2O. Subsequently, 380 mg CTAB and 74 mg FC4 were added to the alkaline solution and stirred at 150 rpm 80 °C for 1 h. Afterwards, 4 mL TEOS was introduced by dropping (1 drop per 2 sec) via a drop funnel. Synthesis parameters are summarized in Figure 14. After reaction time of 2 h (150 rpm, 80 °C), the synthesized DMSN were centrifuged (20 min, 7000 rpm) to remove the solvent and washed three times with ethanol. For extraction, the particles were washed once in an H_2O/ethanol (50 v/v%) mixture, twice in an acidic ethanol solution (30 mL ethanol + 1 drop HCl) and finally washed in ethanol. After drying in oven at 100 °C for 14 h, calcination was performed at 550 °C (5 min; ramp rate: 60 °C h^{-1}) to receive template-free DMSN.

3.3.2 Synthesis Procedure of VINPs

VINPs were synthesized according to the procedure reported by Wang *et al.* (2017)[121]. In a 250 mL round-bottom flask 1 g CTAB was dissolved in 50 mL H_2O. Subsequently, 0.8 mL NaOH (0.1 M) was added and the solution was stirred at 130 rpm 60 °C for 2 h. Afterwards, 20 mL TEOS in cyclohexane (20 v/v%) was introduced dropwise via a syringe pump instrument (76 mL h^{-1}). After 7 days of reaction at 130 rpm 60 °C, the organic solution was manually removed by pipetting and the aqueous solution by centrifugation (20 min, 7000 rpm). The particles were washed, extracted and calcined according to the procedure mentioned in Chapter 3.3.1 to receive plain VINPs. An overview of synthesis parameters for this procedure can be seen on the left side of Figure 15.

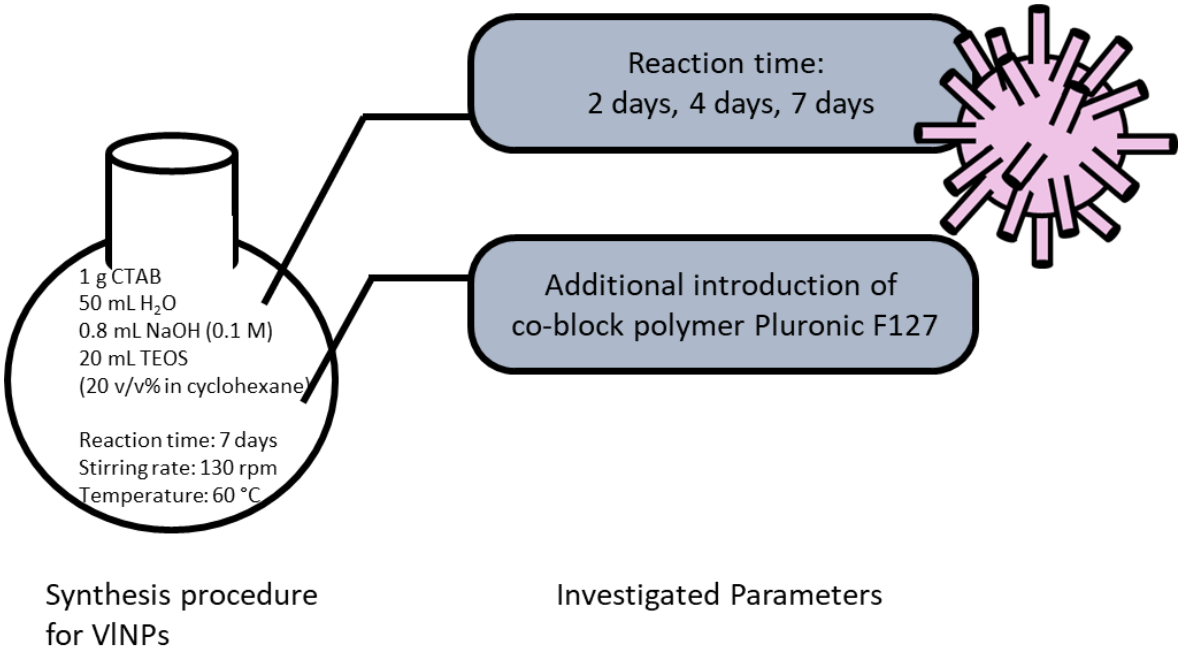

Figure 15. Overview of synthesis parameters of regular synthesis procedure (left) and further investigated parameters (right) for VINPs.

The influence of reaction time on the formation of VINPs was assessed by varying the synthesis duration after the addition of TEOS by 2 days, 4 days and 7 days (Figure 15, right), adapted from Wang *et al.* (2017)[121]. The latter coincided with the parameter used in the regular synthesis procedure and served as a control.

Second, co-block polymer Pluronic F127 was introduced (mass ratio 4:1 to the amount of CTAB) to investigate the influence on the VINPs morphology (Figure 15, right), adapted from von Baeckmann *et al.* (2021)[151].

3.3.3 Synthesis Procedure of NrNPs

For the synthesis of NrNPs, a modified synthesis procedure from Huang *et al.* (2010)[117] and Yu *et al.* (2016)[86] was implemented. 2.42 g CTAB and 605 mL water were introduced in a 1 L round-bottom flask. After CTAB was dissolved, 9.35 mL NH_4OH was added to the solution and stirred vigorously at 700 rpm for 1 h at room temperature (rt). Afterwards, 5.17 mL TEOS was introduced at once. For the formation of NrNPs, the suspension was stirred at 700 rpm for 4 h at rt. To receive plain NrNPs, the solution was removed by centrifugation (20 min, 7000 rpm) and the particles were washed, extracted and calcined according to the procedure mentioned in Chapter 3.3.1. An overview of synthesis parameters for this procedure can be seen on the left side of Figure 16.

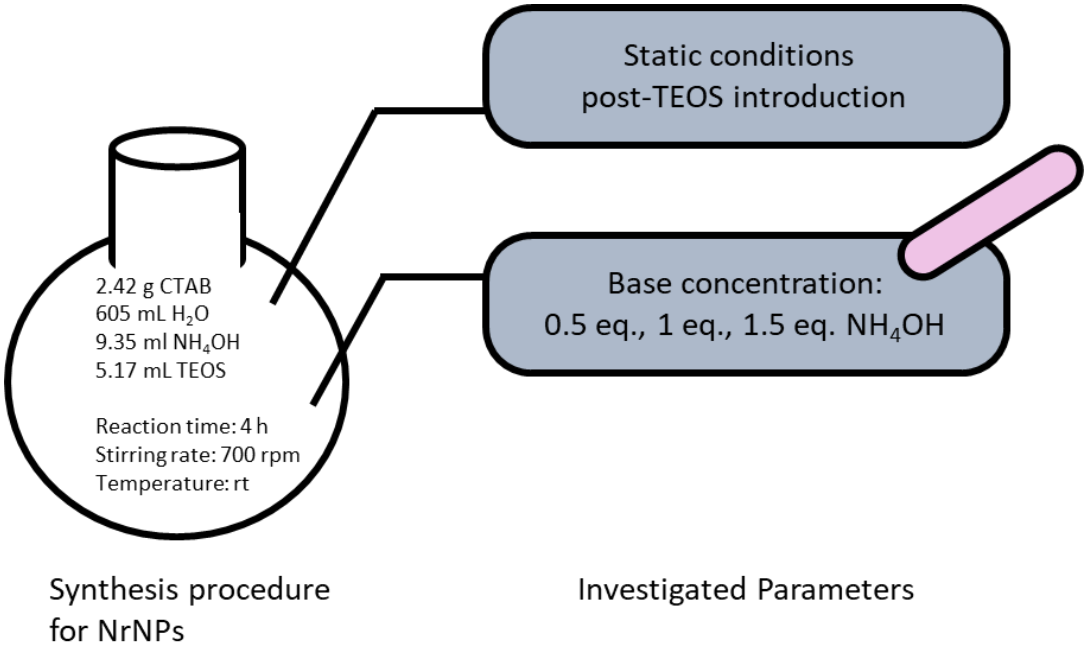

Figure 16. Overview of synthesis parameters of implemented synthesis procedure (left) and further investigated parameters (right) for NrNPs.

The influence of base concentration was investigated by variation of the NH_4OH concentration equivalents (eq.) (0.5 eq., 1 eq. and 1.5 eq) for the synthesis of NrNPs.

To investigate the influence of stirring rate on the NrNPs morphology, synthesis was performed under static conditions after the addition of TEOS. An overview of the investigated parameters for NrNPs synthesis can be found on the right side of Figure 16.

3.4 Functionalization Strategies

MSNs obtained from the reported procedures in Chapter 3.3 were grafted with three different functional groups: PO_3, epoxide and PEG. The goal was to introduce functional groups on the inner pore surfaces and outer surfaces of MSNs.

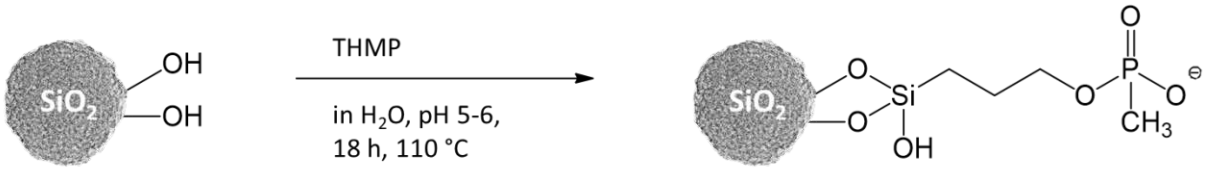

Scheme 1. Chemical reaction scheme and conditions for the preparation of MSN_PO_3 by THMP.

Phosphonated MSNs (MSN_PO_3) were obtained via direct functionalization with commercially available silane THMP. 300 mg MSNs were dispersed overnight in 60 mL nanopure H_2O at 600 rpm, rt in a 250 mL round-bottom flask. Afterwards, a solution of THMP (8 mmol g^{-1} silica) in 15 mL nanopure H_2O, adjusted with diluted HCl solution to pH 5-6, was introduced to the suspension and refluxed at 110 °C at a stirring rate of 700 rpm overnight. The corresponding chemical reaction scheme is illustrated in Scheme 1.[75] On the next day, phosphonated MSNs were centrifuged (7000 rpm, 20 min) to remove the supernatant, washed once with H_2O and three times with ethanol. After drying at 40 °C, MSN_PO_3 were received and analyzed via TGA, N_2 physisorption, DLS, zeta potential analysis and ssNMR.

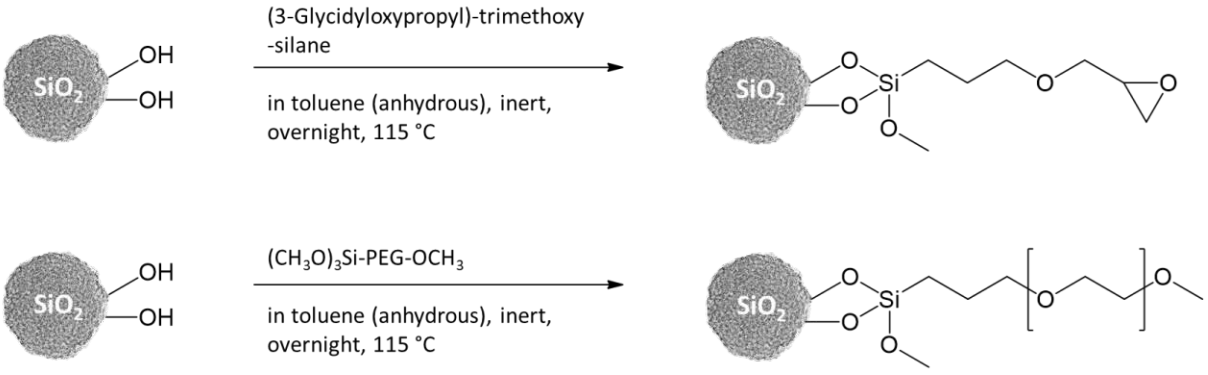

Scheme 2. Chemical reaction scheme and conditions of the post-synthesis functionalization route with commercially available silanes for obtaining MSN_epox (top) and MSN_PEG (bottom).

To obtain epoxide- (MSN_epox) and polyethylene glycol- (MSN_PEG) functionalized MSNs, commercially available silanes were used. 300 mg of plain MSNs were weighed in a 250 mL three-neck round-bottom flask and outgassed under vacuum overnight at 150 °C and 500 rpm stirring rate. After reducing the temperature to 115 °C, the particles were suspended in 90 mL of anhydrous toluene under inert conditions and stirred at

500 rpm overnight. The corresponding silanes (8 mmol g^{-1} silica (3-Glycidyloxypropyl)-trimethoxysilane for MSN_epox and 0.04 mmol g^{-1} $(CH_3O)_3Si$-PEG-OCH_3 for MSN_PEG) were introduced at 115 °C 500 rpm to the well-dispersed solutions to start the overnight reaction. Reaction schemes for the preparation of MSN_epox and MSN_PEG are shown in Scheme 2.[152] Subsequently, the particles were isolated by centrifugation (7000 rpm, 20 min). The functionalized MSNs were washed once with toluene, three times with ethanol and dried at 40 °C. MSN_epox and MSN_PEG were subsequently analyzed via TGA, N_2 physisorption, DLS, zeta potential analysis and ssNMR.

3.5 Instructions for Adsorption Studies

Designed MSNs were evaluated on the adsorption capacity of model toxin paracetamol to determine the applicability as oral nano-detoxifiers. A modified adsorption procedure based on Farjadian *et al.* (2015)[88] was applied. Freshly prepared paracetamol solution (10 mg mL^{-1}) in ethanol (pure, 96 %) was introduced to MSNs in a ratio of 2.8 wt/v% and placed on a shaker at 80 rpm 37 °C for 2 or 6 h. Afterwards, the particles were separated from the solution by centrifugation (7000 rpm, 20 min) and paracetamol-adsorbed solid material dried at 37 °C overnight. Mass loss monitoring via TGA was conducted to quantify adsorbed paracetamol in the material. This experiment was divided into two sections: First, plain DMSN, VlNPs and NrNPs were loaded with paracetamol to find the morphology with the highest adsorption capacity. Second, the experiment was conducted for the functionalized morphology with the highest adsorption capacity.

Similar adsorption attempts were conducted for plain DMSN, VlNPs and NrNPs in a different medium. Paracetamol was dissolved in SGF for a 2 h adsorption procedure to simulate acidic conditions in human stomachs and SIF for a 6 h adsorption procedure for human intestines simulations. Procedures and characterization were performed according to the adsorption procedures reported above. Only centrifugation parameters were adjusted to the aqueous solution to 9000 rpm and 20 min.

The preparation of SGF and SIF for adsorption and release studies was adapted from Caillard *et al.* (2012)[153]. For the preparation of 2 L **SGF** (pH 1.2), 4 g anhydrous NaCl was dissolved in 1.986 L nanopure H_2O and 14 mL HCl (37 %). 2 L **SIF** (pH 7.4) was prepared by dissolving 13.6 g KH_2PO_4 in 500 mL nanopure H_2O. To adjust the pH, 380 mL of NaOH solution (0.2 M) was introduced to the solution together with 1.12 L nanopure H_2O. The pH values were checked for both solutions before application.

3.6 Instructions for Release Studies

To monitor the potential release of paracetamol-adsorbed MSNs, release tests in SGF and SIF were conducted. Conditions and procedure were adapted from Juère *et al.* (2020)[21]. 20 mg particles were combined with 5 mL SGF and shaken at 80 rpm at 37 °C to simulate body movement and temperature. Samples (0.75 mL) were taken after centrifugation (20 min at 9000 rpm) and diluted (in 2.25 mL of corresponding solution) after the first 35 min and subsequently every hour. The volume was replaced with fresh medium, particles were redispersed and put back on the shaker. The solution was changed to SIF after 3 h whereas an intermediate washing step with SIF was included. Samples were also taken from the washing- and solution exchange steps. Afterwards, samples were taken after 1 h, 24 h and 48 h in SIF. Absorptions of diluted samples were measured via UV/vis spectroscopy and concentrations were calculated via calibration lines in corresponding SGF and SIF.

3.7 Tools for Data Analysis and Presentation

Data was analysed and plotted via OriginPro. Other Figures and Schemes were created by Microsoft PowerPoint and ChemDraw. Zotero was used for generation of citations. For language correction, Grammarly was used.

4 Results and Discussion

4.1 Characterization of Plain MSNs

In the following Chapters, analysis results of synthesized MSNs are shown. All descriptions are structured in the same way. First, morphology and corresponding characterization results of the regular synthesis procedures are given. Second, results of parameter studies are described, if applicable.

4.1.1 Characterization of DMSN

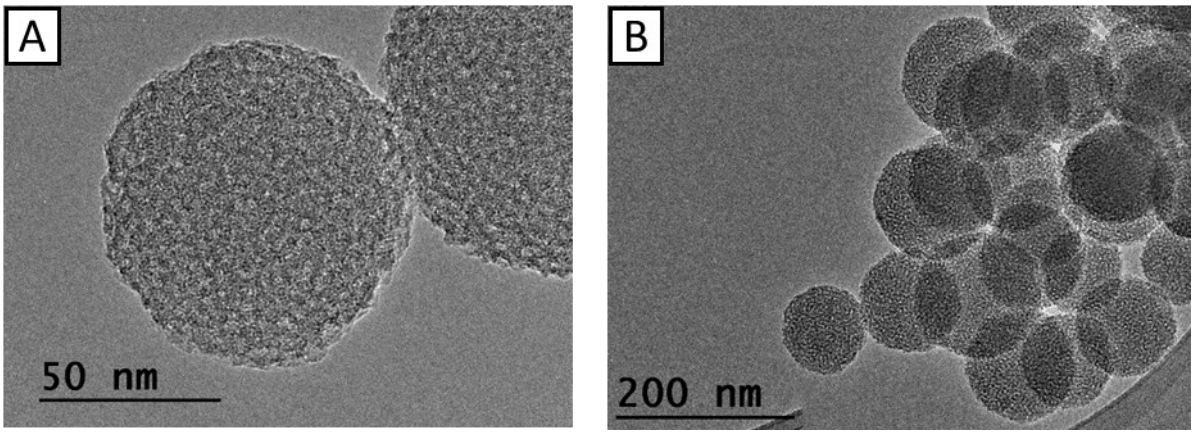

Figure 17. TEM images of DMSN. Image A gives an insight into the pore system of plain DMSN. Image B shows the particle size distribution of DMSN.

DMSN were synthesized as almost monodisperse, spherical porous nanoparticles with a smooth particle surface shown in Figure 17. As measured from TEM images, the average particle size of DMSN was found to be 116 nm.

Zeta potential for DMSN in H_2O was found to be -47 mV. Thus, the surface of synthesized DMSN exhibited a negative surface charge in aqueous solutions.

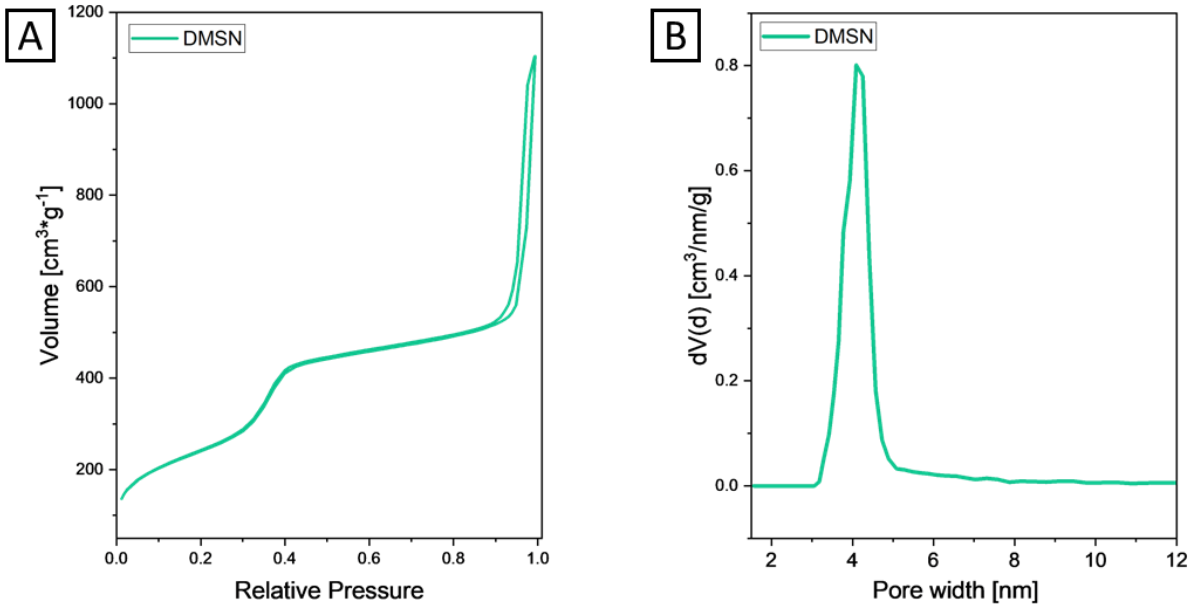

Figure 18. N_2 physisorption results of DMSN. N_2 Adsorption/desorption isotherm (Figure A) with corresponding pore structure analysis via NLDFT model (Figure B) of DMSN at -196 °C. The presence of hysteresis in the N_2 physisorption isotherm (Figure A) and a peak in the mesoporous pore size range (Figure B) indicated mesoporous system of the nanoparticles.

As measured by N_2 physisorption, DMSN showed a surface area of 885 m^2 g^{-1}, mesopore size of 3.8 nm and pore volume of 1.22 cm^3 g^{-1}. Therefore, the presence of the mesopore system was proven. Additionally, the hysteresis in type IV[154] N_2 physisorption isotherms (Figure 18A), as well as the single peak found in the mesoporous range of pore structure analysis (Figure 18B), confirmed a mesoporous system for synthesized DMSN.

Therefore, DMSN were successfully synthesized as MSNs with spherical morphology. A summary of the mentioned results for synthesized DMSN can be found in Table 1 in Chapter 4.1.4.

4.1.2 Characterization of VINPs

4.1.2.1 Characterization results of the regular synthesis procedure of VINPs

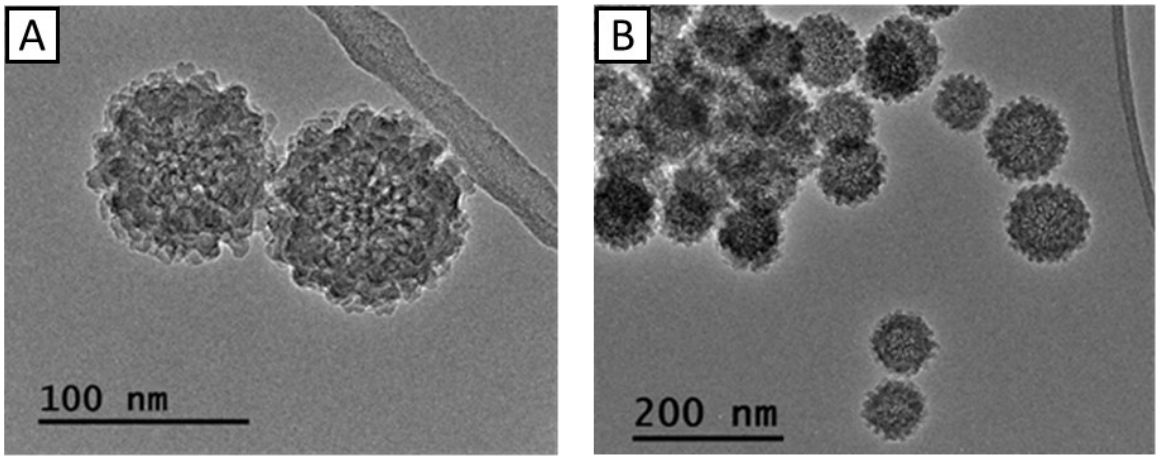

Figure 19. TEM images of VINPs. Image A shows the surface spikes of plain VINPs. Image B gives an insight into the particle size distribution of VINPs.

TEM images (Figure 19) of synthesized VINPs showed a monodisperse, spherical morphology with a rough surface formed by spikes. The average particle size was found to be 96 nm.

The zeta potential of plain VINPs in H_2O was measured as -49 mV, indicating negative surface charge in this solvent.

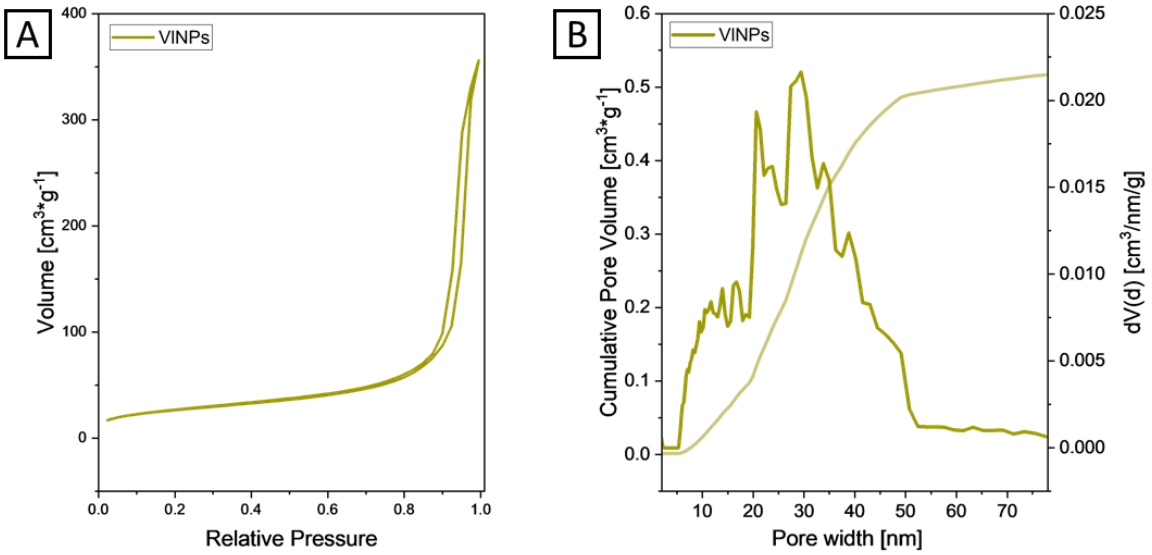

Figure 20. N_2 Physisorption isotherm (Figure A) and pore volume vs pore width received from NLDFT model (Figure B) of VINPs at -196 °C.

The surface area of VINPs was found to be 92 m^2 g^{-1}. The presence of a hysteresis in Figure 20A indicated a mesoporous pore system for VINPs. The pore volume was found to be 0.52 cm^3 g^{-1}. The pore width analysis (Figure 20B, deep orange) showed a broad pore size distribution over the range of 10-40 nm. Noticeable high pore size values defined the low surface area. To further approve the pore size range, the cumulative pore volume analysis graph, plotted in light orange (Figure 20B), was found to be in the same scope. Therefore, the broad pore size range of 10-40 nm was accepted for VINPs. Due to the broad pore size distribution and the introduced VINPs formation by Wang *et al.* (2017)[121], it was assumed that the porous system of this morphology was constructed by the interstices of the surface spikes.

To summarize, spherical VINPs with a rough surface were successfully synthesized. A wide pore size range was found for this morphology, which was ascribed to the interstices of the spikes. A summary of the mentioned results for synthesized VINPs can be found in Table 1 in Chapter 4.1.4.

4.1.2.2 Results of Parameter Studies for VINPs: Reaction Time and Co-block Polymer

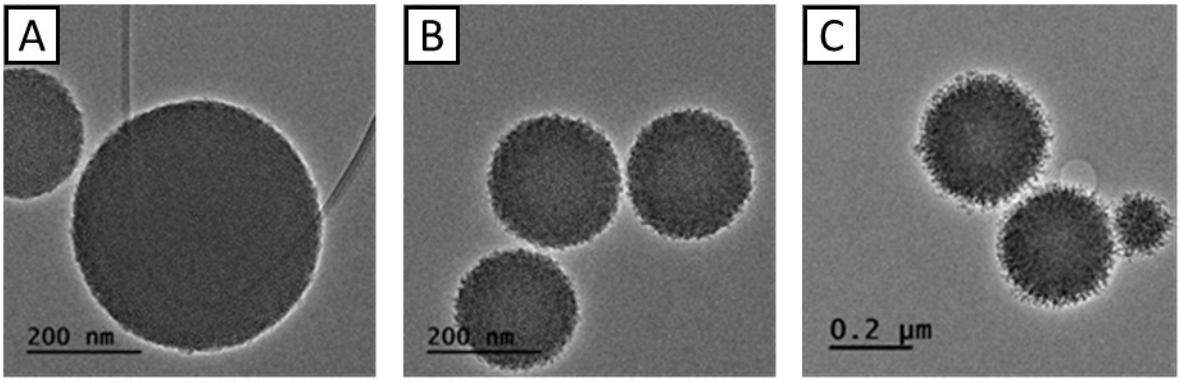

Figure 21. Observed spike growth of VINPs with varied synthesis time monitored by TEM imaging. Image A showed VINPs after 2 days synthesis with the shortest spikes, Image B after 4 days and Image C after 7 days of synthesis with the longest spikes.

Upon the variation of reaction time (2 days, 4 days, 7 days) for the synthesis of VINPs, a difference in the length of spikes was observed. After 2 days, hardly any spikes were visible in the TEM image in Figure 21A. If the reaction was stopped after 4 days, spikes were visible in Figure 21B at a similar magnification. After 7 days reaction, it was finally possible to obtain VINPs with the longest spikes, shown in Figure 21C. Therefore, the parameter “synthesis time” has a noteworthy influence on the surface properties of VINPs. This observation coincided with Wang *et al.* (2017)[121] for the formation of VINPs. They proposed the formation of the spikes after the formation of the spherical body, as described in Chapter 2.4.2 and in Figure 9.

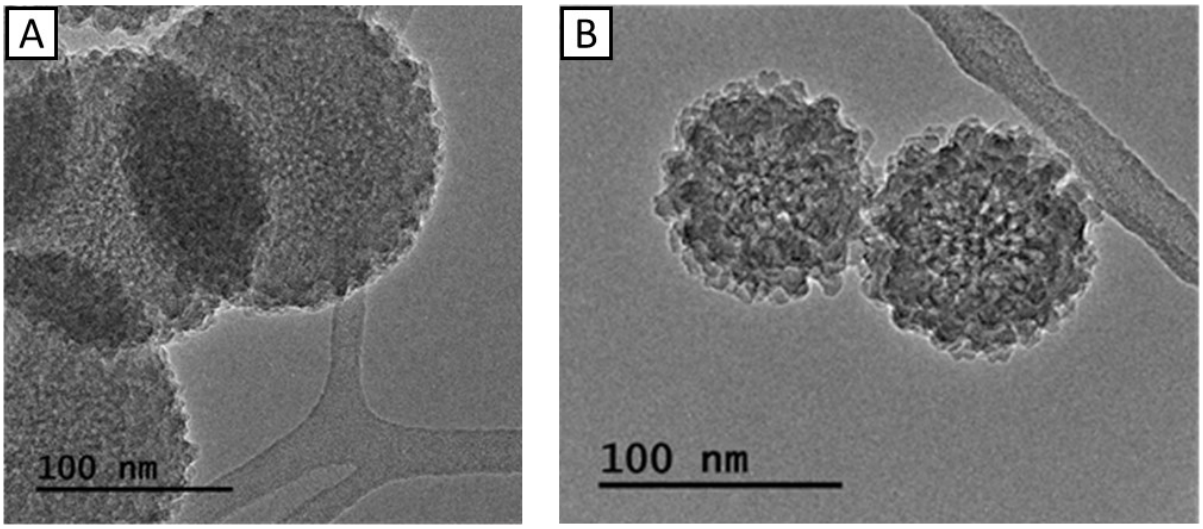

Figure 22. Images of VlNPs with introduced co-block polymer Pluronic F127 during synthesis (Image A) and of VlNPs from regular synthesis procedure (Image B) taken by TEM. Due to the presence of the co-block polymer, larger MSNs with shorter spikes were synthesized.

Another varied parameter was the introduction of the co-block polymer Pluronic F127 for the synthesis of VlNPs, adapted from the synthesis procedure of von Baeckmann *et al.* (2021)[151]. Without co-block polymer, average particle size of 96 nm was observed in Figure 22B. Upon the use of Pluronic F127, bigger particles with an average size of 150 nm were obtained as shown in Figure 22A. In addition, a change in spike size and morphology was detected. An explanation for these phenomena could be the reduction of synthesis speed directed by the co-block polymer. Therefore, a more isotropic-like, shorter spike formation had been favored in the presence of Pluronic F127.

4.1.3 Characterization of NrNPs

4.1.3.1 Characterization Results of Regular Synthesis Procedure of NrNPs

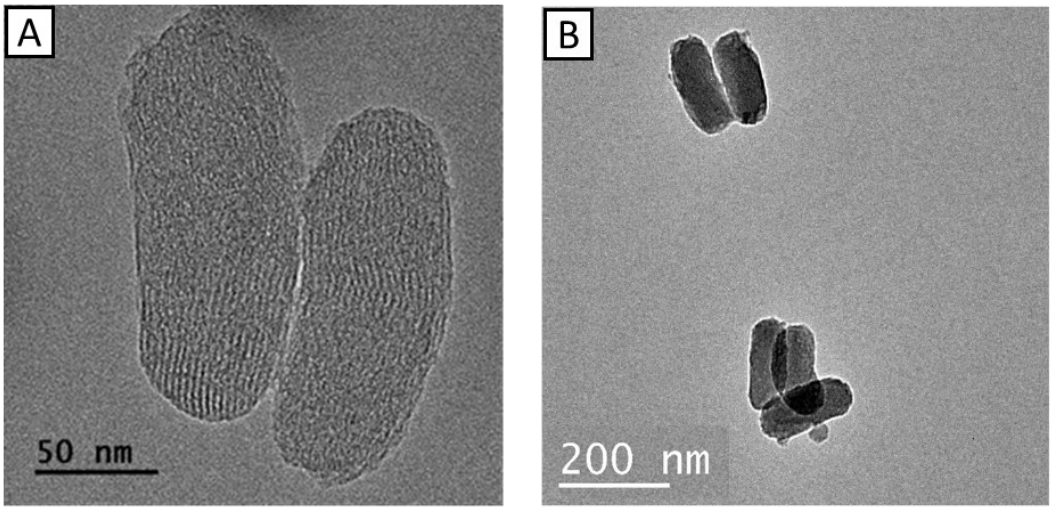

Figure 23. TEM images of NrNPs. Image A gives an insight into the pore properties of NrNPs. Image B demonstrates the particle size distribution of NrNPs.

Synthesized NrNPs were obtained as monodisperse, anisotropic mesoporous nanorods with a smooth surface (Figure 23). The average particle dimensions measured from TEM images were found to be 173 nm in length and 74 nm in width, giving an aspect ratio of 2.3. Zeta potential for NrNPs in H_2O was -44 mV. Therefore, negative surface charge was confirmed for plain NrNPs.

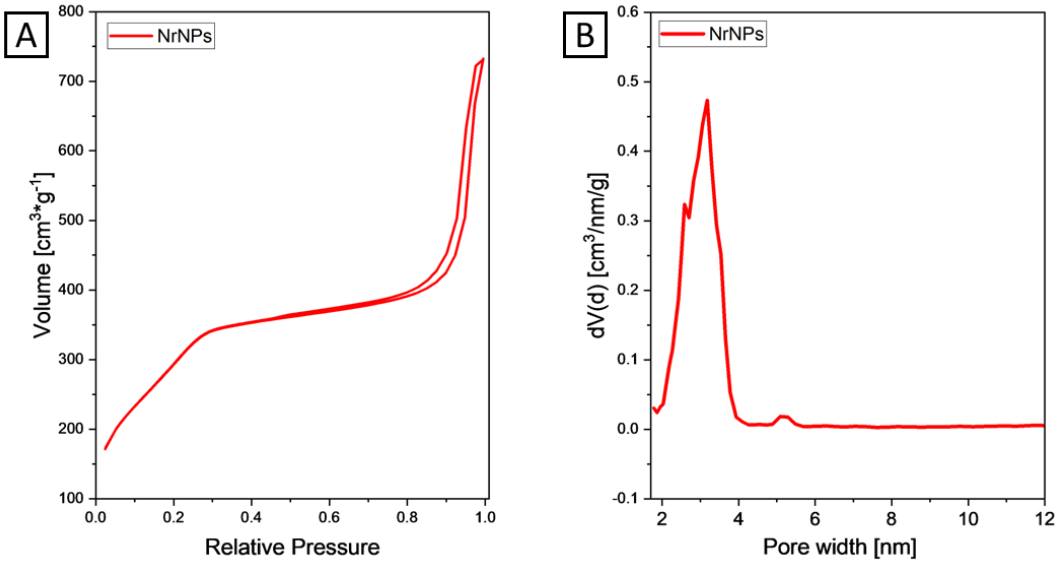

Figure 24. N_2 adsorption and desorption isotherms (Figure A) with corresponding pore structure analysis via NLDFT model (Figure B) of NrNPs measured at -196 °C. The presence of hysteresis in the N_2 physisorption isotherm (Figure A) indicated mesoporous system of the nanorods. This was confirmed by the pore structure analysis. One predominant peak can be found in the mesoporous range for NrNPs (Figure B).

The surface area of plain NrNPs was determined to be 1041 m^2 g^{-1}, the mesopore size 3.2 nm and the pore volume 1.04 cm^3 g^{-1}. The presence of a hysteresis in the N_2 physisorption isotherm and the single predominant peak in the mesopore range in Figure 24 confirmed the mesoporous pore system of NrNPs.

Plain NrNPs were successfully synthesized in a mesoporous, anisotropic morphology with smooth surface properties. A summary of the mentioned results for synthesized NrNPs can be found in Table 1 in Chapter 4.1.4.

4.1.3.2 Results of Parameter Studies for NrNPs: Base Concentration and Stirring Rate

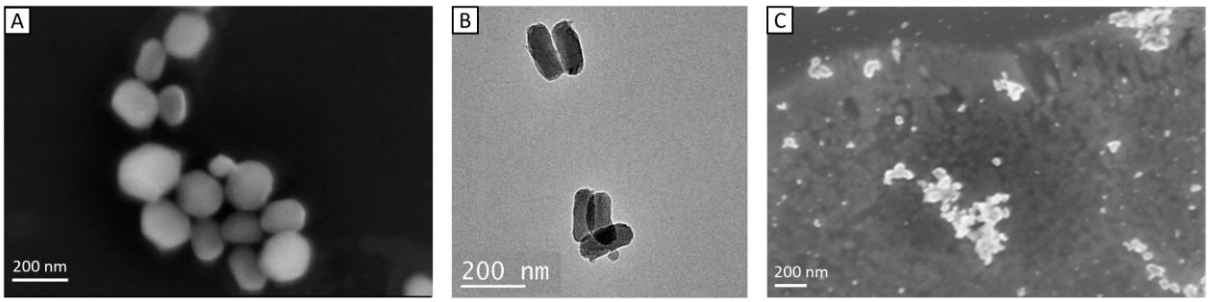

Figure 25. SEM (Figures A and C) and TEM (Figure B) images of synthesized NrNPs after the use of different base concentrations. Left to right: highest to lowest base concentration in synthesis. In Image A, the introduction of 1.5 eq NH_4OH led to a hexagonal shape, in Image B, 1 eq. NH_4OH forming rods and in Image C, 0.5 eq NH_4OH were introduced resulting in crude silica material.

With the variation of base concentration for NrNPs synthesis, the impact on the morphology was observed in Figure 25. 1.5 eq. NH_4OH (with respect to the regular synthesis quantities) led to the formation of hexagonal particles shown in Figure 25A. With 1 eq., NrNPs were formed (Figure 25B). Upon the use of 0.5 eq. NH_4OH, solely crude silica without distinctive morphology was observed in SEM image in Figure 25C. Thus, we conclude the base concentration has a major influence on the formation of the anisotropic shape. At higher pH conditions, particle growth is favored in more than two directions, forming a hexagonal shape rather than a rod-like or spherical shape.

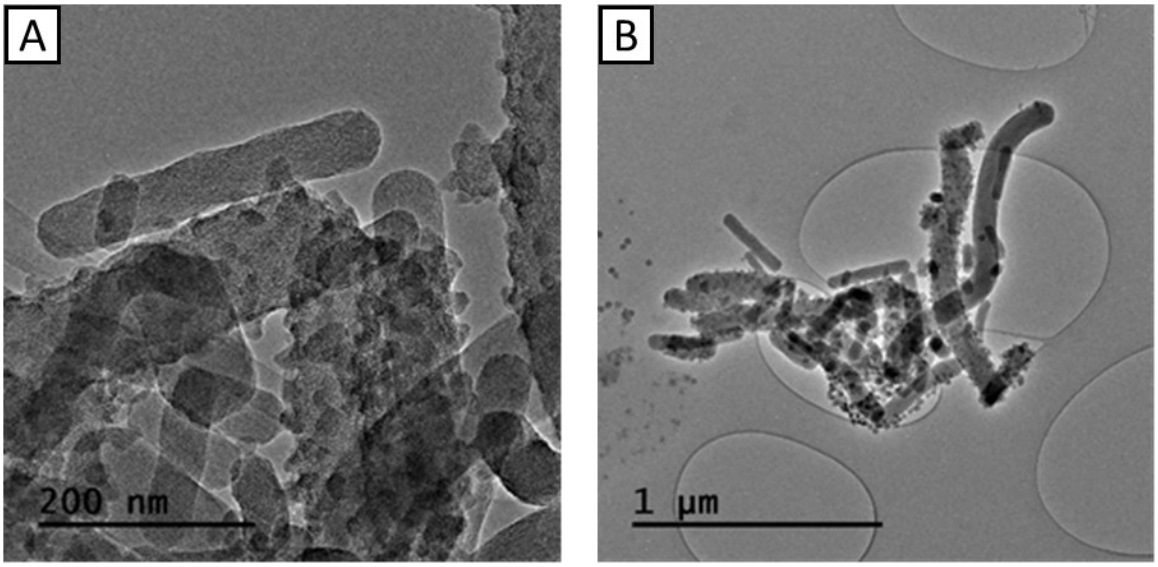

Figure 26. TEM images of NrNPs synthesized without stirring. At higher magnification (Image A), rough surface was observed. At lower magnification visible (Image B), NrNPs synthesized under static conditions turned out to be polydisperse.

During the regular synthesis procedure for NrNPs, vigorous stirring was applied. To investigate the role of stirring rate, NrNPs were reproduced under static conditions. The surface of obtained NrNPs appeared rough as observed by TEM imaging in Figure 26A. Due to the growth under static conditions, the particles resulted in high polydispersity, illustrated in Figure 26B. However, further studies are necessary to confirm whether the rough surface was anchored to the rod-shaped MSNs body or labile upon mechanical influence and storage.

4.1.4 Overview of MSN Morphologies

To summarize the synthesis of plain MSNs, three different morphologies were successfully produced: DMSN, VlNPs and NrNPs. MSNs were found to be in comparable size ranges. Zeta potential values highlighted the similarity between the chemical nature of the surfaces of the template-free, plain synthesized MSNs. Size, zeta potential and N_2 physisorption results are summarized in Table 1.

Table 1. Summary of the analysis results of DMSN, NrNPs and VlNPs. Size of obtained MSNs, zeta potential and surface area, pore size and pore volume as determined by N_2 Physisorption. The average size was measured from TEM images and DLS (DMSN and VlNPs only), giving h_D values.

Sample	Average Size [nm]		Zeta [mV]	Surface Area [$m^2 g^{-1}$]	Pore Size [nm]	Pore Volume [$cm^3 g^{-1}$]
	TEM	h_D				
DMSN	116	158	-47	885	3.8	1.22
VlNPs	96	111	-49	92	10-40	0.52
NrNPs	173x74		-44	1041	3.2	1.04

Under consideration of surface and pore property values, DMSN were found to be the most promising candidates for the application as nano-detoxifiers. Due to promising pore volume and size in the mesoporous range, proper adsorption quantities of paracetamol were pre-assumed. To further improve the detoxification of paracetamol, MSNs were functionalized. Corresponding results were reported in the following Chapter 4.2.

4.2 Characterization of Functionalized MSNs

4.2.1 Characterization of Functionalized DMSN

DMSN, VINPs and NrNPs were grafted with three functional groups: PO_3, epoxide and PEG. For the reasons outlined in the previous Chapter 4.1.4, DMSN were found to be the most promising morphology for preliminary application studies. Thus, special attention was given to functionalization and characterization of this morphology.

Mass loss [wt%] as measured by TGA was used to quantify functionalized species. For DMSN_PO_3 7 wt%, DMSN_epox 9 wt% and for DMSN_PEG 11 wt% mass loss ascribed to functionalization was determined.

Zeta potentials were found to be -46 mV for DMSN_PO_3, -43 mV for DMSN_epox and -41 mV for DMSN_PEG. Compared to the zeta potential of plain DMSN (-47 mV), these values only differed slightly for functionalized DMSN due to the chosen low functionalization rates. All designed particles exhibited negative charge in H_2O.

Table 2 gives a summary of the analysis of functionalized DMSN.

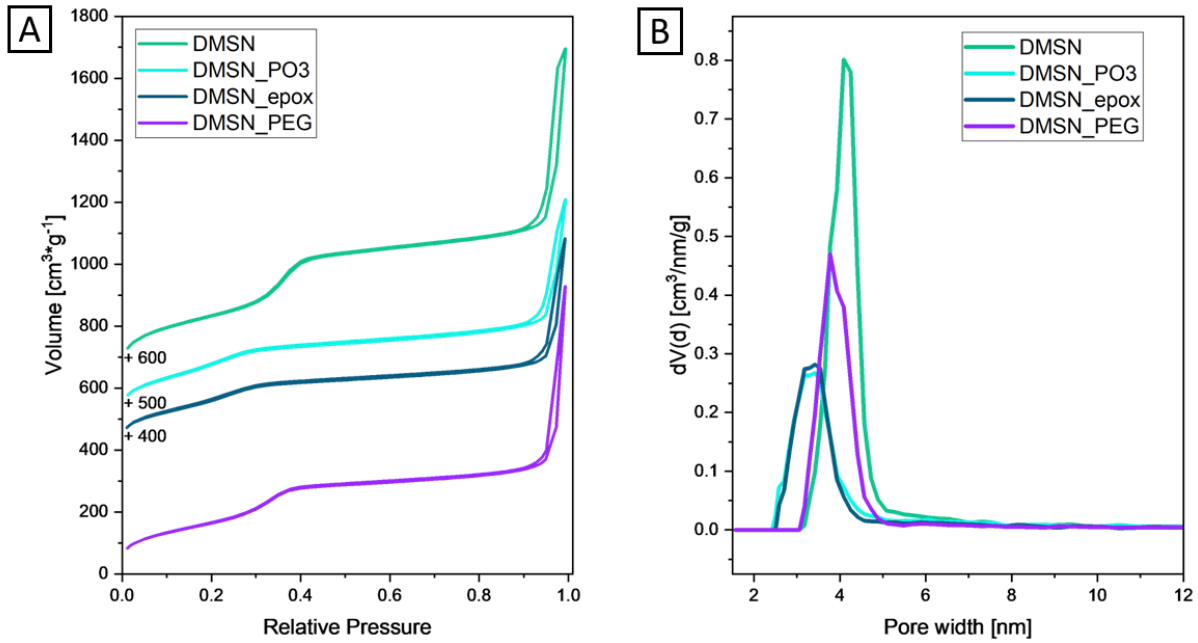

Figure 27. N_2 adsorption and desorption isotherm (Figure A) and pore size distribution (Figure B) of plain and functionalized DMSN measured at -196 °C.

After functionalization, the surface area decreased for all DMSN. Surface area for DMSN_PO_3 was found to be 711 m^2 g^{-1}, for DMSN_epox 642 m^2 g^{-1} and for DMSN_PEG 621 m^2 g^{-1}. An expected trend towards lower surface area values for species functionalized with higher quantity (as summarized in Table 2) was detected.

As shown in Figure 27B and Table 2, pore sizes remained similar to plain DMSN (3.8 nm): 3.4 nm for DMSN_PO_3 and DMSN_epox, 3.8 nm for DMSN_PEG. However, pore volume decreased upon functionalization. The pore volume of DMSN_PO_3 was determined as 0.90 cm^3 g^{-1} and 0.84 cm^3 g^{-1} for DMSN_epox. Interestingly, the highest functionalized species (DMSN_PEG) showed the lowest decline in pore volume (1.08 cm^3 g^{-1} compared to 1.22 cm^3 g^{-1} for plain DMSN). Thus, the functionalization of PEG moieties favored the outer surface rather than the inner pore surface compared to PO_3 and epoxide functionalization.

As the N_2 sorption isotherms (Figure 27A) hysteresis were still present and pore sizes remained in a similar range compared to plain DMSN, we confirmed a conserved mesoporous system after functionalization.

Table 2. Summarized analysis results of functionalized DMSN including values of plain DMSN for comparison. The amount of functionalized moiety was determined by TGA via mass loss compared to plain DMSN mass loss values. Mass loss, zeta potential and N_2 physisorption values are listed.

Sample	Mass loss [wt%]	Zeta [mV]	Surface Area [m^2 g^{-1}]	Pore Size [nm]	Pore Volume [cm^3 g^{-1}]
DMSN		-47	885	3.8	1.22
_PO_3	7	-46	711	3.4	0.90
_epox	9	-43	642	3.4	0.84
_PEG	11	-41	621	3.8	1.08

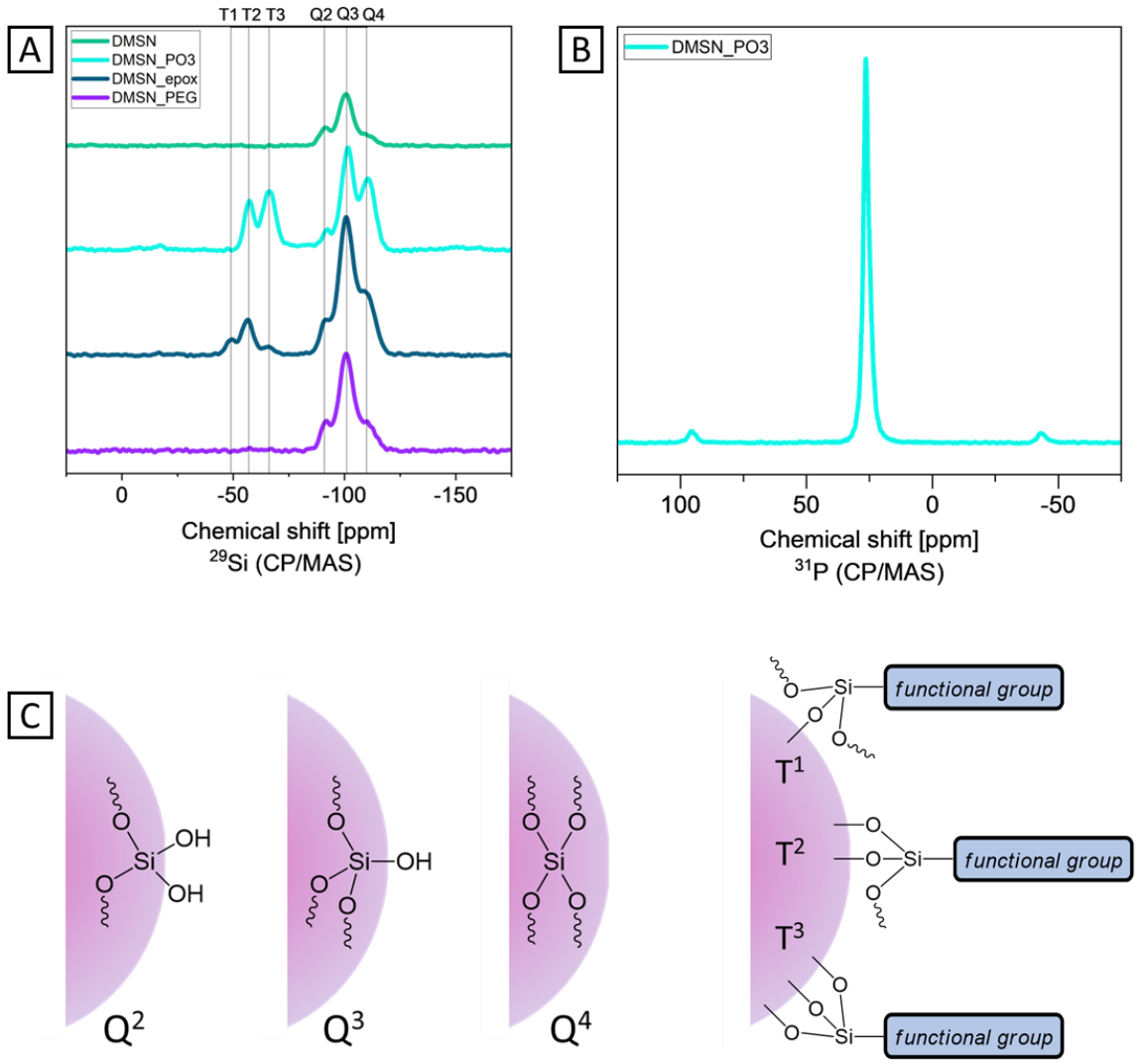

Figure 28. ^{29}Si and ^{31}P ssNMR data of DMSN. Figure A shows the ^{29}Si (CP/MAS) ssNMR spectra of plain DMSN and functionalized species. T and Q species were highlighted by vertical lines. Figure B shows the ^{31}P (CP/MAS) ssNMR spectrum of DMSN_PO_3. The corresponding assignations of Q- and T-species from ^{29}Si ssNMR were illustrated in Figure C. Figure C was created by the author of this thesis, based on Bouchoucha *et al.* (2016)[75].

Corresponding Q-species (Figure 28C) peaks were found for all DMSN, as shown in Figure 28A. Successful functionalization was confirmed by ^{29}Si ssNMR. In Figure 28A, the presence of T-species (T^1 = -49 ppm; T^2 = -58 ppm; T^3 = -66 ppm) for DMSN_PO_3 and DMSN_epox proved proper functionalization (as illustrated in Figure 28C) onto MSNs. No T-species were found for PEG-grafted DMSN. As von Baeckmann *et al.* (2021)[103], a former publication of the research group, reported absence of T-species for commercially available PEG silanes, DMSN_PEG was still assumed to be successfully grafted and applied for further studies.

The ^{31}P ssNMR (Figure 28B) for DMSN_PO_3 showed an intense peak at 26 ppm, confirming the presence of PO_3 species.

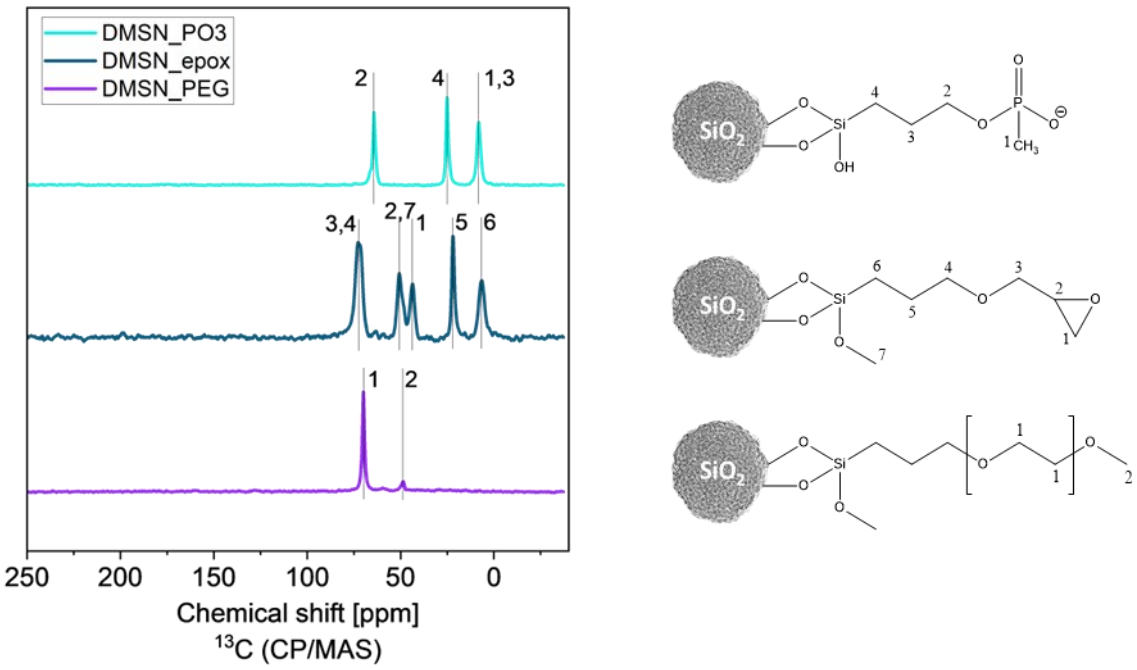

Figure 29. ^{13}C (CP/MAS) ssNMR spectra of functionalized DMSN with corresponding chemical structures. Peaks were assigned and highlighted in the chemical structures of the functional groups (PO_3, epoxide, PEG).

Successful functionalization without degradation or alteration of the moiety was confirmed for all MSNs. Corresponding peaks for all chemical structures were detected in ^{13}C ssNMR spectra, shown in Figure 29 with assigned peaks. For DMSN_PO_3, peaks at 64 ppm, 25 ppm and 8 ppm were found. For DMSN_epox, peaks at 72 ppm, 50 ppm, 44 ppm, 22 ppm and 7 ppm were assigned. DMSN_PEG showed one big peak at 70 ppm for the repetition unit of the polymer and one peak at 48 ppm. Therefore, stable functional groups without impurities and template residues were confirmed for all functionalized DMSN.

4.2.2 Characterization of Functionalized VINPs

Mass loss values were found to be 5 wt% for VINPs-epox and 10 wt% for VINPs_PEG. Zeta potential for VINPs_epox was determined as -39 mV and for VINPs_PEG as -30 mV, indicating negative surface charge.

For VINPs_PO_3, the zeta potential value was found to be higher (-46 mV) compared to plain VINPs (-49 mV) and surface area declined after functionalization. However, no mass loss was determined by TGA measurements. Therefore, the functionalization of VINPs_PO_3 was unsuccessful. Table 3 presents an overview of the analysis values of functionalized VINPs.

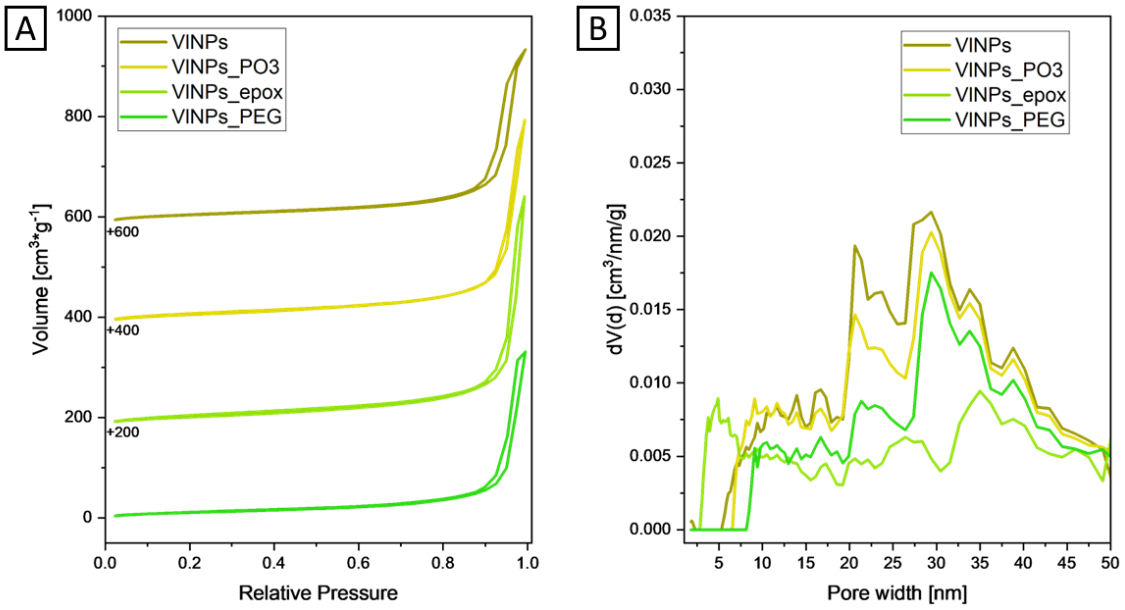

Figure 30. N_2 adsorption and desorption isotherms (Figure A) and pore size distributions (Figure B) of plain and functionalized VINPs at -196 °C.

As determined by N_2 physisorption, the surface area of all functionalized VINPs decreased compared to plain VINPs. The pore size was found to be in a similar wide range for functionalized VINPs. The pore volume changed slightly after functionalization. These values are summarized in Table 3. The minor decrease in pore volume after functionalization was ascribed to the special pore morphology for VINPs, outlined in Chapter 4.1.2. As the hysteresis in the sorption isotherms (Figure 30A) and the pore size range (Figure 30B) were conserved, we confirmed that the material did not lose mesoporosity after functionalization.

Table 3. Analysis overview of functionalized VINPs. Mass loss, zeta potential and N_2 physisorption values are listed.

Sample	Mass loss [wt%]	Zeta Potential [mV]	Surface Area [$m^2 g^{-1}$]	Pore Size [nm]	Pore Volume [$cm^3 g^{-1}$]
VINPs		-49	92	10-16	0.52
_PO3	0	-46	76	10-16	0.54
_epox	5	-39	79	5-16	0.50
_PEG	10	-30	47	10-16	0.42

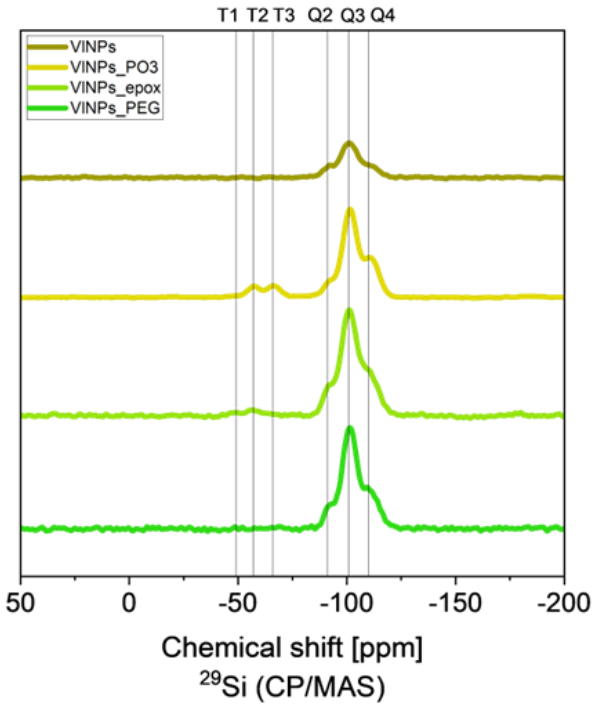

Figure 31. The ^{29}Si (CP/MAS) ssNMR spectra of plain and functionalized VINPs. T and Q species were assigned with vertical lines.

Successful functionalization was proven for VINPs by ^{29}Si ssNMR. Illustrated in Figure 31, peaks for the T-species were found for VINPs_PO_3 and VINPs_epox in the spectra. The description of Q- and T-species assignations can be found in Figure 28C. As previously outlined in Chapter 4.2.1, the absence of T-species for PEG-grafted VINPs cannot be concluded as unsuccessful functionalization. Thus, we confirmed successful functionalization of all VINPs except for VINPs_PO_3.

4.2.3 Characterization of Functionalized NrNPs

Mass loss was quantified as 10 wt% for NrNPs_PO_3, 11 wt% for NrNPs_epox and 7 wt% for NrNPs_PEG. Zeta potential was found for NrNPs_PO_3 to be -45 mV, for NrNPs_epox -42 mV and for NrNPs_PEG -36 mV. Thus, the surface charge for all designed NrNPs was found to be negative in H_2O. Table 4 summarizes the analysis values for plain and functionalized NrNPs.

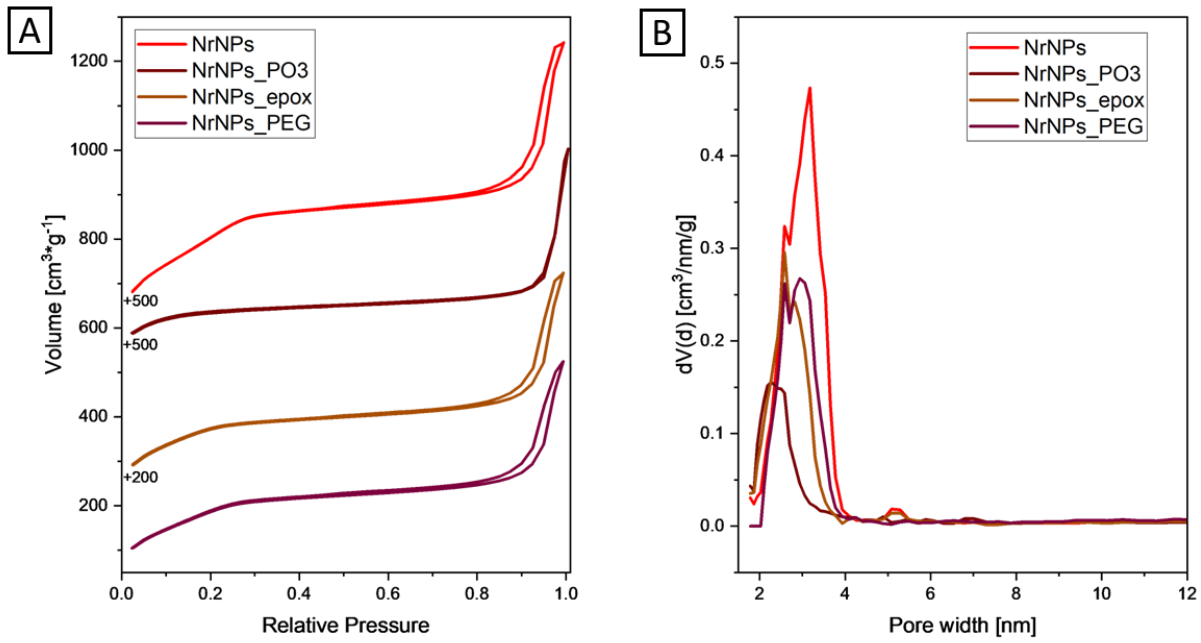

Figure 32. N_2 adsorption and desorption isotherms (Figure A) and pore size distributions (Figure B) of plain and functionalized NrNPs at -196 °C.

For NrNPs, a clear decline in surface area was observed after functionalization. For NrNPs_PO_3, the pore size decreased to 2.3 nm (from 3.2 nm plain NrNPs). For NrNPs_epox and NrNPs_PEG, pore sizes in a similar magnitude were determined. The pore volume decreased for all functionalized species. NrNPs_PO_3 showed for all N_2 physisorption values the strongest decline. These values are summarized in Table 4. The hysteresis in sorption isotherms was barely visible in Figure 32A. Thus, the mesoporosity was lost after PO_3 functionalization of NrNPs. However, the hysteresis of NrNPs_epox and NrNPs_PEG were conserved. Additionally, the pore sizes (Figure 32B) of these materials were in the mesoporous range. Therefore, the mesoporosity was still preserved for NrNPs_epox and NrNPs_PEG.

Table 4. Analysis overview of functionalized NrNPs. Mass loss, zeta potential and N_2 physisorption values are listed.

Sample	Mass loss [wt%]	Zeta Potential [mV]	Surface Area [$m^2 g^{-1}$]	Pore Size [nm]	Pore Volume [$cm^3 g^{-1}$]
NrNPs		-44	1041	3.2	1.04
_PO3	10	-45	478	2.3	0.42
_epox	11	-42	712	2.6	0.75
_PEG	7	-36	671	2.9	0.74

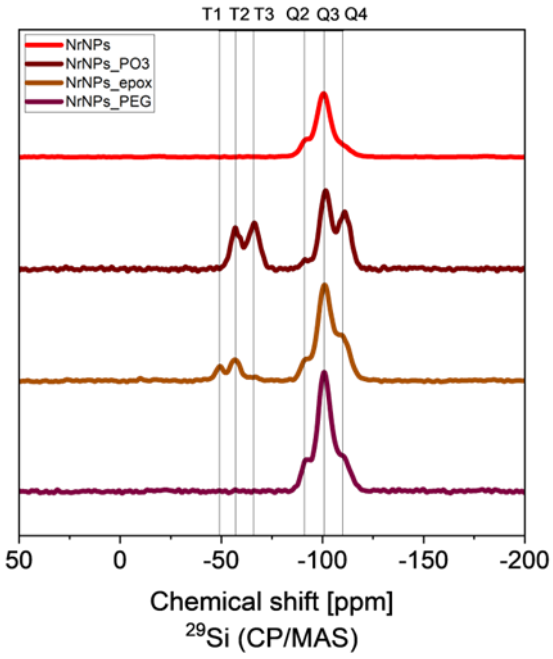

Figure 33. The ^{29}Si (CP/MAS) ssNMR spectra of plain and functionalized NrNPs. T and Q species were assigned with vertical lines.

^{29}Si ssNMR spectra of functionalized NrNPs are shown in Figure 33. The presence of T-species indicated successful functionalization for NrNPs_PO_3 and NrNPs_epox. The description of Q- and T-species assignations is shown in Figure 28C. As outlined in Chapter 4.2.1, the absence of T-species for commercially available PEG was expected and does not conclude unsuccessful functionalization of NrNPs_PEG.

4.3 Colloidal Stability

To investigate the colloidal stability of designed MSNs in H_2O, the particle size distribution and the change of average particle size over time were measured. Additionally, the colloidal stability of plain and functionalized DMSN in the pH range 8-2 was determined via zeta potential measurements. Corresponding graphs are shown in Figure 34 and Figure 35.

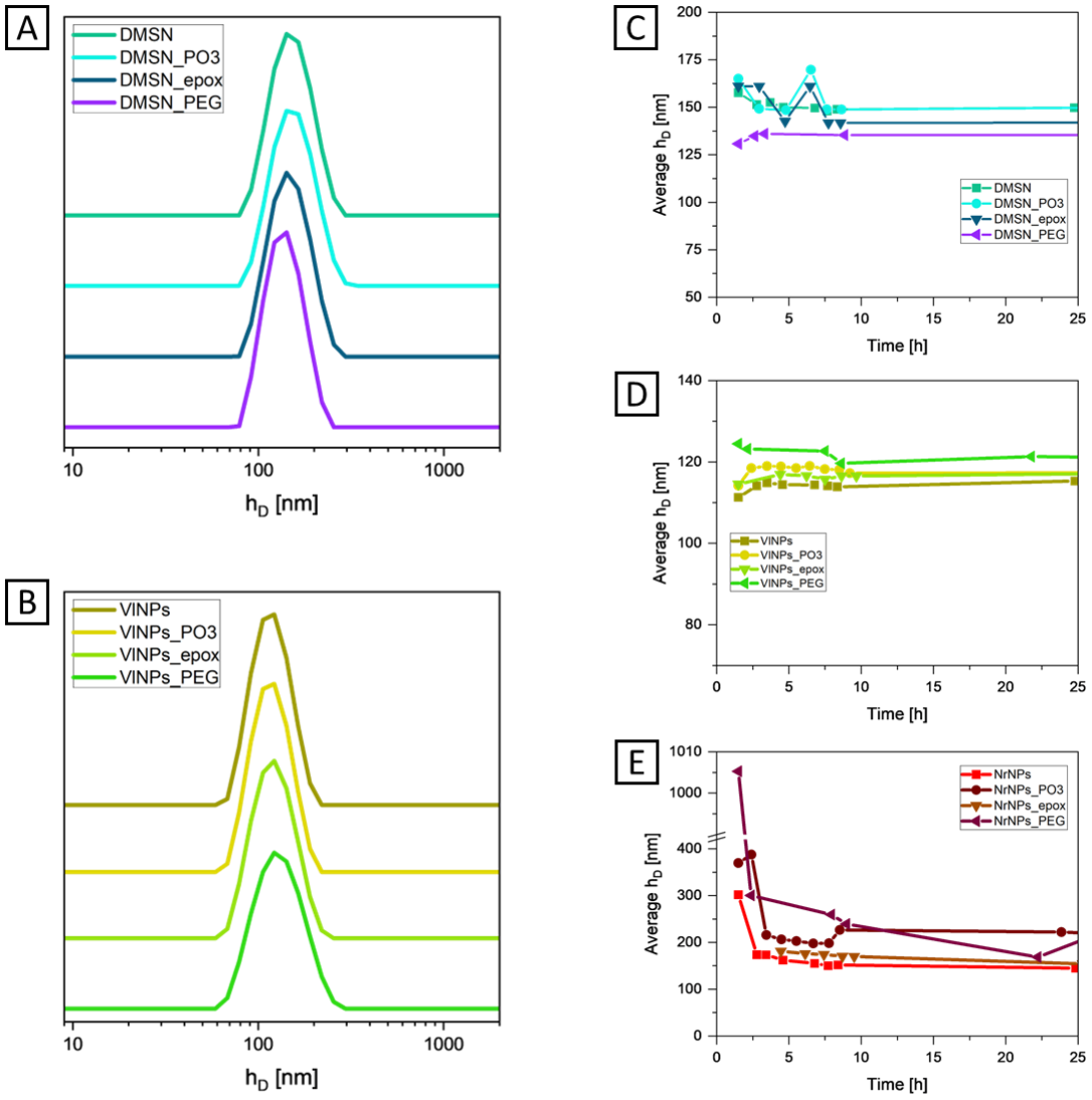

Figure 34. Particle size distribution and long-time h_D measurements for the evaluation of colloidal stability. Particle size distribution of plain and functionalized DMSN (Figure A) and VINPs (Figure B) are given. The plotted graphs suggested no significant agglomeration for all MSNs in H_2O as no intensity was measured in higher h_D regions. As h_D was measured via a model designed for spheres, the particle size distribution of NrNPs was not shown. Long-term stability measurements, average h_D over time in H_2O, for plain and functionalized DMSN (Figure C), VINPs (Figure D) and NrNPs (Figure E) are shown. Throughout 25 h, no significant decomposition was observed for all MSNs. In the first hours, minor size fluctuations were visible for DMSN_PO_3 and DMSN_epox in Figure C. As the h_D was measured via a model for spheres, anisotropic NrNPs showed minor deviations in Figure E.

The particle size distribution was measured to confirm colloidal stability in H_2O of designed plain and functionalized DMSN (Figure 34A) and VINPs (Figure 34B). As no additional peaks were found in lower and higher size ranges apart from the distinct peak, no degradation and agglomeration were detected. Thus, these values indicated colloidal stability in H_2O. As the model for h_D measurements was designed for spherical particles, the particle size distribution of NrNPs was not shown here.

The long-term stability of DMSN was investigated by measurements of average particle sizes as a function of time (Figure 34C). Stability over time was confirmed for plain and functionalized DMSN, as the average h_D did not show any significant deviations over the range of 24 h in H_2O. Therefore, no interparticle aggregation was assumed for plain and functionalized DMSN in the long term. The stability of plain and functionalized VINPs was investigated by the same technique (Figure 34D). As the average h_D was steady for more than 24 h in H_2O, long-term stability was proven for all VINPs without aggregation. The polydispersity index of all DMSN and VINPs was lower than 0.3 during the measurement duration. Thus, long-term colloidal stability in H_2O was proven for these samples. Average h_D as a function of time was measured for plain and functionalized NrNPs. Due to the model for spherical particles, strong deviations were found in the first 4 h for these anisotropic NrNPs. Afterwards, average h_D values were found to be stable for at least 24 h (Figure 34E). Therefore, long-term stability in H_2O without aggregation was also concluded for NrNPs.

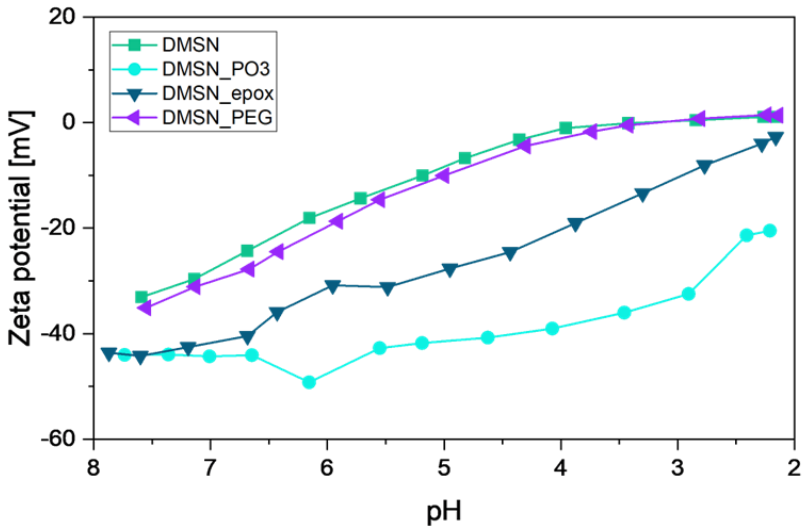

Figure 35. Measured zeta potentials of plain and functionalized DMSN as a function of pH 8 to 2.

Zeta potential as a function of pH was measured to determine the charge and colloidal stability of the particles in neutral to acidic medium. Noticeably, DMSN_PO_3 (-44 mV to -20 mV) exhibited negative charge over the entire pH range, as displayed in Figure 35. DMSN_epox (-44 mV to -3 mV) also showed negative charges in the entire range. Thus, colloidal stability was conserved for these materials in the measured pH range. The zeta potential range for DMSN_PEG reached

from -35 mV to +1 mV with the isoelectric point at pH 3.18. Plain DMSN showed a similar trend. Over pH 8-2, the zeta potential values of plain DMSN were -33 mV to +1 mV with an isoelectric point of 3.29. Therefore, DMSN_PEG and plain DMSN exhibited the protonated form[140,141] in lower pH and were suspected to aggregate.

Colloidal stability is favored for oral nano-detoxifiers to provide full adsorption capacity without interparticle pore blockage. To sum up, colloidal stability was proven due to narrow particle size distributions and long-term steady average h_D over time for all DMSN and VINPs. NrNPs showed deviant data due to the unsuitable measurement model. However, colloidal stability could not be excluded for NrNPs. Steady average h_D over time after 4 h suggested existing colloidal stability for NrNPs. To confirm this proposition, a measurement model for anisotropic NrNPs would be necessary. Because of zeta potential measurements in pH 8-2, we observed enhanced stability for DMSN_PO_3 and DMSN_epox. This was ascribed to electrostatic interparticle repulsion[75,97] as illustrated in Figure 6B. Thus, the adsorption capacity of DMSN_PO_3 and DMSN_epox was further evaluated. However, DMSN and DMSN_PEG were further investigated in preliminary adsorption studies due to the confirmed stability in neutral pH.

4.4 Results of Paracetamol Adsorption Studies

This Chapter reports the results of preliminary adsorption studies of MSNs. MSNs were loaded with paracetamol to gain information on the adsorption capacity. For the application as oral nano-detoxifiers, excellent adsorption capacities were necessary. Hereby, two main experiments were conducted, as previously described in Chapter 3.5. In the first experiment, paracetamol was adsorbed onto plain DMSN, VINPs and NrNPs **in ethanol for 2 h**. Adsorptions in **SGF and SIF** were also attempted.

For the second experiment, the adsorption of paracetamol of plain and functionalized DMSN (**in ethanol for 2 h and 6 h**) was quantified.

4.4.1 Paracetamol Adsorption of Plain DMSN, VINPs and NrNPs

To find the best material for further experiments, plain DMSN, VINPs and NrNPs were loaded with paracetamol **in ethanol for 2 h**.

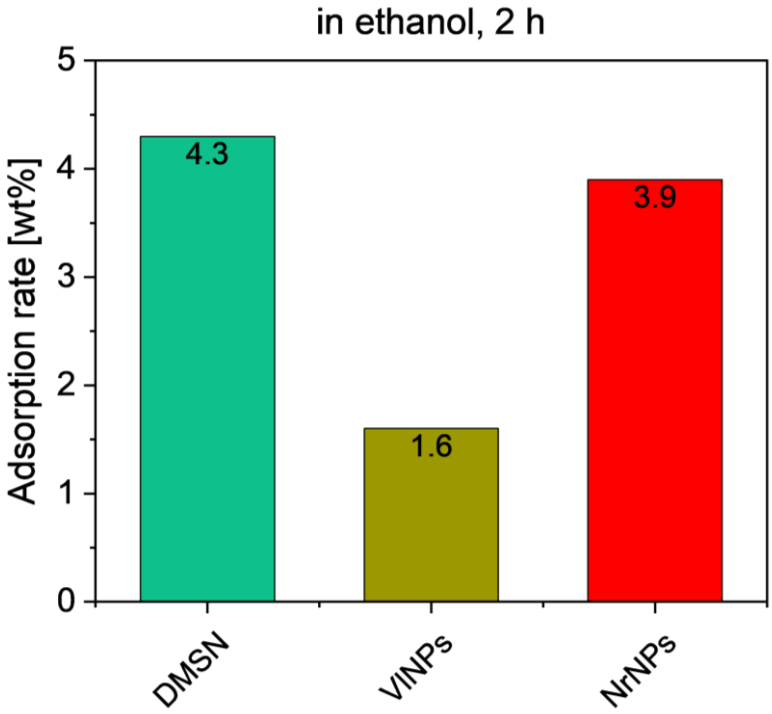

Figure 36. Quantification of adsorbed paracetamol determined by TGA onto plain DMSN, VINPs and NrNPs. Adsorption was practiced in ethanol for 2 h. DMSN (green) showed the highest adsorption rates, followed by NrNPs (red) and VINPs (yellow).

As seen in Figure 36, DMSN showed the highest paracetamol adsorption capacities (4.3 wt%) of all morphologies in ethanol. The adsorption values for NrNPs (3.9 wt%) were found to be in an acceptable range. Solely VlNPs showed significantly low paracetamol adsorption (1.6 wt%). This was ascribed to the special pore morphology as previously outlined in Chapter 4.1.2.

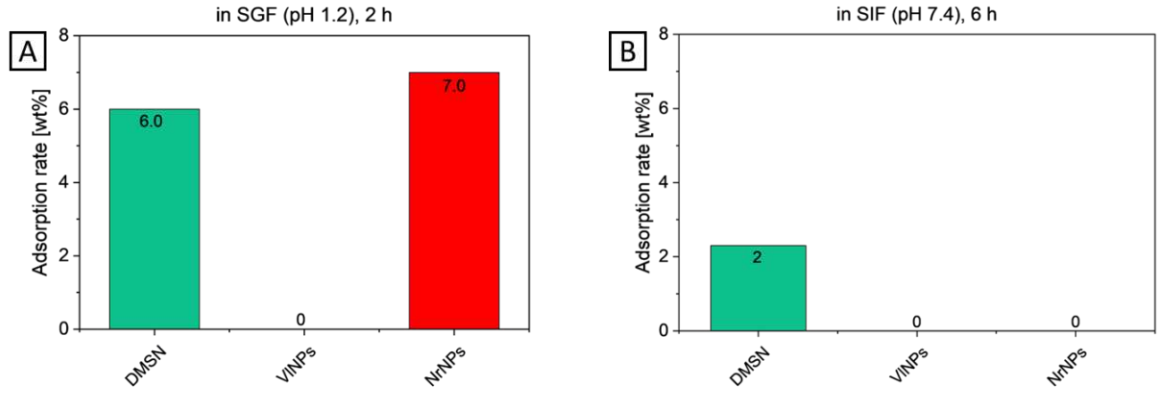

Figure 37. Bar charts of paracetamol adsorption results of DMSN (green), VlNPs and NrNPs (red) in SGF and SIF. Adsorptions were performed in SGF for 2 h (Figure A) and SIF for 6 h (Figure B).

To further simulate stomach and intestine conditions, adsorptions were performed in **SGF for 2 h** and **SIF for 6 h**. This was conducted for plain DMSN, VlNPs and NrNPs. Results are shown in Figure 37. DMSN was the only morphology to adsorb any paracetamol in both media (6 wt% in SGF, 2 wt% in SIF). NrNPs showed adsorption only in SGF (7 wt%). No paracetamol adsorption was measured for VlNPs in SGF and SIF. The significant decrease in adsorption capacity in SIF (pH 7.4) was ascribed to the deprotonation of the silanol surface[140,141], as outlined in Chapter 2.4.4. Due to the loss of hydrogen bond donors in the deprotonated state, paracetamol is less affine to interact with the inner-pore surfaces of the MSNs. Thus, the amount of adsorbed toxin decreased in SIF. As these results did not coincide with the observations from experiments in ethanol, further studies are necessary to optimize the adsorption procedure in SGF and SIF. The influence of aqueous SGF and SIF and accompanying salts and endogenous proteins need to be considered. These compete with paracetamol for adsorption sites of MSNs[155] and thus reduce the loading capacity.

Besides having the highest pore size values, DMSN also exhibited the highest adsorption capacity for model toxin paracetamol. Hence, this material was chosen for further experiments.

4.4.2 Paracetamol Adsorption of Functionalized DMSN

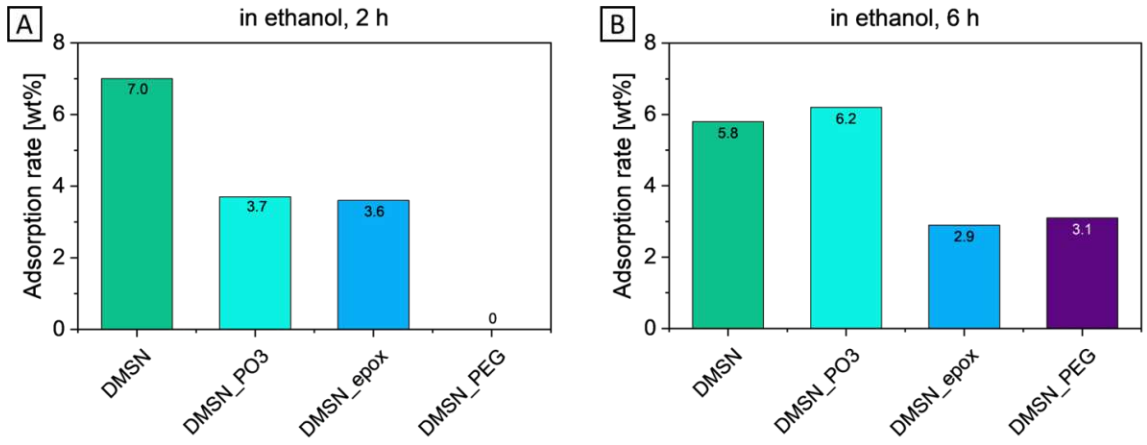

Figure 38. Paracetamol adsorption quantities of plain and functionalized DMSN. Adsorption was performed in ethanol for 2 h (Figure A) and 6 h (Figure B). After 2 h, plain DMSN (green) contained the highest amounts of paracetamol. After 6 h loading, DMSN_PO_3 (cyan) showed the highest adsorption values. DMSN_epox (blue) and DMSN_PEG (violet) showed the lowest amounts of paracetamol adsorption in both cases.

The paracetamol adsorption quantification of plain and functionalized DMSN was illustrated in Figure 38. Adsorptions were conducted **in ethanol for 2 h**, to simulate the time nano-detoxifiers remain in the stomach, and **in ethanol for 6 h** to simulate the time in the intestines.

2 h experiments (Figure 38A) gave the highest adsorption values for plain DMSN (7 wt%), followed by DMSN_PO_3 (3.7 wt%) and DMSN_epox (3.6 wt%). No paracetamol was adsorbed onto DMSN_PEG after 2 h. Hydrogen bonds between paracetamol and DMSN were suspected to be the predominant cause of adsorption. The bigger pore volumes of plain DMSN were another advantage for higher adsorption quantities. In the case of DMSN_PEG, the grafted polymer might have hindered paracetamol from entering the pores in this short period. Additionally, loading time was too short to reach the adsorption equilibrium.

After increasing the loading duration to **6 h** (Figure 38B, Table 5), DMSN_PO_3 was found to have the most paracetamol (6.2 wt%) adsorbed. This functionalization formed the strongest hydrogen bonds with paracetamol in the pores. The adsorbed amounts were lower for plain DMSN (5.8 wt%) and DMSN_epox (2.9 wt%) after 6 h compared to 2 h experiments. However, DMSN_PEG showed adsorption (3.1 wt%) for 6 h experiments. As the 6 h experiments showed adsorptions for all DMSN, these loaded materials were used for further characterization and studies.

Table 5. Summary of paracetamol adsorption results in ethanol for 6 h. Quantification (mass loss) monitored by TGA and surface area measured by N_2 physisorption of DMSN with the decrease (Δ) in surface area for comparison are listed.

Sample	Mass loss [wt%]	Surface Area [$m^2 g^{-1}$]	Δ Surface Area [%]
DMSN_Parac	5.8	731	16
DMSN_PO_3_Parac	6.2	570	20
DMSN_epox_Parac	2.9	582	9
DMSN_PEG_Parac	3.1	563	9

Table 5 summarizes the results and characterization of 6 h adsorption experiments in ethanol. Quantification of paracetamol adsorption and the decrease (%) in surface area after adsorption are listed. After paracetamol adsorption, a decrease in surface area was noticed for all DMSN. This change corresponded with mass loss in the magnitude of three times. Therefore, TGA was a suitable method to quantify adsorbed paracetamol. Corresponding N_2 physisorption isotherms and pore size distribution graphs of adsorbed DMSN are shown in Figure 39.

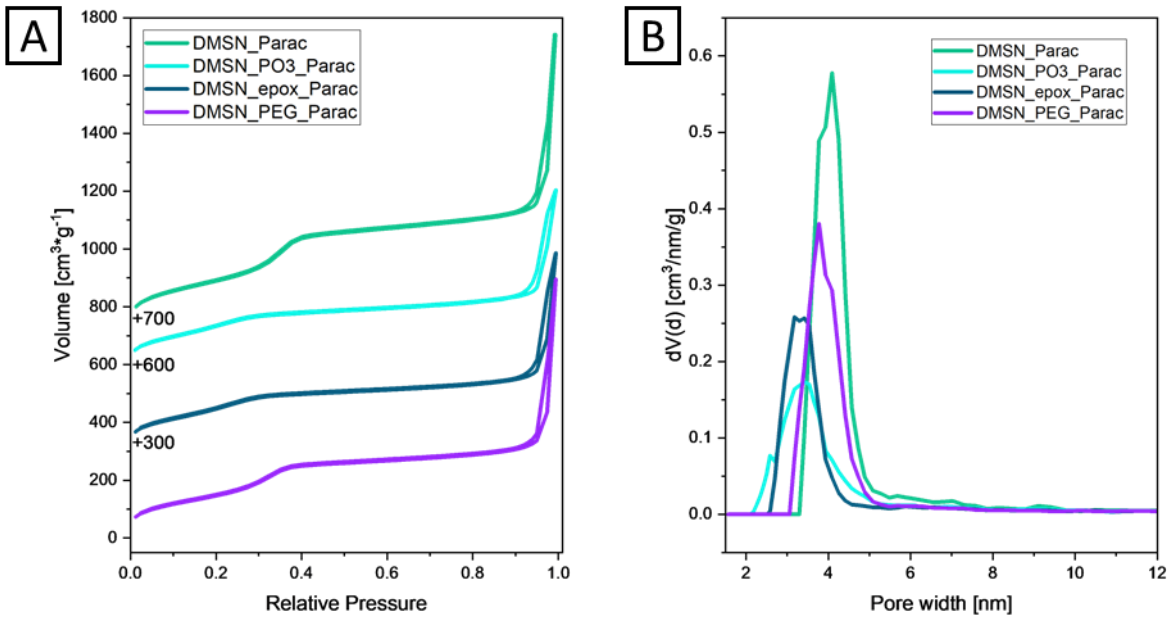

Figure 39. N_2 physisorption isotherms (Figure A) and pore size distribution approximations (Figure B) of paracetamol-adsorbed (6 h, in ethanol) plain and functionalized DMSN measured at -196 °C.

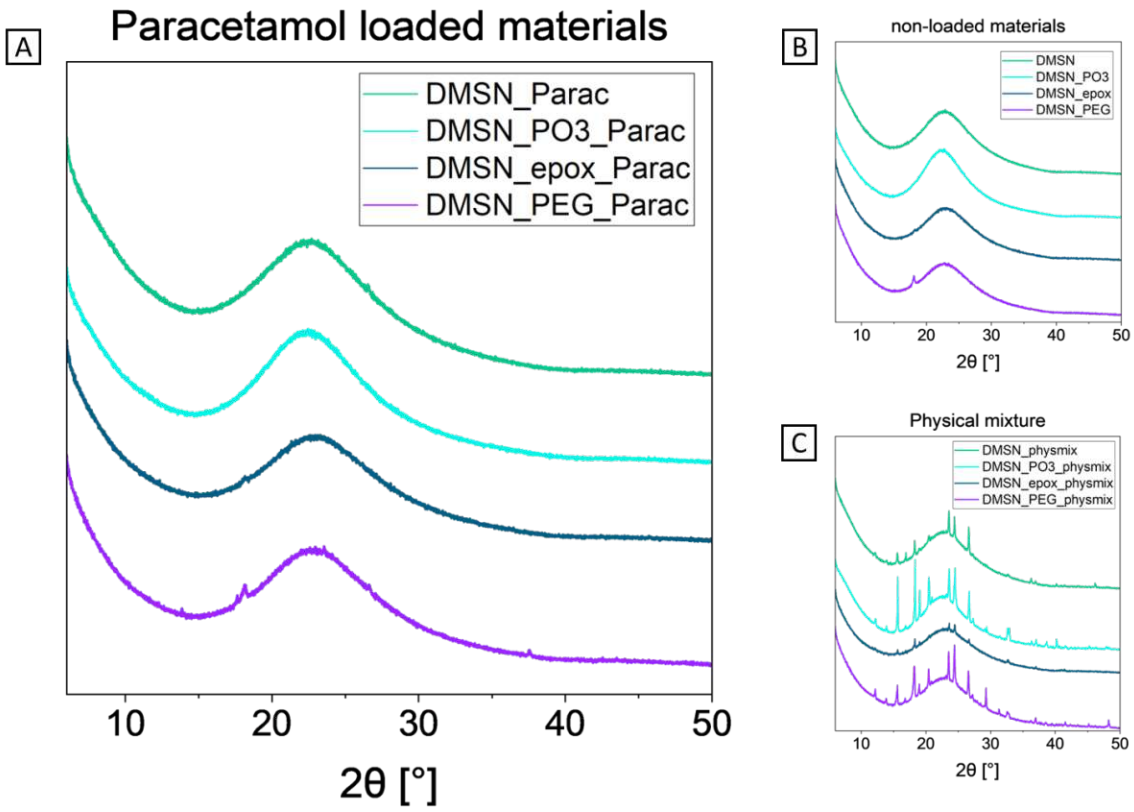

Figure 40. PXRD results of paracetamol adsorbed DMSN. Figure A shows the PXRD pattern of paracetamol-adsorbed (in ethanol, 6 h) plain and functionalized DMSN. Pore confinement of paracetamol was proven due to the absence of crystalline peaks. For comparison, PXRD pattern of non-loaded DMSN (Figure B) and physical mixtures with paracetamol (Figure C) were introduced.

PXRD patterns of loaded DMSN (Figure 40A) were monitored to determine the confinement of paracetamol in the mesopores. Due to the absence of crystalline peaks in the pattern, amorphous paracetamol was confirmed to be adsorbed in the pores only[149,150], as outlined in Chapter 2.4.4. For comparison, PXRD was taken for non-loaded MSNs (Figure 40B). The presence of the small peak at 18° in the DMSN_PEG_Parac pattern was therefore assigned to impurities of the material. To assure the visibility of possible crystalline peaks at given adsorption quantities, PXRD patterns of physical mixtures (Figure 40C) were measured. Sharp crystalline peaks were easily visible for physical mixtures. Thus, the confinement of the model toxin paracetamol was successful for all DMSN.

Due to the higher adsorption capacity for paracetamol and the verified confinement in the mesopores, DMSN_PO_3 was found to be the best material for adsorption experiments performed in ethanol for 6 h. The higher affinity to paracetamol was ascribed to the introduced functional groups, as DMSN_PO_3 holds more hydrogen bond acceptors[98] compared to plain silanol. Another suitable candidate for paracetamol adsorption was plain DMSN. The formation of hydrogen bonds between paracetamol and plain silanol groups was favored compared to DMSN_epox and DMSN_PEG. Another contributing factor could be the steric hindrance of the PEG moieties, which shielded the diffusion of paracetamol.

4.5 Results of Release Studies

Paracetamol-adsorbed functionalized DMSN (6 h, in ethanol) were evaluated for release together with adsorbed plain VINPs and NrNPs (2 h, in ethanol). These experiments were conducted to monitor the potential release of confined paracetamol in SGF and SIF. Corresponding release graphs are shown in Figure 41.

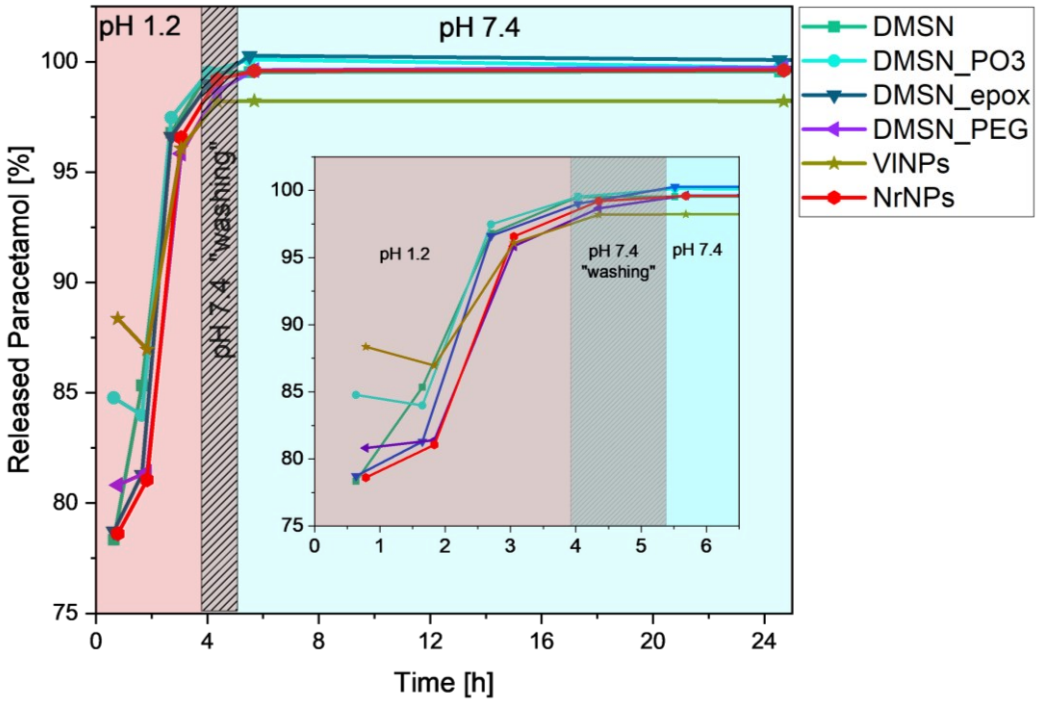

Figure 41. Paracetamol release rate (normalized to the total released amount for each MSN) as a function of time (in h). Samples taken from release in SGF were highlighted in pink, from SIF in blue. The performed washing step is indicated by a dashed background.

Most paracetamol was released in the first hours. The drug concentration after the change of solution was found to be significantly low. Solely minor paracetamol quantities below the limit of Lambert-Beer were monitored in UV/vis for samples taken after 6 h. Consequently, a different approach to monitor release in alkaline medium would be necessary to gain more accurate results for UV/vis measurements.

All MSNs showed similar release curves. Solely for VINPs, faster release for the first 2 h was observed in Figure 41. This was ascribed to the specific pore morphology for VINPs, outlined in Chapter 4.1.2. Compared to other morphologies, paracetamol could only be loosely adsorbed at the interstices of surface spikes resulting in faster release.

For the application as oral nano-detoxifiers, toxins must not be released in the body at all. Thus, further studies to improve the confinement of the toxin are necessary.

5 Conclusions and Perspectives

5.1 Design of Silica-Based Oral Nano-Detoxifiers

To summarize, the preparation of suitable silica-based oral nano-detoxifiers was accomplished. In the scope of this project, we were able to control the morphology of the silica-based oral nano-detoxifiers. Three different morphologies were successfully synthesized: DMSN, VINPs and NrNPs. The influence of selected parameters on these syntheses was observed. Due to the high porosity, DMSN were found to be the best morphologies for the application as oral nano-detoxifiers. Summary and perspectives on paracetamol adsorption were further outlined in the following Chapter 5.2.

PO_3 and epoxide were introduced as functional groups for the preservation of colloidal stability[75,97] and to enhance the model toxin adsorption capacity[98,99]. The stability of the best candidate DMSN_PO_3 in harsh stomach acidity and colloidal stability were confirmed in this project. PEG functionalization was performed to reduce the formation of protein corona in GIT serum.[101–103] The reduced protein corona formation would need to be confirmed in further studies. Additionally, the size of the protein corona on the particles needs to be observed to be able to predict further aspects and difficulties in the performance in biological systems.[18,93]

For further studies, it would be advisable to increase the particle size of MSNs.[75,89,90] Preventing epithelium transfer of toxin-adsorbed nano-detoxifiers into the bloodstream is crucial for the safety of patients. For large-scale industry production, synthesis procedures need to be adapted for up-scaling.

5.2 Summary and Perspectives of Adsorption Studies

Preliminary adsorption studies of the model toxin paracetamol onto plain MSNs again highlighted the highest loading capacity for DMSN compared to other morphologies. Furthermore, the comparison of the paracetamol adsorption capacity of plain and functionalized DMSN in ethanol revealed the best quantities for DMSN_PO_3 and plain DMSN. This was ascribed to the hydrogen donors and acceptors in the surface structures for sufficient hydrogen bond formation.[98,144] With confirmed colloidal stability and sufficient adsorption capacity, DMSN_PO_3 was found to be the best oral nano-detoxifier for model toxin paracetamol in ethanol.

The main adsorption studies were performed in ethanol. Using SGF and SIF as adsorption medium was attempted for plain MSNs. In SGF, higher adsorption capacities were determined compared to SIF. The reason was ascribed to the pH of the media. In pH 1.2 of SGF, protonated silanol groups of plain MSNs exhibit more possible hydrogen binding sites compared to the deprotonated silanol groups at pH 7.4 of SIF.[140,141] For further studies, the incorporation of functional groups with pK_a > 7.4 and hydrogen binding sites could be attempted. The functional groups would not deprotonate in SIF. Thus, hydrogen bonds with paracetamol would be ensured in neutral pH. However, the colloidal stability would not be conserved due to the lack of interparticle repulsion. DMSN_PO_3 was not tested for paracetamol adsorption in SGF and SIF yet. However, due to the pK_a 2 of PO_3 functional groups[75], the number of hydrogen bond contributors could be decreased in SIF due to deprotonation. Thus, we expect lower adsorption capacities for DMSN_PO_3.

However, the presence of hydrogen bonds needs to be proven by shifts observed in Fourier-Transform Infrared Spectroscopy.[156] In the course of this project, the amount of adsorbed drug was too low to be visible in the spectra.

Former studies on MSNs adsorption conducted by Bui *et al.* (2011)[157] showed lower adsorption capacities for paracetamol compared to other common drugs. They concluded higher adsorption affinities for cationic drugs through a wide pH range. Additionally, increased hydrophobicity gave higher adsorption rates. Another attempt in this study was to introduce trimethylsilyl surface functionalization on the MSNs. This led to increased adsorption rates at higher pH conditions. This effect was attributed to the higher hydrophobicity of the material. Thus, for further detoxification studies, the use of cationic or hydrophobic toxins might lead to higher adsorption capacity. In this case, electrostatic interactions would contribute to adsorption. Additionally, the use of hydrophobic functional groups could provide better adsorption in aqueous medium.

5.3 Summary and Perspectives of Release Studies

Another important aspect is the release rate of adsorbed paracetamol in SGF and SIF. Excessive amounts of paracetamol were released after the first minutes for all tested MSNs. For detoxification, the toxin must not be released at all. The goal is to fully remove all toxins from the body. Thus, an additional system to trap the toxin inside the pores is striving for further studies. A strategy towards protein corona formation in the intestines or particle agglomeration could be utilized to seal the pores after toxin adsorption. However, the influence of changed material properties on the safety of the patients would need to be considered. Additionally, another measurement method for lower toxin concentrations released, such as High-Performance Liquid

Chromatography, would be suitable. Thus, smaller sample volumes would be needed, leading to better accuracy of the experiment.

Depending on health status, environment and eating behavior, the composition of enzymes in GIT media and bowel emptying frequency could differ drastically between individuals.[45] Thus, creating an “one-fits-all” medium is hardly realizable. For further oral detoxification studies, including additional parameters of GIT, such as the presence of degrading enzymes[50], is recommended. In this way, the safety of individual patients can be ensured.

5.4 Further Perspectives on Selectivity

Although the adsorption of model toxin paracetamol onto designed silica-based oral nano-detoxifiers was observed in this master’s project, the adsorption selectivity of metabolites will need to be further attended. The metabolite NAPQI directly influences the hepatotoxicity of paracetamol overdose.[131] Thus, a pathway for the selective removal of NAPQI would be the final goal of this research project. Inspired by the natural excretion[132], glutathione functionalization could be aimed for the selective removal of NAPQI. The sulfated and glucuronided metabolites of paracetamol were reported to be less harmful than NAPQI.[129,130] However, these metabolites could still be used as noninvasive model toxins for further selectivity studies. For enhanced adsorption affinity of acetaminophen sulfate, thiol groups would be suitable. As the chemical structure of acetaminophen glucuronide exhibits the large glucuronide residue and hydrogen binding sites, designing functional groups representing perfect fitting “key-lock” hosts for the large glucuronide residue could offer a solution for selective adsorption.[158]

For another approach, the deprotonation of the metabolites at pH 7.4 of SIF could be used. The pK_a of acetaminophen sulfate[159] was reported as -2.2 and 3.2 for acetaminophen glucuronide[160]. The structures would be negatively charged at pH 7.4 compared to paracetamol[126] (pK_a 9.3). Thus, positively charged functional groups could enhance the affinity of MSNs for metabolites due to electrostatic interactions. In this case, the low adsorption capacity of paracetamol is suitable for the selective removal of metabolites. Thus, the drug would still be present in the body for therapeutical purposes. However, this approach could not be used for the real toxin NAPQI[161], as the pK_a of this compound is 19.1. Therefore, this metabolite would not be charged in the pH range of the GIT.

6 References

(1) National Capital Poison Center. *National Poison Controll Call Statistics, 2021*. https://www.poison.org/poison-statistics-national (accessed 2023-06-15).

(2) Eddleston, M. Patterns and Problems of Deliberate Self-poisoning in the Developing World. *QJM* **2000**, *93* (11), 715–731. https://doi.org/10.1093/qjmed/93.11.715.

(3) Graham, L. M.; Nguyen, T. M.; Lee, S. B. Nanodetoxification: Emerging Role of Nanomaterials in Drug Intoxication Treatment. *Nanomed.* **2011**, *6* (5), 921–928. https://doi.org/10.2217/nnm.11.75.

(4) Juère, E.; Florek, J.; Bouchoucha, M.; Jambhrunkar, S.; Wong, K. Y.; Popat, A.; Kleitz, F. *In Vitro* Dissolution, Cellular Membrane Permeability, and Anti-Inflammatory Response of Resveratrol-Encapsulated Mesoporous Silica Nanoparticles. *Mol. Pharm.* **2017**, *14* (12), 4431–4441. https://doi.org/10.1021/acs.molpharmaceut.7b00529.

(5) Li, L.; Liu, T.; Fu, C.; Tan, L.; Meng, X.; Liu, H. Biodistribution, Excretion, and Toxicity of Mesoporous Silica Nanoparticles after Oral Administration Depend on Their Shape. *Nanomedicine Nanotechnol. Biol. Med.* **2015**, *11* (8), 1915–1924. https://doi.org/10.1016/j.nano.2015.07.004.

(6) Uges, D. R. A. What Is the Definition of a Poisoning? *J. Clin. Forensic Med.* **2001**, *8* (1), 30–33. https://doi.org/10.1054/jcfm.2000.0465.

(7) Paracelsus. *Labyrintus Und Irrgang Der Vermeinten Artzet*; von Bodenstein, A., Ed.; Perna, 1574.

(8) Müller, D.; Desel, H. Common Causes of Poisoning. *Dtsch. Ärztebl. Int.* **2013**, *110* (41), 690–700. https://doi.org/10.3238/arztebl.2013.0690.

(9) Mowry, J. B.; Spyker, D. A.; Brooks, D. E.; McMillan, N.; Schauben, J. L. 2014 Annual Report of the American Association of Poison Control Centers' National Poison Data System (NPDS): 32nd Annual Report. *Clin. Toxicol.* **2015**, *53* (10), 962–1147. https://doi.org/10.3109/15563650.2015.1102927.

(10) Presgrave, R. D. F.; Camacho, L. A. B.; Villas Boas, M. H. S. A Profile of Unintentional Poisoning Caused by Household Cleaning Products, Disinfectants and Pesticides. *Cad. Saúde Pública* **2008**, *24* (12), 2901–2908. https://doi.org/10.1590/S0102-311X2008001200019.

(11) Gaw, C. E.; Osterhoudt, K. C. Ethanol Intoxication of Young Children. *Pediatr. Emerg. Care* **2019**, *35* (10), 722–730. https://doi.org/10.1097/PEC.0000000000001946.

(12) Jones, L. O. Poisoning. *Anaesth. Intensive Care Med.* **2006**, *7* (4), 132–134. https://doi.org/10.1383/anes.2006.7.4.132.

(13) Wennig, R.; Eyer, F.; Schaper, A.; Zilker, T.; Andresen-Streichert, H. Mushroom Poisoning. *Dtsch. Ärztebl. Int.* **2020**, *117*, 701–708. https://doi.org/10.3238/arztebl.2020.0701.

(14) Taylor, S. L.; Stratton, J. E.; Nordlee, J. A. Histamine Poisoning (Scombroid Fish Poisoning): An Allergy-Like Intoxication. *J. Toxicol. Clin. Toxicol.* **1989**, *27* (4–5), 225–240. https://doi.org/10.3109/15563658908994420.
(15) Hungerford, J. M. Scombroid Poisoning: A Review. *Toxicon* **2010**, *56* (2), 231–243. https://doi.org/10.1016/j.toxicon.2010.02.006.
(16) Eddleston, M. Novel Clinical Toxicology and Pharmacology of Organophosphorus Insecticide Self-Poisoning. *Annu. Rev. Pharmacol. Toxicol.* **2019**, *59* (1), 341–360. https://doi.org/10.1146/annurev-pharmtox-010818-021842.
(17) Kloske, M.; Witkiewicz, Z. Novichoks – The A Group of Organophosphorus Chemical Warfare Agents. *Chemosphere* **2019**, *221*, 672–682. https://doi.org/10.1016/j.chemosphere.2019.01.054.
(18) Janjua, T. I.; Cao, Y.; Kleitz, F.; Linden, M.; Yu, C.; Popat, A. Silica Nanoparticles: A Review of Their Safety and Current Strategies to Overcome Biological Barriers. *Adv. Drug Deliv. Rev.* **2023**, *203*, 115115. https://doi.org/10.1016/j.addr.2023.115115.
(19) Abeer, M. M.; Rewatkar, P.; Qu, Z.; Talekar, M.; Kleitz, F.; Schmid, R.; Lindén, M.; Kumeria, T.; Popat, A. Silica Nanoparticles: A Promising Platform for Enhanced Oral Delivery of Macromolecules. *J. Controlled Release* **2020**, *326*, 544–555. https://doi.org/10.1016/j.jconrel.2020.07.021.
(20) Florek, J.; Caillard, R.; Kleitz, F. Evaluation of Mesoporous Silica Nanoparticles for Oral Drug Delivery – Current Status and Perspective of MSNs Drug Carriers. *Nanoscale* **2017**, *9* (40), 15252–15277. https://doi.org/10.1039/C7NR05762H.
(21) Juère, E.; Del Favero, G.; Masse, F.; Marko, D.; Popat, A.; Florek, J.; Caillard, R.; Kleitz, F. Gastro-Protective Protein-Silica Nanoparticles Formulation for Oral Drug Delivery: In Vitro Release, Cytotoxicity and Mitochondrial Activity. *Eur. J. Pharm. Biopharm.* **2020**, *151*, 171–180. https://doi.org/10.1016/j.ejpb.2020.03.015.
(22) Tollemeto, M.; Huang, Z.; Christensen, J. B.; Mørck Nielsen, H.; Rønholt, S. Mucoadhesive Dendrons Conjugated to Mesoporous Silica Nanoparticles as a Drug Delivery Approach for Orally Administered Biopharmaceuticals. *ACS Appl. Mater. Interfaces* **2023**, *15* (7), 8798–8810. https://doi.org/10.1021/acsami.2c16502.
(23) Eurostat. *Accidents and injuries statistics 2020*. https://ec.europa.eu/eurostat/statistics-explained/index.php?title=Accidents_and_injuries_statistics#Healthcare_for_injuries.2C_poisoning_and_other_consequences_of_external_causes (accessed 2024-01-23).
(24) Eurostat. *Causes of death - standardised death rate by NUTS 2 region of residence. Online data code: hlth_cd_asdr2*. https://ec.europa.eu/eurostat/databrowser/view/hlth_cd_asdr2/default/table?lang=en (accessed 2024-01-23).
(25) STATISTIK AUSTRIA. *Todesursachenstatistik. Gestorbene in Österreich ab 1970 nach Todesursachen und Geschlecht*.

https://www.statistik.at/statistiken/bevoelkerung-und-soziales/bevoelkerung/gestorbene/todesursachen (accessed 2024-01-23).
(26) KFV Kuratorium für Verkehrssicherheit. *Vorsicht giftig! Jährlich rund 800 Kinder-Vergiftungsunfälle*. https://www.kfv.at/vorsicht-giftig-jaehrlich-rund-800-kinder-vergiftungsunfaelle/ (accessed 2024-01-23).
(27) Bundesministerium für Soziales, Gesundheit, Pflege und Konsumentenschutz (BMSGPK). *Suizid und Suizidprävention in Österreich*. https://www.sozialministerium.at/dam/jcr:802889bf-4033-4280-ac4e-6ad2ef02eda5/Suizidbericht_2023.pdf.
(28) Ornillo, C.; Harbord, N. Fundaments of Toxicology—Approach to the Poisoned Patient. *Adv. Chronic Kidney Dis.* **2020**, *27* (1), 5–10. https://doi.org/10.1053/j.ackd.2019.12.001.
(29) Jacobsen, D. The Relative Efficacy of Antidotes. *J. Toxicol. Clin. Toxicol.* **1995**, *33* (6), 705–708. https://doi.org/10.3109/15563659509010633.
(30) Chacko, B.; Peter, J. V. Antidotes in Poisoning. *Indian J. Crit. Care Med.* **2019**, *23* (4), 241–249. https://doi.org/10.5005/jp-journals-10071-23310.
(31) Joshi, P. B.; Chavali, M.; Tripati, G. K.; Tondwalkar, S. Medical Applications of Activated Carbon. In *Activated Carbon*; Verma, C., Quraishi, M. A., Eds.; The Royal Society of Chemistry, 2023; pp 42–54. https://doi.org/10.1039/BK9781839169861-00042.
(32) Kim, J.-J.; Kim, Y.-S.; Kumar, V. Heavy Metal Toxicity: An Update of Chelating Therapeutic Strategies. *J. Trace Elem. Med. Biol.* **2019**, *54*, 226–231. https://doi.org/10.1016/j.jtemb.2019.05.003.
(33) Jacobsen, D.; McMartin, K. E. Antidotes for Methanol and Ethylene Glycol Poisoning. *J. Toxicol. Clin. Toxicol.* **1997**, *35* (2), 127–143. https://doi.org/10.3109/15563659709001182.
(34) Marraffa, J. M.; Cohen, V.; Howland, M. A. Antidotes for Toxicological Emergencies: A Practical Review. *Am. J. Health. Syst. Pharm.* **2012**, *69* (3), 199–212. https://doi.org/10.2146/ajhp110014.
(35) Prescott, L. F.; Illingworth, R. N.; Critchley, J. A.; Stewart, M. J.; Adam, R. D.; Proudfoot, A. T. Intravenous N-Acetylcystine: The Treatment of Choice for Paracetamol Poisoning. *BMJ* **1979**, *2* (6198), 1097–1100. https://doi.org/10.1136/bmj.2.6198.1097.
(36) Heard, K. J. Acetylcysteine for Acetaminophen Poisoning. *N. Engl. J. Med.* **2008**, *359* (3), 285–292. https://doi.org/10.1056/NEJMct0708278.
(37) Bruno, G. R.; Howland, M. A.; McMeeking, A.; Hoffman, R. S. Long-Acting Anticoagulant Overdose: Brodifacoum Kinetics and Optimal Vitamin K Dosing. *Ann. Emerg. Med.* **2000**, *36* (3), 262–267. https://doi.org/10.1067/mem.2000.108317.
(38) Benson, B. E.; Hoppu, K.; Troutman, W. G.; Bedry, R.; Erdman, A.; Höjer, J.; Mégarbane, B.; Thanacoody, R.; Caravati, E. M. Position Paper Update: Gastric

Lavage for Gastrointestinal Decontamination. *Clin. Toxicol.* **2013**, *51* (3), 140–146. https://doi.org/10.3109/15563650.2013.770154.
(39) American Academy of Clinical Toxicology; European Association of Poisons Centres and Clinical Toxicologists,. Position Paper: Gastric Lavage. *J. Toxicol. Clin. Toxicol.* **2004**, *42* (7), 933–943. https://doi.org/10.1081/CLT-200045006.
(40) Eddleston, M.; Haggalla, S.; Reginald, K.; Sudarshan, K.; Senthilkumaran, M.; Karalliedde, L.; Ariaratnam, A.; Sheriff, M. H. R.; Warrell, D. A.; Buckley, N. A. The Hazards of Gastric Lavage for Intentional Self-Poisoning in a Resource Poor Location. *Clin. Toxicol.* **2007**, *45* (2), 136–143. https://doi.org/10.1080/15563650601006009.
(41) Yeates, P. J. A.; Thomas, S. H. L. Effectiveness of Delayed Activated Charcoal Administration in Simulated Paracetamol (Acetaminophen) Overdose: Delayed Activated Charcoal Efficacy. *Br. J. Clin. Pharmacol.* **2000**, *49* (1), 11–14. https://doi.org/10.1046/j.1365-2125.2000.00107.x.
(42) Zellner, T.; Prasa, D.; Färber, E.; Hoffmann-Walbeck, P.; Genser, D.; Eyer, F. The Use of Activated Charcoal to Treat Intoxications. *Dtsch. Ärztebl. Int.* **2019**, *116*, 311–317. https://doi.org/10.3238/arztebl.2019.0311.
(43) Bouchard, J.; Lavergne, V.; Roberts, D. M.; Cormier, M.; Morissette, G.; Ghannoum, M. Availability and Cost of Extracorporeal Treatments for Poisonings and Other Emergency Indications: A Worldwide Survey. *Nephrol. Dial. Transplant.* **2017**, *32* (4), 699–706. https://doi.org/10.1093/ndt/gfw456.
(44) Morishita, M.; Peppas, N. A. Is the Oral Route Possible for Peptide and Protein Drug Delivery? *Drug Discov. Today* **2006**, *11* (19–20), 905–910. https://doi.org/10.1016/j.drudis.2006.08.005.
(45) Durán-Lobato, M.; Niu, Z.; Alonso, M. J. Oral Delivery of Biologics for Precision Medicine. *Adv. Mater.* **2020**, *32* (13), 1901935. https://doi.org/10.1002/adma.201901935.
(46) Chisaka, H.; Matsushima, Y.; Wada, F.; Saeki, S.; Hachisuka, K. Dynamics of Capsule Swallowing by Healthy Young Men and Capsule Transit Time from the Mouth to the Stomach. *Dysphagia* **2007**, *21* (4), 275–279. https://doi.org/10.1007/s00455-006-9054-3.
(47) Caffarel-Salvador, E.; Abramson, A.; Langer, R.; Traverso, G. Oral Delivery of Biologics Using Drug-Device Combinations. *Curr. Opin. Pharmacol.* **2017**, *36*, 8–13. https://doi.org/10.1016/j.coph.2017.07.003.
(48) Johansson, M. E. V.; Sjövall, H.; Hansson, G. C. The Gastrointestinal Mucus System in Health and Disease. *Nat. Rev. Gastroenterol. Hepatol.* **2013**, *10* (6), 352–361. https://doi.org/10.1038/nrgastro.2013.35.
(49) Boegh, M.; García-Díaz, M.; Müllertz, A.; Nielsen, H. M. Steric and Interactive Barrier Properties of Intestinal Mucus Elucidated by Particle Diffusion and Peptide Permeation. *Eur. J. Pharm. Biopharm.* **2015**, *95*, 136–143. https://doi.org/10.1016/j.ejpb.2015.01.014.

(50) Boland, M. Human Digestion – a Processing Perspective. *J. Sci. Food Agric.* **2016**, *96* (7), 2275–2283. https://doi.org/10.1002/jsfa.7601.
(51) Juère, E.; Caillard, R.; Marko, D.; Del Favero, G.; Kleitz, F. Smart Protein-Based Formulation of Dendritic Mesoporous Silica Nanoparticles: Toward Oral Delivery of Insulin. *Chem. – Eur. J.* **2020**, *26* (23), 5195–5199. https://doi.org/10.1002/chem.202000773.
(52) Iriarte-Mesa, C.; Jobst, M.; Bergen, J.; Kiss, E.; Ryoo, R.; Kim, J.-C.; Crudo, F.; Marko, D.; Kleitz, F.; Del Favero, G. Morphology-Dependent Interaction of Silica Nanoparticles with Intestinal Cells: Connecting Shape to Barrier Function. *Nano Lett.* **2023**, *23* (16), 7758–7766. https://doi.org/10.1021/acs.nanolett.3c00835.
(53) Goldberg, M.; Gomez-Orellana, I. Challenges for the Oral Delivery of Macromolecules. *Nat. Rev. Drug Discov.* **2003**, *2* (4), 289–295. https://doi.org/10.1038/nrd1067.
(54) Rojas, S.; Baati, T.; Njim, L.; Manchego, L.; Neffati, F.; Abdeljelil, N.; Saguem, S.; Serre, C.; Najjar, M. F.; Zakhama, A.; Horcajada, P. Metal–Organic Frameworks as Efficient Oral Detoxifying Agents. *J. Am. Chem. Soc.* **2018**, *140* (30), 9581–9586. https://doi.org/10.1021/jacs.8b04435.
(55) Anselmo, A. C.; Mitragotri, S. Nanoparticles in the Clinic: An Update. *Bioeng. Transl. Med.* **2019**, *4* (3), e10143. https://doi.org/10.1002/btm2.10143.
(56) Anselmo, A. C.; Mitragotri, S. Nanoparticles in the Clinic: An Update Post COVID -19 Vaccines. *Bioeng. Transl. Med.* **2021**, *6* (3), e10246. https://doi.org/10.1002/btm2.10246.
(57) Muhammad, F.; Nguyen, T. D. T.; Raza, A.; Akhtar, B.; Aryal, S. A Review on Nanoparticle-Based Technologies for Biodetoxification. *Drug Chem. Toxicol.* **2017**, *40* (4), 489–497. https://doi.org/10.1080/01480545.2016.1277736.
(58) Comenge, J.; Sotelo, C.; Romero, F.; Gallego, O.; Barnadas, A.; Parada, T. G.-C.; Domínguez, F.; Puntes, V. F. Detoxifying Antitumoral Drugs via Nanoconjugation: The Case of Gold Nanoparticles and Cisplatin. *PLoS ONE* **2012**, *7* (10), e47562. https://doi.org/10.1371/journal.pone.0047562.
(59) Hu, X.; Tulsieram, K. L.; Zhou, Q.; Mu, L.; Wen, J. Polymeric Nanoparticle–Aptamer Bioconjugates Can Diminish the Toxicity of Mercury in Vivo. *Toxicol. Lett.* **2012**, *208* (1), 69–74. https://doi.org/10.1016/j.toxlet.2011.10.006.
(60) Wei, W.; Du, J.; Li, J.; Yan, M.; Zhu, Q.; Jin, X.; Zhu, X.; Hu, Z.; Tang, Y.; Lu, Y. Construction of Robust Enzyme Nanocapsules for Effective Organophosphate Decontamination, Detoxification, and Protection. *Adv. Mater.* **2013**, *25* (15), 2212–2218. https://doi.org/10.1002/adma.201205138.
(61) Howell, B.; Chauhan, A. Uptake of Amitriptyline and Nortriptyline with Liposomes, Proteins, and Serum: Implications for Drug Detoxification. *J. Colloid Interface Sci.* **2008**, *319* (1), 81–93. https://doi.org/10.1016/j.jcis.2007.11.018.
(62) Herrmann, I. K.; Urner, M.; Koehler, F. M.; Hasler, M.; Roth-Z'Graggen, B.; Grass, R. N.; Ziegler, U.; Beck-Schimmer, B.; Stark, W. J. Blood Purification Using

Functionalized Core/Shell Nanomagnets. *Small* **2010**, *6* (13), 1388–1392. https://doi.org/10.1002/smll.201000438.
(63) Lestari, W. W.; Meilani, R.; Nurcahyo, I. F.; Larasati, L.; Dendy, D. In Situ Electro-Synthesis of EDTA-Modified MIL-100(Fe) as an Enhanced Candidate Detoxifying Agent for Pb(II) and Its Adsorption Characteristics. *J. Inorg. Organomet. Polym. Mater.* **2023**, *34*, 1028–1039. https://doi.org/10.1007/s10904-023-02868-6.
(64) Gibson, G. G.; Skett, P. *Introduction to Drug Metabolism*; Chapman and Hall: London, 1986.
(65) Xu, P.; Guo, S.; Yu, H.; Li, X. Mesoporous Silica Nanoparticles (MSNs) for Detoxification of Hazardous Organophorous Chemicals. *Small* **2014**, *10* (12), 2404–2412. https://doi.org/10.1002/smll.201303633.
(66) Vidaurre-Agut, C.; Rivero-Buceta, E.; Romaní-Cubells, E.; Clemments, A. M.; Vera-Donoso, C. D.; Landry, C. C.; Botella, P. Protein Corona over Mesoporous Silica Nanoparticles: Influence of the Pore Diameter on Competitive Adsorption and Application to Prostate Cancer Diagnostics. *ACS Omega* **2019**, *4* (5), 8852–8861. https://doi.org/10.1021/acsomega.9b00460.
(67) Pangestu, A.; Lestari, W. W.; Wibowo, F. R.; Larasati, L. Green Electro-Synthesized MIL-101(Fe) and Its Aspirin Detoxification Performance Compared to MOF-808. *J. Inorg. Organomet. Polym. Mater.* **2022**, *32* (5), 1828–1839. https://doi.org/10.1007/s10904-022-02235-x.
(68) Leroux, J.-C. Injectable Nanocarriers for Biodetoxification. *Nat. Nanotechnol.* **2007**, *2* (11), 679–684. https://doi.org/10.1038/nnano.2007.339.
(69) Howell, B. A.; Chauhan, A. Current and Emerging Detoxification Therapies for Critical Care. *Materials* **2010**, *3* (4), 2483–2505. https://doi.org/10.3390/ma3042483.
(70) Wang, L.; Han, K.; Jiang, X.; Mao, C.; Li, X.; Zhou, M. Recent Advances in Blood Toxin Removal Technology. *Sustain. Mater. Technol.* **2024**, *39*, e00828. https://doi.org/10.1016/j.susmat.2024.e00828.
(71) Rojas, S.; Guillou, N.; Horcajada, P. Ti-Based nanoMOF as an Efficient Oral Therapeutic Agent. *ACS Appl. Mater. Interfaces* **2019**, *11* (25), 22188–22193. https://doi.org/10.1021/acsami.9b06472.
(72) Salek, A.; Selmi, M.; Njim, L.; Umek, P.; Mejanelle, P.; Moussa, F.; Douki, W.; Hosni, K.; Baati, T. Titanate Nanotubes as an Efficient Oral Detoxifying Agent against Drug Overdose: Application in Rat Acetaminophen Poisoning. *Nanoscale Adv.* **2023**, *5* (11), 2950–2962. https://doi.org/10.1039/D2NA00874B.
(73) Mekaru, H.; Lu, J.; Tamanoi, F. Development of Mesoporous Silica-Based Nanoparticles with Controlled Release Capability for Cancer Therapy. *Adv. Drug Deliv. Rev.* **2015**, *95*, 40–49. https://doi.org/10.1016/j.addr.2015.09.009.
(74) Yang, Y.; Zhang, M.; Song, H.; Yu, C. Silica-Based Nanoparticles for Biomedical Applications: From Nanocarriers to Biomodulators. *Acc. Chem. Res.* **2020**, *53* (8), 1545–1556. https://doi.org/10.1021/acs.accounts.0c00280.

(75) Bouchoucha, M.; Côté, M.-F.; C.-Gaudreault, R.; Fortin, M.-A.; Kleitz, F. Size-Controlled Functionalized Mesoporous Silica Nanoparticles for Tunable Drug Release and Enhanced Anti-Tumoral Activity. *Chem. Mater.* **2016**, *28* (12), 4243–4258. https://doi.org/10.1021/acs.chemmater.6b00877.
(76) Diagboya, P. N. E.; Dikio, E. D. Silica-Based Mesoporous Materials; Emerging Designer Adsorbents for Aqueous Pollutants Removal and Water Treatment. *Microporous Mesoporous Mater.* **2018**, *266*, 252–267. https://doi.org/10.1016/j.micromeso.2018.03.008.
(77) von Baeckmann, C.; Guillet-Nicolas, R.; Renfer, D.; Kählig, H.; Kleitz, F. A Toolbox for the Synthesis of Multifunctionalized Mesoporous Silica Nanoparticles for Biomedical Applications. *ACS Omega* **2018**, *3* (12), 17496–17510. https://doi.org/10.1021/acsomega.8b02784.
(78) Bouchoucha, M.; C.-Gaudreault, R.; Fortin, M.-A.; Kleitz, F. Mesoporous Silica Nanoparticles: Selective Surface Functionalization for Optimal Relaxometric and Drug Loading Performances. *Adv. Funct. Mater.* **2014**, *24* (37), 5911–5923. https://doi.org/10.1002/adfm.201400524.
(79) Wu, S.-H.; Mou, C.-Y.; Lin, H.-P. Synthesis of Mesoporous Silica Nanoparticles. *Chem. Soc. Rev.* **2013**, *42* (9), 3862. https://doi.org/10.1039/c3cs35405a.
(80) Tiemann, M.; Weinberger, C. Selective Modification of Hierarchical Pores and Surfaces in Nanoporous Materials. *Adv. Mater. Interfaces* **2021**, *8* (4), 2001153. https://doi.org/10.1002/admi.202001153.
(81) Bobo, D.; Robinson, K. J.; Islam, J.; Thurecht, K. J.; Corrie, S. R. Nanoparticle-Based Medicines: A Review of FDA-Approved Materials and Clinical Trials to Date. *Pharm. Res.* **2016**, *33* (10), 2373–2387. https://doi.org/10.1007/s11095-016-1958-5.
(82) 21CFR172.480, Title 21; CFR Code of Federal Regulations, 2018; Vol. 3, 2018.
(83) Lindén, M. Biodistribution and Excretion of Intravenously Injected Mesoporous Silica Nanoparticles: Implications for Drug Delivery Efficiency and Safety. In *The Enzymes*; Elsevier, 2018; Vol. 43, pp 155–180. https://doi.org/10.1016/bs.enz.2018.07.007.
(84) Croissant, J. G.; Fatieiev, Y.; Khashab, N. M. Degradability and Clearance of Silicon, Organosilica, Silsesquioxane, Silica Mixed Oxide, and Mesoporous Silica Nanoparticles. *Adv. Mater.* **2017**, *29* (9), 1604634. https://doi.org/10.1002/adma.201604634.
(85) Hao, N.; Liu, H.; Li, L.; Chen, D.; Li, L.; Tang, F. *In Vitro* Degradation Behavior of Silica Nanoparticles Under Physiological Conditions. *J. Nanosci. Nanotechnol.* **2012**, *12* (8), 6346–6354. https://doi.org/10.1166/jnn.2012.6199.
(86) Yu, M.; Wang, J.; Yang, Y.; Zhu, C.; Su, Q.; Guo, S.; Sun, J.; Gan, Y.; Shi, X.; Gao, H. Rotation-Facilitated Rapid Transport of Nanorods in Mucosal Tissues. *Nano Lett.* **2016**, *16* (11), 7176–7182. https://doi.org/10.1021/acs.nanolett.6b03515.

(87) Zheng, N.; Li, J.; Xu, C.; Xu, L.; Li, S.; Xu, L. Mesoporous Silica Nanorods for Improved Oral Drug Absorption. *Artif. Cells Nanomedicine Biotechnol.* **2018**, *46* (6), 1132–1140. https://doi.org/10.1080/21691401.2017.1362414.
(88) Farjadian, F.; Ahmadpour, P.; Samani, S. M.; Hosseini, M. Controlled Size Synthesis and Application of Nanosphere MCM-41 as Potent Adsorber of Drugs: A Novel Approach to New Antidote Agent for Intoxication. *Microporous Mesoporous Mater.* **2015**, *213*, 30–39. https://doi.org/10.1016/j.micromeso.2015.04.002.
(89) Lu, F.; Wu, S.-H.; Hung, Y.; Mou, C.-Y. Size Effect on Cell Uptake in Well-Suspended, Uniform Mesoporous Silica Nanoparticles. *Small* **2009**, *5* (12), 1408–1413. https://doi.org/10.1002/smll.200900005.
(90) Kim, H. L.; Lee, S. B.; Jeong, H. J.; Kim, D. W. Enhanced Tumor Targetability of PEGylated Mesoporous Silica Nanoparticles on in Vivo Optical Imaging According to Their Size. *RSC Adv* **2014**, *4* (59), 31318–31322. https://doi.org/10.1039/C4RA03905J.
(91) Sun, B.; Zhou, G.; Zhang, H. Synthesis, Functionalization, and Applications of Morphology-Controllable Silica-Based Nanostructures: A Review. *Prog. Solid State Chem.* **2016**, *44* (1), 1–19. https://doi.org/10.1016/j.progsolidstchem.2016.01.001.
(92) Berardi, A.; Baldelli Bombelli, F. Oral Delivery of Nanoparticles - Let's Not Forget about the Protein Corona. *Expert Opin. Drug Deliv.* **2019**, *16* (6), 563–566. https://doi.org/10.1080/17425247.2019.1610384.
(93) Von Baeckmann, C.; Kählig, H.; Lindén, M.; Kleitz, F. Irreversible Adsorption of Serum Proteins onto Nanoparticles. *Part. Part. Syst. Charact.* **2021**, *38* (1), 2000273. https://doi.org/10.1002/ppsc.202000273.
(94) Souris, J. S.; Lee, C.-H.; Cheng, S.-H.; Chen, C.-T.; Yang, C.-S.; Ho, J. A.; Mou, C.-Y.; Lo, L.-W. Surface Charge-Mediated Rapid Hepatobiliary Excretion of Mesoporous Silica Nanoparticles. *Biomaterials* **2010**, *31* (21), 5564–5574. https://doi.org/10.1016/j.biomaterials.2010.03.048.
(95) Clemments, A. M.; Muniesa, C.; Landry, C. C.; Botella, P. Effect of Surface Properties in Protein Corona Development on Mesoporous Silica Nanoparticles. *RSC Adv* **2014**, *4* (55), 29134–29138. https://doi.org/10.1039/C4RA03277B.
(96) Tarn, D.; Ashley, C. E.; Xue, M.; Carnes, E. C.; Zink, J. I.; Brinker, C. J. Mesoporous Silica Nanoparticle Nanocarriers: Biofunctionality and Biocompatibility. *Acc. Chem. Res.* **2013**, *46* (3), 792–801. https://doi.org/10.1021/ar3000986.
(97) Lu, J.; Liong, M.; Zink, J. I.; Tamanoi, F. Mesoporous Silica Nanoparticles as a Delivery System for Hydrophobic Anticancer Drugs. *Small* **2007**, *3* (8), 1341–1346. https://doi.org/10.1002/smll.200700005.
(98) Huynh, R. P. S.; Evans, D. R.; Lian, J. X.; Spasyuk, D.; Siahrostrami, S.; Shimizu, G. K. H. Creating Order in Ultrastable Phosphonate Metal–Organic Frameworks

via Isolable Hydrogen-Bonded Intermediates. *J. Am. Chem. Soc.* **2023**, *145* (39), 21263–21272. https://doi.org/10.1021/jacs.3c05279.

(99) Rother, D.; Sen, T.; East, D.; Bruce, I. J. Silicon, Silica and Its Surface Patterning/Activation with Alkoxy- and Amino-Silanes for Nanomedical Applications. *Nanomed.* **2011**, *6* (2), 281–300. https://doi.org/10.2217/nnm.10.159.

(100) Wang, J.-Q.; Sun, J.; Cheng, W.-G.; Dong, K.; Zhang, X.-P.; Zhang, S.-J. Experimental and Theoretical Studies on Hydrogen Bond-Promoted Fixation of Carbon Dioxide and Epoxides in Cyclic Carbonates. *Phys. Chem. Chem. Phys.* **2012**, *14* (31), 11021. https://doi.org/10.1039/c2cp41698k.

(101) Cauda, V.; Schlossbauer, A.; Bein, T. Bio-Degradation Study of Colloidal Mesoporous Silica Nanoparticles: Effect of Surface Functionalization with Organo-Silanes and Poly(Ethylene Glycol). *Microporous Mesoporous Mater.* **2010**, *132* (1–2), 60–71. https://doi.org/10.1016/j.micromeso.2009.11.015.

(102) Pelaz, B.; Del Pino, P.; Maffre, P.; Hartmann, R.; Gallego, M.; Rivera-Fernández, S.; De La Fuente, J. M.; Nienhaus, G. U.; Parak, W. J. Surface Functionalization of Nanoparticles with Polyethylene Glycol: Effects on Protein Adsorption and Cellular Uptake. *ACS Nano* **2015**, *9* (7), 6996–7008. https://doi.org/10.1021/acsnano.5b01326.

(103) von Baeckmann, C.; Kählig, H.; Lindén, M.; Kleitz, F. On the Importance of the Linking Chemistry for the PEGylation of Mesoporous Silica Nanoparticles. *J. Colloid Interface Sci.* **2021**, *589*, 453–461. https://doi.org/10.1016/j.jcis.2020.12.004.

(104) Faria, M.; Björnmalm, M.; Thurecht, K. J.; Kent, S. J.; Parton, R. G.; Kavallaris, M.; Johnston, A. P. R.; Gooding, J. J.; Corrie, S. R.; Boyd, B. J.; Thordarson, P.; Whittaker, A. K.; Stevens, M. M.; Prestidge, C. A.; Porter, C. J. H.; Parak, W. J.; Davis, T. P.; Crampin, E. J.; Caruso, F. Minimum Information Reporting in Bio–Nano Experimental Literature. *Nat. Nanotechnol.* **2018**, *13* (9), 777–785. https://doi.org/10.1038/s41565-018-0246-4.

(105) Stöber, W.; Fink, A.; Bohn, E. Controlled Growth of Monodisperse Silica Spheres in the Micron Size Range. *J. Colloid Interface Sci.* **1968**, *26* (1), 62–69. https://doi.org/10.1016/0021-9797(68)90272-5.

(106) Unger, K.; Rupprecht, H.; Valentin, B.; Kircher, W. The Use of Porous and Surface Modified Silicas as Drug Delivery and Stabilizing Agents. *Drug Dev. Ind. Pharm.* **1983**, *9* (1–2), 69–91. https://doi.org/10.3109/03639048309048546.

(107) Beck, J. S.; Vartuli, J. C.; Roth, W. J.; Leonowicz, M. E.; Kresge, C. T.; Schmitt, K. D.; Chu, C. T. W.; Olson, D. H.; Sheppard, E. W.; McCullen, S. B.; Higgins, J. B.; Schlenker, J. L. A New Family of Mesoporous Molecular Sieves Prepared with Liquid Crystal Templates. *J. Am. Chem. Soc.* **1992**, *114* (27), 10834–10843. https://doi.org/10.1021/ja00053a020.

(108) Zhao, D.; Feng, J.; Huo, Q.; Melosh, N.; Fredrickson, G. H.; Chmelka, B. F.; Stucky, G. D. Triblock Copolymer Syntheses of Mesoporous Silica with Periodic

50 to 300 Angstrom Pores. *Science* **1998**, *279* (5350), 548–552. https://doi.org/10.1126/science.279.5350.548.

(109) Han, Y.-J.; Stucky, G. D.; Butler, A. Mesoporous Silicate Sequestration and Release of Proteins. *J. Am. Chem. Soc.* **1999**, *121* (42), 9897–9898. https://doi.org/10.1021/ja992138r.

(110) Lai, C.-Y.; Trewyn, B. G.; Jeftinija, D. M.; Jeftinija, K.; Xu, S.; Jeftinija, S.; Lin, V. S.-Y. A Mesoporous Silica Nanosphere-Based Carrier System with Chemically Removable CdS Nanoparticle Caps for Stimuli-Responsive Controlled Release of Neurotransmitters and Drug Molecules. *J. Am. Chem. Soc.* **2003**, *125* (15), 4451–4459. https://doi.org/10.1021/ja028650l.

(111) Nam, L.; Coll, C.; Erthal, L.; De La Torre, C.; Serrano, D.; Martínez-Máñez, R.; Santos-Martínez, M.; Ruiz-Hernández, E. Drug Delivery Nanosystems for the Localized Treatment of Glioblastoma Multiforme. *Materials* **2018**, *11* (5), 779. https://doi.org/10.3390/ma11050779.

(112) Pal, N.; Bhaumik, A. Soft Templating Strategies for the Synthesis of Mesoporous Materials: Inorganic, Organic–Inorganic Hybrid and Purely Organic Solids. *Adv. Colloid Interface Sci.* **2013**, *189–190*, 21–41. https://doi.org/10.1016/j.cis.2012.12.002.

(113) Florek, J.; Guillet-Nicolas, R.; Kleitz, F. Ordered Mesoporous Silica: Synthesis and Applications. In *Functional Materials: For Energy, Sustainable Development and Biomedical Sciences*; Leclerc, M., Gauvin, R., Eds.; Walter de Gruyter GmbH & Co KG, 2014; pp 61–100.

(114) Pal, N.; Lee, J.-H.; Cho, E.-B. Recent Trends in Morphology-Controlled Synthesis and Application of Mesoporous Silica Nanoparticles. *Nanomaterials* **2020**, *10* (11), 2122. https://doi.org/10.3390/nano10112122.

(115) Han, L.; Zhou, Y.; He, T.; Song, G.; Wu, F.; Jiang, F.; Hu, J. One-Pot Morphology-Controlled Synthesis of Various Shaped Mesoporous Silica Nanoparticles. *J. Mater. Sci.* **2013**, *48* (17), 5718–5726. https://doi.org/10.1007/s10853-013-7501-8.

(116) Li, F.; Wang, Z.; Stein, A. Shaping Mesoporous Silica Nanoparticles by Disassembly of Hierarchically Porous Structures. *Angew. Chem. Int. Ed.* **2007**, *46* (11), 1885–1888. https://doi.org/10.1002/anie.200604147.

(117) Huang, X.; Teng, X.; Chen, D.; Tang, F.; He, J. The Effect of the Shape of Mesoporous Silica Nanoparticles on Cellular Uptake and Cell Function. *Biomaterials* **2010**, *31* (3), 438–448. https://doi.org/10.1016/j.biomaterials.2009.09.060.

(118) Hao, N.; Li, L.; Tang, F. Roles of Particle Size, Shape and Surface Chemistry of Mesoporous Silica Nanomaterials on Biological Systems. *Int. Mater. Rev.* **2017**, *62* (2), 57–77. https://doi.org/10.1080/09506608.2016.1190118.

(119) Cai, Q.; Luo, Z.-S.; Pang, W.-Q.; Fan, Y.-W.; Chen, X.-H.; Cui, F.-Z. Dilute Solution Routes to Various Controllable Morphologies of MCM-41 Silica with a

Basic Medium. *Chem. Mater.* **2001**, *13* (2), 258–263. https://doi.org/10.1021/cm990661z.

(120) Wang, Y.; Song, H.; Yu, M.; Xu, C.; Liu, Y.; Tang, J.; Yang, Y.; Yu, C. Room Temperature Synthesis of Dendritic Mesoporous Silica Nanoparticles with Small Sizes and Enhanced mRNA Delivery Performance. *J. Mater. Chem. B* **2018**, *6* (24), 4089–4095. https://doi.org/10.1039/C8TB00544C.

(121) Wang, W.; Wang, P.; Tang, X.; Elzatahry, A. A.; Wang, S.; Al-Dahyan, D.; Zhao, M.; Yao, C.; Hung, C.-T.; Zhu, X.; Zhao, T.; Li, X.; Zhang, F.; Zhao, D. Facile Synthesis of Uniform Virus-like Mesoporous Silica Nanoparticles for Enhanced Cellular Internalization. *ACS Cent. Sci.* **2017**, *3* (8), 839–846. https://doi.org/10.1021/acscentsci.7b00257.

(122) Jin, H.; Liu, Z.; Ohsuna, T.; Terasaki, O.; Inoue, Y.; Sakamoto, K.; Nakanishi, T.; Ariga, K.; Che, S. Control of Morphology and Helicity of Chiral Mesoporous Silica. *Adv. Mater.* **2006**, *18* (5), 593–596. https://doi.org/10.1002/adma.200502038.

(123) Herdiana, Y.; Wathoni, N.; Shamsuddin, S.; Muchtaridi, M. Scale-up Polymeric-Based Nanoparticles Drug Delivery Systems: Development and Challenges. *OpenNano* **2022**, *7*, 100048. https://doi.org/10.1016/j.onano.2022.100048.

(124) Liu, Y.; Yao, Y.; Fu, J.; Hu, W.; Feng, J.; Wan, J.; Yu, C. Large-Scale Synthesis of Fractal Silica Nanoparticles: Understanding the Impact of Solvents. *Microporous Mesoporous Mater.* **2021**, *316*, 110976. https://doi.org/10.1016/j.micromeso.2021.110976.

(125) Williams, R.; Karuranga, S.; Malanda, B.; Saeedi, P.; Basit, A.; Besançon, S.; Bommer, C.; Esteghamati, A.; Ogurtsova, K.; Zhang, P.; Colagiuri, S. Global and Regional Estimates and Projections of Diabetes-Related Health Expenditure: Results from the International Diabetes Federation Diabetes Atlas, 9th Edition. *Diabetes Res. Clin. Pract.* **2020**, *162*, 108072. https://doi.org/10.1016/j.diabres.2020.108072.

(126) National Center for Biotechnology Information. *PubChem Compound Summary for CID 1983, Acetaminophen*. https://pubchem.ncbi.nlm.nih.gov/compound/Acetaminophen#section=Computed-Properties (accessed 2024-03-15).

(127) Drugbank Online. *Acetaminophen*. https://go.drugbank.com/drugs/DB00316 (accessed 2024-03-15).

(128) Lee, W. M. Acetaminophen and the U.S. Acute Liver Failure Study Group: Lowering the Risks of Hepatic Failure. *Hepatology* **2004**, *40* (1), 6–9. https://doi.org/10.1002/hep.20293.

(129) Chen, W.; Koenigs, L. L.; Thompson, S. J.; Peter, R. M.; Rettie, A. E.; Trager, W. F.; Nelson, S. D. Oxidation of Acetaminophen to Its Toxic Quinone Imine and Nontoxic Catechol Metabolites by Baculovirus-Expressed and Purified Human Cytochromes P450 2E1 and 2A6. *Chem. Res. Toxicol.* **1998**, *11* (4), 295–301. https://doi.org/10.1021/tx9701687.

(130) Franco, F. W.; Malonn, M. C. Acetaminophen pharmacokinetic and toxicological aspects: a review. *Rev. Científica Multidiscip. Núcleo Conhecimento* **2021**, *9* (12), 18–27. https://doi.org/10.32749/nucleodoconhecimento.com.br/health/acetaminophen-pharmacokinetic.

(131) Albano, E.; Rundgren, M.; Harvison, P. J.; Nelson, S. D.; Moldeus, P. Mechanisms of N-Acetyl-p-Benzoquinone Imine Cytotoxicity. *Mol. Pharmacol.* **1985**, *28*, 306–311.

(132) Gonzalez, F. J. Role of Cytochromes P450 in Chemical Toxicity and Oxidative Stress: Studies with CYP2E1. *Mutat. Res. Mol. Mech. Mutagen.* **2005**, *569* (1–2), 101–110. https://doi.org/10.1016/j.mrfmmm.2004.04.021.

(133) Mitchell, J. R.; Thorgeirsson, S. S.; Potter, W. Z.; Jollow, D. J.; Keiser, H. Acetaminophen-induced Hepatic Injury: Protective Role of Glutathione in Man and Rationale for Therapy. *Clin. Pharmacol. Ther.* **1974**, *16* (4), 676–684. https://doi.org/10.1002/cpt1974164676.

(134) Jones, A. L. Mechanism of Action and Value of N-Acetylcysteine in the Treatment of Early and Late Acetaminophen Poisoning: A Critical Review. *J. Toxicol. Clin. Toxicol.* **1998**, *36* (4), 277–285. https://doi.org/10.3109/15563659809028022.

(135) Buckley, N. A.; Buckley, N.; Whyte, I. M.; O'Connell, D. L.; Dawson, A. H. Oral or Intravenous *N* -Acetylcysteine: Which Is the Treatment of Choice for Acetaminophen (Paracetamol) Poisoning? *J. Toxicol. Clin. Toxicol.* **1999**, *37* (6), 759–767. https://doi.org/10.1081/CLT-100102453.

(136) Betten, D. P.; Vohra, R. B.; Cook, M. D.; Matteucci, M. J.; Clark, R. F. Antidote Use in the Critically Ill Poisoned Patient. *J. Intensive Care Med.* **2006**, *21* (5), 255–277. https://doi.org/10.1177/0885066606290386.

(137) Miotke-Wasilczyk, M.; Józefowicz, M.; Strankowska, J.; Kwela, J. The Role of Hydrogen Bonding in Paracetamol–Solvent and Paracetamol–Hydrogel Matrix Interactions. *Materials* **2021**, *14* (8), 1842. https://doi.org/10.3390/ma14081842.

(138) Liu, Y.; Yang, G.; Jin, S.; Xu, L.; Zhao, C. Development of High-Drug-Loading Nanoparticles. *ChemPlusChem* **2020**, *85* (9), 2143–2157. https://doi.org/10.1002/cplu.202000496.

(139) Spaltro, A.; Pila, M. N.; Colasurdo, D. D.; Noseda Grau, E.; Román, G.; Simonetti, S.; Ruiz, D. L. Removal of Paracetamol from Aqueous Solution by Activated Carbon and Silica. Experimental and Computational Study. *J. Contam. Hydrol.* **2021**, *236*, 103739. https://doi.org/10.1016/j.jconhyd.2020.103739.

(140) O'Reilly, J. P.; Butts, C. P.; I'Anso, I. A.; Shaw, A. M. Interfacial pH at an Isolated Silica−Water Surface. *J. Am. Chem. Soc.* **2005**, *127* (6), 1632–1633. https://doi.org/10.1021/ja0443326.

(141) Rosenholm, J. M.; Czuryszkiewicz, T.; Kleitz, F.; Rosenholm, J. B.; Lindén, M. On the Nature of the Brønsted Acidic Groups on Native and Functionalized

Mesoporous Siliceous SBA-15 as Studied by Benzylamine Adsorption from Solution. *Langmuir* **2007**, *23* (8), 4315–4323. https://doi.org/10.1021/la062450w.

(142) Ong, S.; Zhao, X.; Eisenthal, K. B. Polarization of Water Molecules at a Charged Interface: Second Harmonic Studies of the Silica/Water Interface. *Chem. Phys. Lett.* **1992**, *191* (3–4), 327–335. https://doi.org/10.1016/0009-2614(92)85309-X.

(143) Shaw, A. M.; Hannon, T. E.; Li, F.; Zare, R. N. Adsorption of Crystal Violet to the Silica−Water Interface Monitored by Evanescent Wave Cavity Ring-Down Spectroscopy. *J. Phys. Chem. B* **2003**, *107* (29), 7070–7075. https://doi.org/10.1021/jp027636s.

(144) Narayan, R.; Gadag, S.; Garg, S.; Nayak, U. Y. Understanding the Effect of Functionalization on Loading Capacity and Release of Drug from Mesoporous Silica Nanoparticles: A Computationally Driven Study. *ACS Omega* **2022**, *7* (10), 8229–8245. https://doi.org/10.1021/acsomega.1c03618.

(145) Bolis, V.; Fubini, B.; Marchese, L.; Martra, G.; Costa, D. Hydrophilic and Hydrophobic Sites on Dehydrated Crystalline and Amorphous Silicas. *J. Chem. Soc. Faraday Trans.* **1991**, *87* (3), 497. https://doi.org/10.1039/ft9918700497.

(146) Musso, G. E.; Bottinelli, E.; Celi, L.; Magnacca, G.; Berlier, G. Influence of Surface Functionalization on the Hydrophilic Character of Mesoporous Silica Nanoparticles. *Phys. Chem. Chem. Phys.* **2015**, *17* (21), 13882–13894. https://doi.org/10.1039/C5CP00552C.

(147) Yang, P.; Gai, S.; Lin, J. Functionalized Mesoporous Silica Materials for Controlled Drug Delivery. *Chem. Soc. Rev.* **2012**, *41* (9), 3679. https://doi.org/10.1039/c2cs15308d.

(148) Guillet-Nicolas, R.; Popat, A.; Bridot, J.-L.; Monteith, G.; Qiao, S. Z.; Kleitz, F. pH-Responsive Nutraceutical-Mesoporous Silica Nanoconjugates with Enhanced Colloidal Stability. *Angew. Chem. Int. Ed.* **2013**, *52* (8), 2318–2322. https://doi.org/10.1002/anie.201208840.

(149) Rengarajan, G. T.; Enke, D.; Steinhart, M.; Beiner, M. Stabilization of the Amorphous State of Pharmaceuticals in Nanopores. *J. Mater. Chem.* **2008**, *18* (22), 2537. https://doi.org/10.1039/b804266g.

(150) Juère, E.; Kleitz, F. On the Nanopore Confinement of Therapeutic Drugs into Mesoporous Silica Materials and Its Implications. *Microporous Mesoporous Mater.* **2018**, *270*, 109–119. https://doi.org/10.1016/j.micromeso.2018.04.031.

(151) von Baeckmann, C.; Rubio, G. M. D. M.; Kählig, H.; Kurzbach, D.; Reithofer, M. R.; Kleitz, F. Evaporation-Induced Self-Assembly of Small Peptide-Conjugated Silica Nanoparticles. *Angew. Chem. Int. Ed.* **2021**, *60* (42), 22700–22705. https://doi.org/10.1002/anie.202108378.

(152) Brühwiler, D. Postsynthetic Functionalization of Mesoporous Silica. *Nanoscale* **2010**, *2* (6), 887. https://doi.org/10.1039/c0nr00039f.

(153) Caillard, R.; Subirade, M. Protein Based Tablets as Reversible Gelling Systems for Delayed Release Applications. *Int. J. Pharm.* **2012**, *437* (1–2), 130–136. https://doi.org/10.1016/j.ijpharm.2012.07.039.

(154) Sing, K. S. W. Physisorption of Nitrogen by Porous Materials. *J. Porous Mater.* **1995**, *2* (1), 5–8. https://doi.org/10.1007/BF00486564.
(155) Andersson, J.; Rosenholm, J.; Areva, S.; Lindén, M. Influences of Material Characteristics on Ibuprofen Drug Loading and Release Profiles from Ordered Micro- and Mesoporous Silica Matrices. *Chem. Mater.* **2004**, *16* (21), 4160–4167. https://doi.org/10.1021/cm0401490.
(156) Jović, B.; Panić, M.; Radnović, N.; Živojević, K.; Mladenović, M.; Crnojević, V.; Knežević, N. Investigation of the Surface Interactions of Selected Amides with Mesoporous Silica Using FTIR Spectroscopy and Hyperspectral Imaging. *J. Mol. Struct.* **2020**, *1219*, 128562. https://doi.org/10.1016/j.molstruc.2020.128562.
(157) Bui, T. X.; Kang, S.-Y.; Lee, S.-H.; Choi, H. Organically Functionalized Mesoporous SBA-15 as Sorbents for Removal of Selected Pharmaceuticals from Water. *J. Hazard. Mater.* **2011**, *193*, 156–163. https://doi.org/10.1016/j.jhazmat.2011.07.043.
(158) Schmuck, C.; Schwegmann, M. Recognition of Anionic Carbohydrates by an Artificial Receptor in Water. *Org. Lett.* **2005**, *7* (16), 3517–3520. https://doi.org/10.1021/ol051230r.
(159) Drugbank online. *Metabolite Acetaminophen sulfate*. https://go.drugbank.com/metabolites/DBMET00653 (accessed 2024-03-21).
(160) Drugbank online. *Metabolite Acetaminophen glucuronide*. https://go.drugbank.com/metabolites/DBMET00580 (accessed 2024-03-21).
(161) Drugbank online. *Metabolite NAPQI*. https://go.drugbank.com/metabolites/DBMET00243 (accessed 2024-03-21).